

**ELECTRON DENSITY AT JUPITER USING THE GALILEO PLASMA WAVE
INSTRUMENT**

by
Jay Alan Ansher

A thesis submitted in partial fulfillment
of the requirements for the Doctor of
Philosophy degree in Physics
in the Graduate College of
The University of Iowa

December 2001

Thesis supervisor: Professor Donald A. Gurnett

Graduate College
The University of Iowa
Iowa City, Iowa

CERTIFICATE OF APPROVAL

PH.D. THESIS

This is to certify that the Ph.D. thesis of

Jay Alan Ansher

has been approved by the Examining Committee
for the thesis requirement for the Doctor of
Philosophy degree in Physics at the July 2001 graduation.

Thesis committee: _____
Thesis supervisor

Member

Member

Member

Member

This doctoral dissertation is dedicated to the memory of my grandfather, Sanford Lieber, and to the memory of Karen Phelps.

The stars are laughing at us, as we crawl on and on across this antheap.

Andy Partridge of XTC
"Across This Antheap" from Oranges and Lemons

ACKNOWLEDGMENTS

There is a long list of people I would like to thank, who have helped me along the way while I have been writing my dissertation. The first person I would like to thank is Dr. Donald Gurnett. He has shown me a great deal of patience and assistance. I feel very fortunate to have been able to learn from him and work with him on this project, and others since my days as an undergraduate. My parents, Richard and Roslyn, have supported me since the beginning. Without their encouragement and advice I would never have been able to endure the long process of graduate school. My grandparents, Bess and Sanford Lieber also have been a great source of support throughout my education. My grandfather, who earned a college degree in chemistry, helped foster my interests in science at a young age. His continued support and interest in my studies in later years inspired me to continue into graduate school. His death in December of 2000 was a great loss for me and for my family, but his work ethic and love for knowledge will stay with me throughout my life. My other family members' continued interest and enthusiasm for my work has been a great asset. I also wish to thank my sister, Lynn, who has been a companion to me as she walks her own path through graduate school.

Karen Phelps, an administrative assistant with the physics department at the University of Iowa, also made a large difference in my life. Her encouragement and faith in me gave me the motivation to work harder when I felt I could not. Karen had been in the physics department since 1990. She was extremely helpful to me doing her normal job, but also was always there to offer a kind word or some encouragement as a friend. Karen died suddenly of pancreatic cancer in the summer of 1998. Her hard working

attitude, grounded common sense, and strong will always inspired me. I will fondly remember our conversations in her office. She was frequently willing to lend an ear whether I was having a run of good luck or bad. She had a unique way with many of the graduate students in the department. I am saddened that I cannot share my joy with my grandfather, Sanford, or Karen upon completing this dissertation, but I am grateful for their advice, encouragement, and friendship.

I would like to thank my committee members, Dr. Craig Kletzing, Dr. William Klink, Dr. Norbert Malik, and Dr. Robert Merlino for their time and interest in my project. I have also received a great deal of assistance in the preparation of this work. Joe Groene has written most of the computer programs that were involved in the data analysis. The voluminous task of data processing was carried out by quite a few research assistants: Scott Malowitz, Chris Anson, Ed Thomsen, Ngoc Nguyen, Jiansheng Chen, Sean McKay, Humphrey Otita, Aaron Peck, Jon VandeGeest, Yousef Awad, and Mary Ernst. Without their dedicated help, I would not have had any data on which to base a dissertation.

Others in the physics department I would like to thank include Kathy Kurth, Robin Paterson, Jean Hospodarsky, Marilyn Simpson, Christine Stevens, Deborah Foreman, Cheryl Reardon, Dorene Nott, Katie Schaub, and Mary Ann Spilger. Each of these people, as current or former administrative assistants in the department, especially Kathy Kurth, frequently helped me with all the details that are required to survive a graduate student career. They assisted with airline tickets, photocopying, typing, application forms, and a zoo of other administrative details. They capably handled each of these details, which made my life much easier. In addition, Dr. William Kurth and Dr. James A. Van Allen, who sparked my interest in space physics while an undergraduate at Iowa, and Larry Granroth have all been valuable sources of advice and information

during my time here. I would also like to acknowledge helpful conversations with Dr. Benjamin Chandran who showed an interest in the later stages of my work when he arrived at Iowa. Some thanks are owed to Dr. Krishan Khurana and Dr. Margaret Kivelson at UCLA along with Dr. Fran Bagenal at the University of Colorado. They all provided valuable advice and data from their own work that has assisted me in my research.

On a more personal note, I would like to thank my close friends for all their support while I have been working on my Ph.D. Erick and Jana Zawojewski provided me with a place to stay for a significant period of time. Lee and Stephanie Brintle, Lynne Carothers, Neil and Michelle Dodgen, Chris and Carol Piker, Ryan and Jaci Minikis, and Bryce Wade were all kind enough to offer me temporary lodging as well. My close friends John Spiegel, Todd Young, Susan Stewart, and Chris and Jennifer Wilkins have all been there to help me out in various ways whenever I needed them. The University of Iowa Ski and Snowboard club took a great deal of my time but gave back a great deal of reward. I am grateful for the friends I made in the club as well as for the breaks it gave me from my work. Of special note is Brian Davis. He showed up as my officemate for eighteen months at Iowa and became a very close friend. His similar outlook on life provided a healthy perspective and gave me a break from my work when I needed it. The fact that I am writing this indicates that those breaks were a good thing. Had I not finished this Ph.D., Brian's influence might have been altogether differently viewed. And last but not least I would like to thank the members and associates of SPACHouse from Rice University. Chris, Vince, Pete, Dirk, Bemo, Colin, Cormac, Bart, and Paul have all been great friends and without watching them go on to their own successes while still having a great time, I would never have deemed it possible for myself. I may not have

finished the fastest Ph.D. ever, but I had a good time along the way and wouldn't trade the experiences for anything.

ABSTRACT

The plasma wave instrument on board the Galileo spacecraft is used to determine the electron density in Jupiter's magnetosphere. Ordinary mode radio waves are detected in the form of non-thermal continuum radiation trapped in the magnetosphere at frequencies above the electron plasma frequency. By identifying the low-frequency cutoff of continuum radiation as the plasma frequency, the local electron density can be calculated. This technique is used with plasma wave data from the Galileo primary mission to generate an electron density data set with approximately 37-second time resolution. The density data set is used to examine the electron density profile of the Jovian plasma sheet between radial distances of 20 and 140 R_J from Jupiter. The average electron density in the plasma sheet decreases with radial distance according to a power law that scales as $(1/r)^{2.14}$. With the addition of data closer to Jupiter, one sees a change to a steeper power law, approximately $(1/r)^{6.55}$ inside about 20 R_J .

The density data is used in conjunction with data from the Galileo magnetometer instrument and a model of Jupiter's plasma sheet to study pressure balance across the plasma sheet. Assuming the plasma sheet is in a quasi-static state, and the magnetic field lines in the plasma sheet have negligible curvature, the sum of magnetic and particle pressures across the plasma sheet should stay constant. By varying the temperature parameter, best fits for the constant total pressure and corresponding temperature are determined. These values yield pressure and temperature profiles of Jupiter's plasma sheet between approximately 20 and 140 R_J . Typical temperatures determined using this technique are about 10^8 K, corresponding to energies of about 10 keV. The average total

pressure decreases with radial distance from Jupiter as a power law proportional to $(1/r)^{2.23}$. Density and pressure may vary by a factor of 2 or more from these averages. The scatter is likely due to short time-scale variability of density and pressure in the magnetosphere.

TABLE OF CONTENTS

		Page
LIST OF TABLES		xii
LIST OF FIGURES.....		xiii
CHAPTER		
I.	INTRODUCTION.....	1
II.	PLANETARY MAGNETOSPHERES.....	7
	Magnetospheric Physics at the Earth	7
	The Jovian Magnetosphere	9
	Large-scale Plasma Processes	11
	Substorms.....	14
	Small-scale Structure	16
	Summary	19
III.	CONTINUUM RADIATION CUTOFF TECHNIQUE.....	41
	The Role of Continuum Radiation.....	41
	Electron Density From Galileo Plasma Wave Data.....	44
IV.	ELECTRON DENSITY PROFILE AND SURVEY	67
	Radial Density Profile of the Plasma Sheet	67
	Global Density Display.....	70
	Magnetopause Encounters	73
V.	PLASMA SHEET MODELS.....	96
	Plasma Sheet and Magnetodisc Models.....	96
	Identification of the Plasma Sheet in the Data.....	98
	Use of the Khurana Current Sheet Model.....	99
VI.	PRESSURE BALANCE ACROSS THE PLASMA SHEET	108
	Magneto-hydrodynamic Pressure Balance.....	108
	The Least-squares Fitting Program.....	111
	Analysis of Program Output	113
	Pressure and Temperature.....	115
VII.	SUMMARY AND RESULTS	136

VIII.	FUTURE RESEARCH	143
	General Comments About the Data Set	143
	Analysis Projects.....	143
REFERENCES	147

LIST OF TABLES

Table	Page
1. Data Quality Flags	50
2. Pressure Fit Categories.....	119
3. Radial Profile Fit Parameters	140

LIST OF FIGURES

Figure	Page
1. The Galileo spacecraft	3
2. Galileo's primary mission trajectory	5
3. A simple cartoon of Earth's magnetosphere.....	21
4. A more detailed cartoon of the Earth's magnetosphere.....	23
5. A general picture of plasma convection at the Earth	25
6. A comparison of magnetic field lines	27
7. The disc model of the Jovian magnetosphere	29
8. The co-rotating active sector model.....	31
9. The co-rotating convection model	33
10. The transient convection model	35
11. Fingers of dense plasma.....	37
12. Electron density at Jupiter.....	39
13. A sample 24-hour color spectrogram.....	51
14. A diagram of index of refraction versus frequency	53
15. A simple cartoon of continuum radiation	55
16. The electron plasma frequency at Jupiter	57
17. A sample power spectrum from Galileo	59
18. A spectrogram with the plasma frequency.....	61
19. An example of wave superposition.....	63
20. Plasma sheet crossings.....	65
21. Plasma sheet density.	76

22. Fitted plasma sheet density	78
23. Jupiter's electron density profile	80
24. Two different power laws	82
25. The Khurana model.....	84
26. A global density display.....	86
27. Stretched density display	88
28. Global density display with crossings.....	90
29. Magnetopause encounters	92
30. Model magnetopause locations from Voyager	94
31. Four different magnetodisc models.....	102
32. Density and magnetic field strength.....	104
33. One plasma sheet crossing	106
34. Idealized pressure balance	120
35. Temperature and pressure	122
36. Deviations from the best fit.....	124
37. The best fit temperatures.....	126
38. Radial temperature profile	128
39. Total pressure.....	130
40. Radial total pressure profile.....	132
41. Tail magnetopause geometry	134
42. Jupiter's Magnetosphere	141

CHAPTER I: INTRODUCTION

The study of the Jovian magnetosphere began when low-frequency radio noise was detected in the area of the sky around Jupiter [Burke and Franklin, 1955]. Jupiter is an incredibly powerful radio source. The magnetosphere of Jupiter, as observed from Earth, has an angular size on the sky equivalent to four full moons. Jupiter's magnetosphere is a very large and complex system characterized by interactions of charged particles with strong electric and magnetic fields. It is these interactions which generate the intense radio emission observed coming from Jupiter. One of the key characteristics to understanding these electrodynamic processes is the plasma density. Jupiter's nearest moon, Io, ejects about 1000 kg of sulfur, oxygen, sodium, and potassium each second. This gas is quickly ionized by solar radiation. It is believed that because of this source of plasma deep within the system, the magnetosphere of Jupiter behaves very differently than Earth's magnetosphere. By contrast, much of the plasma in the Earth's magnetosphere is ionized hydrogen and helium from the solar wind. This plasma is believed to enter from outside the magnetosphere at the magnetopause boundary. This external source provides the dominant fraction of plasma at the Earth.

Because spacecraft made previous measurements of density near Jupiter during brief flybys of the planet, little is known about the long-term behavior of the plasma and dynamics in its magnetosphere. Density data were available only at limited locations within the Jovian system and only over a time interval of several days. The Galileo spacecraft (Figure 1) however, is making multiple orbits of Jupiter over a period of several years. The plasma wave instrument is collecting data at radial distances from the

planet beyond about 10 Jovian radii (R_J), and at all longitudes. The trajectory of the spacecraft for the primary mission can be seen in Figure 2. A density data set obtained from the plasma wave data allows examination of the Jovian plasma environment on long time scales, and comparison with global models of Jupiter's magnetosphere. With such a data set, a better comparison of the structure and dynamics of the magnetospheres of Jupiter and the Earth may be made. An important subject this data set can address is the ultimate fate of the plasma that is produced near the moon Io: Where does the plasma from Io go? It is assumed likely that this plasma somehow leaves the system down Jupiter's long magnetotail (sometimes extending as far as the orbit of Saturn), but it not yet well understood how the plasma is transported.

Figure 1. The Galileo spacecraft. The plasma wave instrument utilizes the electric dipole antenna elements mounted at the end of the magnetometer boom.

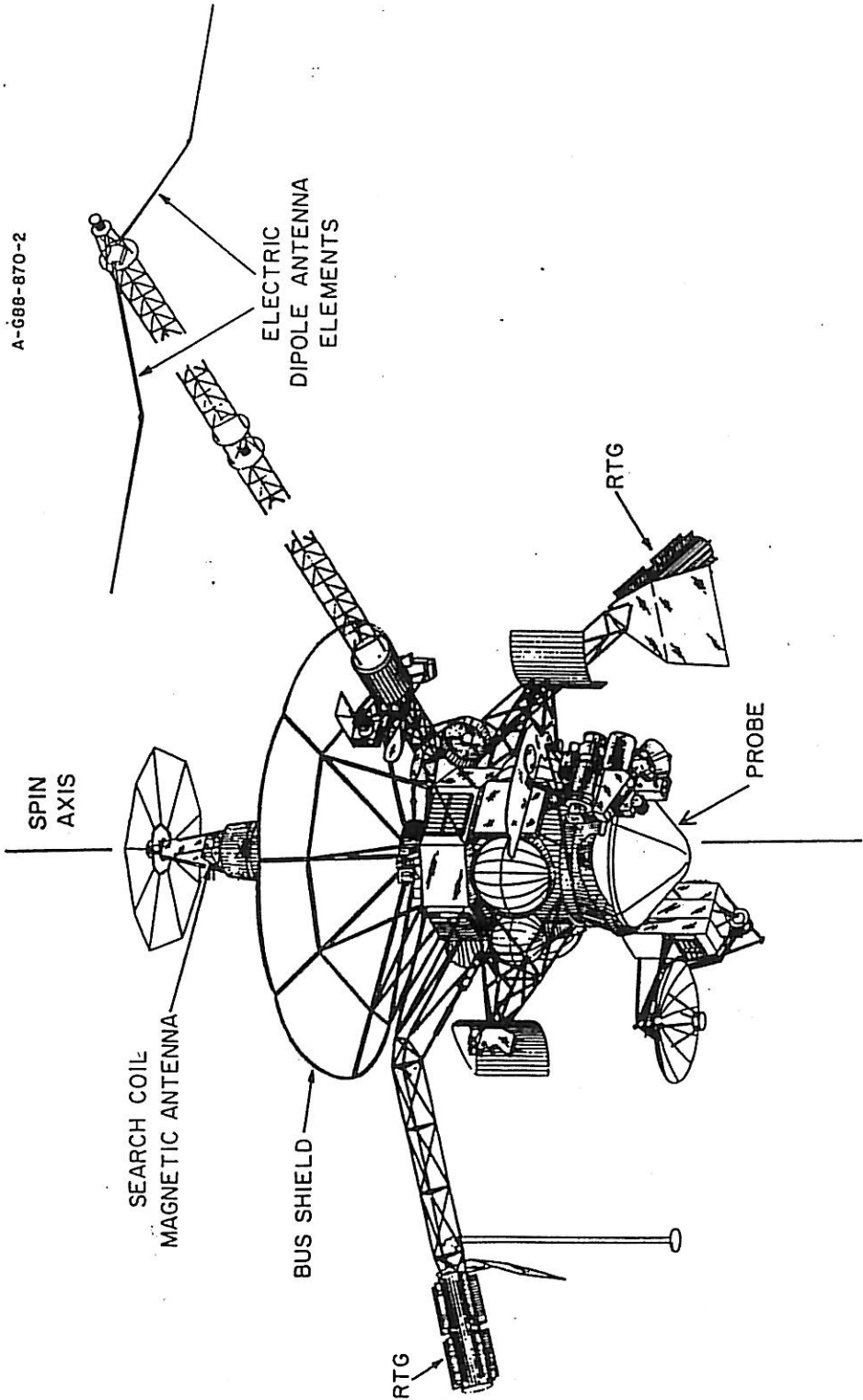
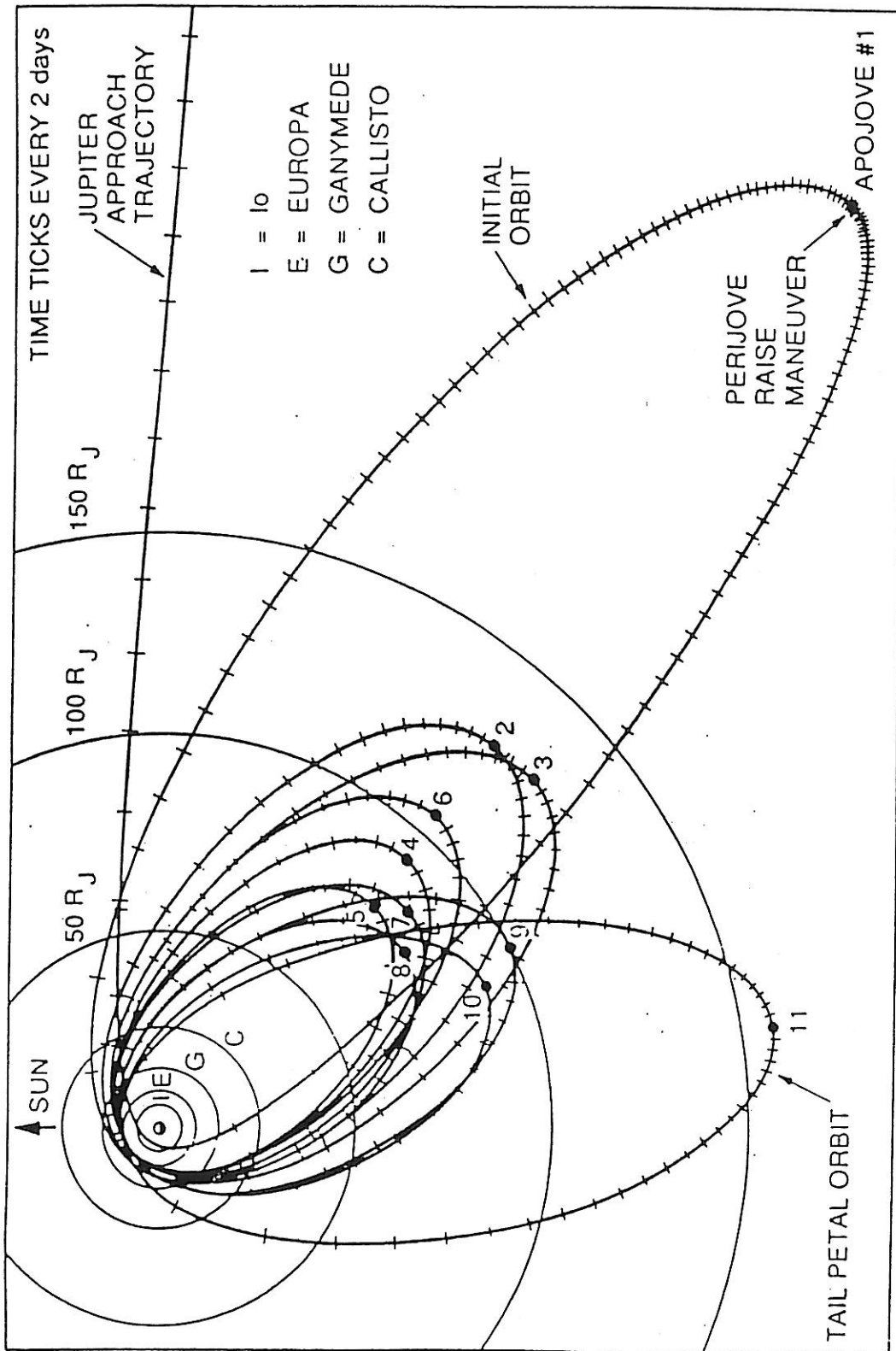


Figure 2. Galileo's primary mission trajectory. Galileo made eleven orbits, including ten encounters with the Galilean satellites of Jupiter. During this primary mission, the spacecraft encountered radial distances between 10 and 150 R_J , and all longitudes.



CHAPTER II: PLANETARY MAGNETOSPHERES

Understanding the global picture of plasma transport at Jupiter draws upon several different areas of magnetospheric physics. Pieces of the global transport puzzle involve magnetospheric interaction with the solar wind, magnetic substorms, and small-scale plasma motions in both the inner and outer magnetosphere. While magnetospheric convection is partially understood at the Earth, studying plasma motions at Jupiter proves to be a greater challenge. Three important differences make the Jovian system much more complicated: Jupiter's magnetic field is much stronger than the Earth's magnetic field, Jupiter spins much faster on its axis than the Earth, and Jupiter's moon Io, located deep inside the magnetosphere, provides a large plasma source. It is not yet well understood what effect these differences have on the global dynamics of the system. The Galileo measurements, taken over longer time scales and larger regions of the magnetosphere, may allow better understanding of these dynamics.

Magnetospheric Physics at the Earth

The solar wind is a hot, tenuous, ionized gas that flows outward from the Sun in all directions. Near the orbit of the Earth, the solar wind has a mean velocity of about 350 km/s, a temperature around 10^5 K, and typical plasma densities on the order of 10 particles per cubic centimeter of space [Tascione, 1988; Kivelson and Russell, 1995]. A weak interplanetary magnetic field (IMF) convects outward with the solar wind. This field is variable in direction and magnitude because its source, the solar magnetic field, is also variable. As the solar wind plasma flows outward, the IMF is carried along with it, because of the high electrical conductivity of the plasma. This "frozen-in-flux" condition

allows the IMF to sweep past the Earth's magnetosphere as the solar wind expands into interplanetary space. When the IMF impinges on the Earth's intrinsic magnetic field, a coupling with the Earth's field takes place. Because the plasma is carried along with the field lines of the IMF, such an interaction allows the deposit of solar wind plasma (mainly protons, electrons, and alpha particles) into the Earth's magnetosphere. The boundary of influence of the Earth's magnetic field is known as the magnetopause. Figure 3 shows a simplified model of the main components of a typical magnetosphere. On the sunward side of the Earth, the magnetopause is located an average of about $10 R_E$ away from the Earth, though this stand-off distance varies with solar wind activity. Several mechanisms have been proposed which may individually, or in combination, allow the plasma to enter the magnetosphere at the nose of the magnetopause: merging of magnetic field lines [Vasyliunas, 1975], diffusion of particles across the magnetopause, and electromagnetic drift of particles across the boundary [Hill, 1983].

Once inside the magnetosphere, the Earth's intrinsic magnetic field (which rotates at the same rate as the Earth rotates about its axis) governs the motions of the plasma. In addition to particles from the solar wind, fresh plasma is slowly supplied by the high altitude ionosphere and plasmasphere of the Earth [Tascione, 1988; Kivelson and Russell, 1995]. Within about 4 or 5 R_E of the planet's center, plasma co-rotates with the Earth's field, according to the same frozen-in-flux principle. The Van Allen radiation belts are one example of this type of trapped particle population. In the outer magnetosphere, as the influence of the magnetic field decreases, inertial and electrodynamic effects diminish the effect of co-rotation. Plasma motions in the magnetosphere generate large-scale electric potentials. These huge potentials, in turn create complex current systems, which result in the bulk transport of charged particles. Mega-ampere currents flow in the magnetosphere and in the ionosphere, according to the electrical conductivity of the

medium, but move most easily along field lines. With a steady-state flow of solar wind plasma and embedded IMF, these complex currents and convection patterns form complete closed circuits. Cartoon maps of these currents and convection patterns can be seen in Figures 4 and 5. These composite pictures of plasma convection at the Earth are the general results of multiple models and theoretical predictions [Tascione, 1988; Kivelson and Russell, 1995]. The launching of numerous rockets and satellites since the 1950's, along with ground based instruments and detectors have experimentally verified that these general convection patterns do exist in the Earth's magnetosphere and ionosphere.

The Jovian Magnetosphere

Jupiter is located 5.2 astronomical units (AU) from the Sun. One AU is the average distance between the Sun and Earth. The temperature and average speed of the solar wind at Jupiter's orbital distance are roughly the same as near the Earth. The electron and proton densities decrease with radial distance from the sun according to a $(1/r)^2$ power law. At the distance of Jupiter's orbit, there are about 0.4 particles per cubic centimeter of space. If the solar wind is still present at the orbital distance of Jupiter, and if Jupiter also has a magnetic field, then we should expect to see a magnetosphere around Jupiter. This is, indeed the case, however there are three major differences between Jupiter and the Earth that make Jupiter's magnetosphere very unique.

The intrinsic magnetic field of Jupiter is different than the Earth's in some important ways. Jupiter is believed to have a great mantle of liquid "metallic" hydrogen. Jupiter's tremendous size and gravitational pull compresses the hydrogen in its mantle until electron shells overlap such that it behaves as a metal. This metallic hydrogen acts as an electrical conductor and produces a magnetic dipole moment of 1.6×10^{11} Tesla-km³, compared to 8.0×10^6 Tesla-km³ at the Earth. The slightly less substantial solar

wind at Jupiter and the large difference in planetary field strengths combine to create an immense magnetospheric cavity in the solar wind that is about 100 times the size of the Earth's magnetosphere [Dessler, 1983]. The magnetic axis of Jupiter is tilted almost 10 degrees from the spin axis. The Earth's magnetic axis is tilted about 12 degrees from its spin axis. Jupiter's magnetic field however, happens to be "upside down" compared to the Earth's. Jupiter's north magnetic pole is in the northern geographic hemisphere, while the Earth's north magnetic pole is in the southern hemisphere.

Jupiter has a very rapid spin rate, and completes one rotation about every 10 hours. Due to frozen-in-flux effects similar to those in the solar wind, plasma in Jupiter's magnetosphere generally tends to be locked into rotation at the same rate as the planet. As is the case at the Earth, this co-rotation is not perfect, but has been shown to be more rigid at smaller radial distances [Hill, 1979; 1980; McNutt et al., 1979]. At the Earth, the spin rate and the resulting "centrifugal" force is much less; the solar wind is the dominant energy source for driving plasma motions. The dynamics of the Jupiter system are driven by the kinetic energy imparted to the plasma by the rapid rotation of the planet and its co-rotating magnetic field.

Of Jupiter's four Galilean satellites, Io orbits closest to Jupiter. Io is located deep inside the magnetosphere, about $5.9 R_J$ from the planet. Because Io is so close to Jupiter, it is subject to tremendous gravitational tidal stresses. These stresses knead and heat the interior of Io, producing numerous volcanoes and geysers, which are routinely observed on its surface. Earth based telescopes have long detected clouds of sulfur, oxygen, sodium and related chemical compounds around Io. Close up photographs from the two Voyager spacecraft have even revealed volcanoes in the act of erupting. Io is the most geologically active object in the Solar system and routinely resurfaces itself through volcanic eruptions. Because of the low escape velocity at the surface of Io, much of the

material ejected from these volcanoes escapes into orbit around Jupiter. When solar ultraviolet light interacts with these molecules, photo-ionization occurs, and provides a source of fresh plasma deep in the interior of Jupiter's magnetosphere. About one ton of newly ionized material is produced every second in the vicinity of Io. This material forms a donut shaped structure around Jupiter at the orbital distance of Io, and is called the Io plasma torus [Dessler, 1983]. The Earth's magnetosphere has no such structure, nor is there a large, localized plasma source deep inside the magnetosphere. Plasma in the Earth's magnetosphere is supplied by the solar wind, with some plasma also coming from the plasmasphere.

Large-scale Plasma Processes

At the Earth, the main source of plasma and kinetic energy is believed to be the solar wind. As the solar wind streams past Earth at about 350 km/s, interactions take place at the nose of the magnetopause and allow energy and particles to be transmitted across the magnetopause boundary into the magnetosphere [Tascione, 1988; Kivelson and Russell, 1995]. The two major models are the "open" magnetosphere and the "closed" magnetosphere. Rough sketches of the difference between these two models are depicted in Figure 6. When the interplanetary magnetic field is oriented with a northward component, little interaction with the Earth's intrinsic field takes place at the nose of the magnetopause. When the IMF is oriented in a southward direction, as in the open model, energy is transferred through a process known as magnetic reconnection [Dungey, 1961; 1965]. The Earth's field and the solar wind field can merge with each other at an "X-line", allowing some of the solar wind field lines to become connected to the Earth. These are called open field lines, and allow solar wind particles direct access to the magnetosphere. In the closed model, there is no connectivity between the Earth's field and the solar wind magnetic field. In this model, particles may enter the magnetosphere

by simple diffusion, or by magnetic field drift across the magnetopause boundary. The open model is well supported by observation, because magnetospheric activity and the plasma flow described previously seem to be well correlated with the north-south orientation of the IMF and solar wind activity [Tascione, 1988; Kivelson and Russell, 1995]. Since the main sources of both plasma and energy at Jupiter are inside its own magnetosphere, it is unclear if a solar wind interaction plays an important role in magnetospheric dynamics there.

Several major models currently exist which attempt to describe large-scale spin-periodic motions in Jupiter's magnetosphere [Hill, et al., 1983; Vasyliunas, 1983]. Because this dissertation involves plasma density measurements, the fashion in which these models address plasma density is of particular interest. Because the plasma source (Io) is in the plane of Jupiter's rotational equator, most of the material starts out confined there. Upon ionization, however, electromagnetic forces play a large role in the subsequent motion. For example, the tilt of Jupiter's magnetic field with respect to the spin axis can alter particle orbits, and change the latitudinal distributions of plasma away from that expected due to direct injection from Io.

One of the simplest models for periodic plasma motions in Jupiter's magnetosphere is the disc model, or offset tilted dipole model, which describes a plasma disc that is centered along the magnetic equatorial plane, and therefore tilted 10 degrees from the spin equatorial plane. As the disc rotates, it appears to wobble up and down. An observer in the spin equatorial plane would encounter the so-called magnetodisc twice per rotation period as it rotates past: once as the disc sweeps past from north to south, and once from south to north [Hill et al., 1983]. This rigid magnetodisc model is depicted in Figure 7. There is some dispute among more detailed models as to whether this magnetodisc is rigid, bent, warped, or wavy. Differences in magnetodisc models depend

on the relative strengths of magnetic, gravitational, and centrifugal forces. Each of these forces can play a role in distributing the plasma to different latitudes and radial extents. For example, the magnetic forces tend to confine the plasma along the magnetic equator, but centrifugal forces due to Jupiter's rapid rotation tend to redistribute the plasma toward the rotational (jovigraphic) equator. There are also uncertainties about the longitudinal symmetry of the magnetodisc. Differences in Jupiter's dayside and nightside magnetosphere at larger radial distances may be reflected in plasma densities and distribution in the magnetodisc. By examining the plasma density data, we can place observational constraints on the thickness of the disc at different longitudes, magnetic latitudes, and radial distances.

The magnetic anomaly model, or co-rotating active sector model shown in very basic terms in Figure 8, describes a situation in which particular, persistent magnetospheric phenomena are observed to co-rotate with the planet. A stationary observer at the jovigraphic equator would see these phenomena rotate past his position once per rotation. In this model, observed higher order moments in Jupiter's magnetic field produce an area of weaker surface field. This area of weaker field, being tied to Jupiter's intrinsic field, is fixed in longitude with respect to the interior of the planet [Hill et al., 1983]. This fixed longitude system is called System-III longitude, and is set up so that Jupiter's dipole field is tilted toward a System-III longitude (λ_{III}) of about 200 degrees. The so-called active sector, or weak-field anomaly is located between about 160 and 320 degrees λ_{III} , and is observed even at large radial distances from Jupiter. The anomaly is characterized by higher plasma densities, higher plasma temperatures, and increased radio emissions from the active sector [Hill, et al., 1983].

A large-scale plasma convection model related to Jupiter's asymmetric magnetic field called the co-rotating convection model [Hill et al., 1981; Hill and Dessler, 1991]

assumes a global pattern of plasma transport and neglects smaller scale variations of plasma density. Within the active sector, the plasma density in the Io torus is somewhat greater than at other longitudes. This model, shown in Figure 9, assumes a greater flux tube content in the active sector, resulting in increased radial outflow in that region as compared with other longitudes. Less dense, slower moving plasma flows inward on the opposite side of the planet, as viewed in the co-rotating reference frame. The dense plasma makes its radial trip to the outer magnetosphere on time scales of a few Jupiter rotation periods. At large radial distances, the plasma is lost to a "planetary wind" due to spin periodic openings of closed field lines to the magnetotail. An advantage of this model is that the convection pattern provides a large portion of the energy required to power observed magnetospheric phenomena, and provides a possible explanation for plasma transport from the Io torus to the outer regions of the Jovian system.

Substorms

At Earth, a phenomenon known as a magnetospheric substorm is frequently observed [Akasofu, 1968]. A substorm occurs when a magnetic "x-line" forms in the equatorial region of the magnetotail. This reconnection causes plasma to be accelerated sunward, populating the inner magnetosphere and the ring current [Tascione, 1988; Kivelson and Russell, 1995]. This sudden increase in high energy plasma can lead to spectacular auroral displays as particles precipitate along the magnetic field lines into the high latitude atmosphere of the Earth. Such events also increase the electrical activity in the magnetosphere, and can interfere with communications satellites as well as power generating stations on the ground. A similar acceleration process on the more distant side of the x-line sends a blob of plasma anti-sunward, allowing plasma to leave the magnetosphere and escape back into the solar wind down the long magnetotail. This substorm phenomenon cycles plasma from solar wind magnetic field lines, through the

Earth's magnetosphere, and back into the solar wind. It is the dominant global plasma transport mechanism at the Earth.

The "growth phase" model of substorms suggests that the magnetosphere goes through several phases before releasing the stored up energy provided by the solar wind. In the growth phase, solar wind magnetic field lines undergo magnetic merging at the nose of the magnetopause. These field lines, and the plasma associated with them are convected from the front of the magnetosphere back toward the tail as the open ends are dragged anti-sunward by the solar wind. As the field lines are piled upon each other in the Earth's magnetotail, the magnetic field strength in the tail increases, storing a large amount of energy. The field lines become more stretched and the plasma sheet becomes thinner. This phase can last up to an hour. The expansion phase, which follows, lasts only a few minutes and is triggered when instabilities in the tail result in magnetic merging similar to the merging that occurs at the magnetopause. If an x-line forms in the tail, as depicted in Figure 6, the stored magnetic field energy can be quickly released and plasma can be very suddenly accelerated sunward, injecting high energy plasma into the inner magnetosphere, but sending much of the plasma in the opposite tailward direction. After expansion, the magnetosphere returns to a more relaxed state during the recovery phase. After recovery, the magnetosphere appears much as it did prior to the original growth phase and the process can repeat. Because magnetic merging is important in this model, growth phase substorms are more efficient during times of southward IMF, and are well explained using an open magnetospheric model [Tascione, 1988; Kivelson and Russell, 1995]. It is unknown whether Jupiter experiences substorms in this same manner. Because the dominant energy source in Jupiter's magnetosphere is its rapid spin rate rather than the solar wind, the presence of substorms seems unlikely. There has, however, been evidence of Jovian auroral enhancements, energetic particle populations,

and other phenomena that are attributed to substorm activity at the Earth. With an orbiting spacecraft that can study these phenomena over long time periods, more careful study of these phenomena may be made.

Small-scale Structure

The use of the density data set to identify small-scale structures in the Jovian magnetosphere is another part of this research project. As the plasma at Jupiter is spun around like a centrifuge, a radially outward directed "centrifugal" force opposes a radially inward gravitational force. The radial distance at which the two forces are equal, is given by the relation:

$$\frac{GMm}{r^2} = mr\Omega_J^2 \quad (1)$$

where G is the universal gravitational constant, M is the mass of Jupiter, m is the mass of a particle in Jupiter's gravitational field, r is the radial distance from the center of the planet, and Ω_J is the rotational frequency of Jupiter. Simple substitution shows that at radial distances beyond about $2.2 R_J$, the outward force dominates. This situation is analogous to a Rayleigh-Taylor gravitational instability. Since the source of plasma (Io) is located at $5.9 R_J$ from the planet, this denser plasma in the inner region of the magnetosphere must flow radially away from the planet. There, presumably a less dense medium flows inward, taking the place of the denser plasma, which is eventually convected out of the system. The exchange of radial position of these different density plasmas is known as interchange, and the entire process is called "interchange instability" because the distribution of plasma is unstable [Thorne, 1983; Richardson and McNutt, 1987]. The denser plasma is in a higher potential energy state in the centrifugal-gravitational potential.

There are theoretical predictions about how the interchange motions take place. A theoretical eddy-diffusion model [Siscoe and Summers, 1981] involves small-scale motions of closely neighboring flux tubes about 6 - 8 R_J from Jupiter (just outside the Io plasma torus). Flux tubes, situated at different radial distances and containing different amounts of plasma change places by way of random, turbulent eddies. The size scale of these eddies is estimated to be about 0.1 - 0.2 R_J based on the "graininess" seen in Voyager 1 plasma measurements [Bagenal et al., 1980]. Because the flux tubes are immediately exposed to the next adjacent neighbor, they continue these turbulent exchanges until the dense plasma has moved outward from its source in the Io torus and the less dense plasma has moved inward. The lifetimes of these eddies are found to be independent of their size.

The transient convection model [Pontius et al., 1986; Pontius and Hill, 1989] is a different model, in which individual flux tubes move outward individually through the less dense medium. In this model, instead of diffusively exchanging plasma with immediately neighboring tubes through turbulent eddies, the flux tubes retain their basic structure and plasma content while moving steadily, radially outward. Their individual plasma content is generally different from the longitudinally independent averaged values assumed by the other models. The same equations that govern plasma transport in the larger-scale corotating convection model are used in this transient convection picture. The radial and azimuthal dimensions of the elliptically shaped transient flux tubes assumed by the Pontius and Hill [1989] model are between 0.01 and 0.1 Jovian radii near the Io plasma torus. A cartoon illustration of this process is shown in Figure 10. In this figure, blobs of plasma (flux tubes of finite width and length) are shown detaching from the rotating Io torus, and moving radially outward through Jupiter's magnetic field.

Yang et al. [1992, 1994] approach the problem of small-scale plasma transport using a computational interchange simulation. They use numerical computer simulations of an asymmetric torus and show evidence of discretely forming "fingers" of plasma moving outward under the influence of Jupiter's centrifugal acceleration. The simulations use a computer code called the RCM-J (the Earth-oriented Rice Convection Model modified for application to Jupiter) [Harel et al., 1981; Wolf, 1983; Wolf et al., 1991]. The simulation region is limited to the equatorial plane at radial distances between 5 and $20R_J$. This computer code assumes ideal magneto-hydrodynamics to calculate particle trajectories by mapping the two dimensional magnetospheric equator onto a two-dimensional ionosphere assuming perfectly conducting magnetic field lines. The simulations employ an outer torus density boundary that decreases by steps with radial distance from Jupiter, and a longitudinal density asymmetry based on the magnetic anomaly model. Runs of the computer code that include an energetic particle population and a coriolis force show development of higher density "fingers" of plasma, shown in Figure 11, that reach outward from the Io torus and move through the surrounding lower density medium. These fingers form predominantly in the denser region of the asymmetric torus and have scale sizes of about $1 R_J$ at a distance of $9 R_J$ from the planet. The best estimate of separation between finger structures is about 15 degrees of longitude, or about 25 minutes of Jupiter rotation. In the computer simulations, this outreaching of plasma fingers constitutes the primary means of plasma transport [Yang, 1994].

There is also some experimental evidence of small-scale plasma motions at Jupiter. The Galileo plasma wave technique described for determining the electron density was previously performed at the Earth [Gurnett and Shaw, 1973; Gurnett, 1975], and also at Jupiter with Voyager plasma wave data [Gurnett et al., 1981; Ansher et al.,

1992; Ansher 1994]. Those analyses seemed to support the model of discrete flux tubes of differing plasma density participating in interchange motions. The density data from the Voyager plasma wave instruments, displayed in Figure 12, showed small-scale density structures less than one R_J in size. Their properties were similar to those expected in heavily loaded plasma flux tubes. Ansher et al. [1992] analyzed a power spectrum of the observed size scales of the density structures, and concluded that there were no preferred scale sizes. The power spectrum was not suggestive of a fully turbulent process like the eddy-diffusion model predicts. A turbulent process would likely have produced a Kolmogorov spectrum, with power proportional to frequency to the $-5/3$ power. Instead the spectrum seemed to be proportional to $(1/f)$ which was more indicative of discrete, square-wave like density structures.

Summary

Using the density measurements from the Galileo mission, global models of Jupiter's magnetosphere, can be tested by mapping the electron density in the magnetosphere. Features such as the magnetodisc should be clearly identifiable in the data. The general properties of Jupiter's plasma sheet, tail lobes, and other major magnetospheric features can be described with the constructed data set. Theoretical models based upon our understanding of the physics at work at Jupiter, and predictions for the structure and dynamics of these important components of the Jovian system can be compared with our data. There are already some limited, direct in-situ measurements of the density in these regions from the brief flybys by the Voyager [Ansher et al., 1992; Bridge et al., 1979; Gurnett et al., 1979; 1981; McNutt et al., 1981, Scarf et al., 1979], Ulysses, and Pioneer missions. But only Galileo, and its extended mission in orbit around the giant planet, can provide enough measurements to test these theories and predictions thoroughly. The use of Galileo's plasma wave instrument to create a density

data set assists in understanding the large-scale motions, small-scale structure, and time dependent behavior. The large structures such as the magnetodisc, and the tail lobes will be examined at many different radial distances and longitudes. Density is a key indicator of the location of the plasma sheet and magnetodisc.

Future examination of the data set may help explain the true shape (rigid, bent or wavy), and dynamics of the magnetodisc. Persistent longitudinal variations in density would appear in the density data as well. Such measurements may help evaluate the accuracy of some of the models proposed to explain longitudinal asymmetries in Jupiter's magnetosphere. Careful analysis of the data set may help determine if Jupiter experiences magnetospheric substorms as the Earth does. The long time periods that Galileo has spent in Jupiter's environment assures that the spacecraft has visited some of the same locations more than once. In this way, time dependent phenomena may be studied.

It is intended that future study of this density data will answer some of the questions involving what happens to the plasma as it is distributed throughout Jupiter's system. The high time resolution of the density data may help explain which of the small-scale transport models (if any of them) best approximates plasma motion at Jupiter. That type of comparison may also give insight into changes in the Jovian system over time since the 1979 Voyager encounters. It should be noted that other instruments on board Galileo are also capable of (and have been designed for) measuring plasma density at Jupiter. The value of the electron density data used in this research is that the time resolution is higher than that of the other plasma instrument on board, and it provides additional measurements of the density which can be used for comparison.

Figure 3. A simple cartoon of Earth's magnetosphere. Shown are several of the boundaries in the magnetosphere, caused by the interaction with the solar wind. From Tascione [1988].

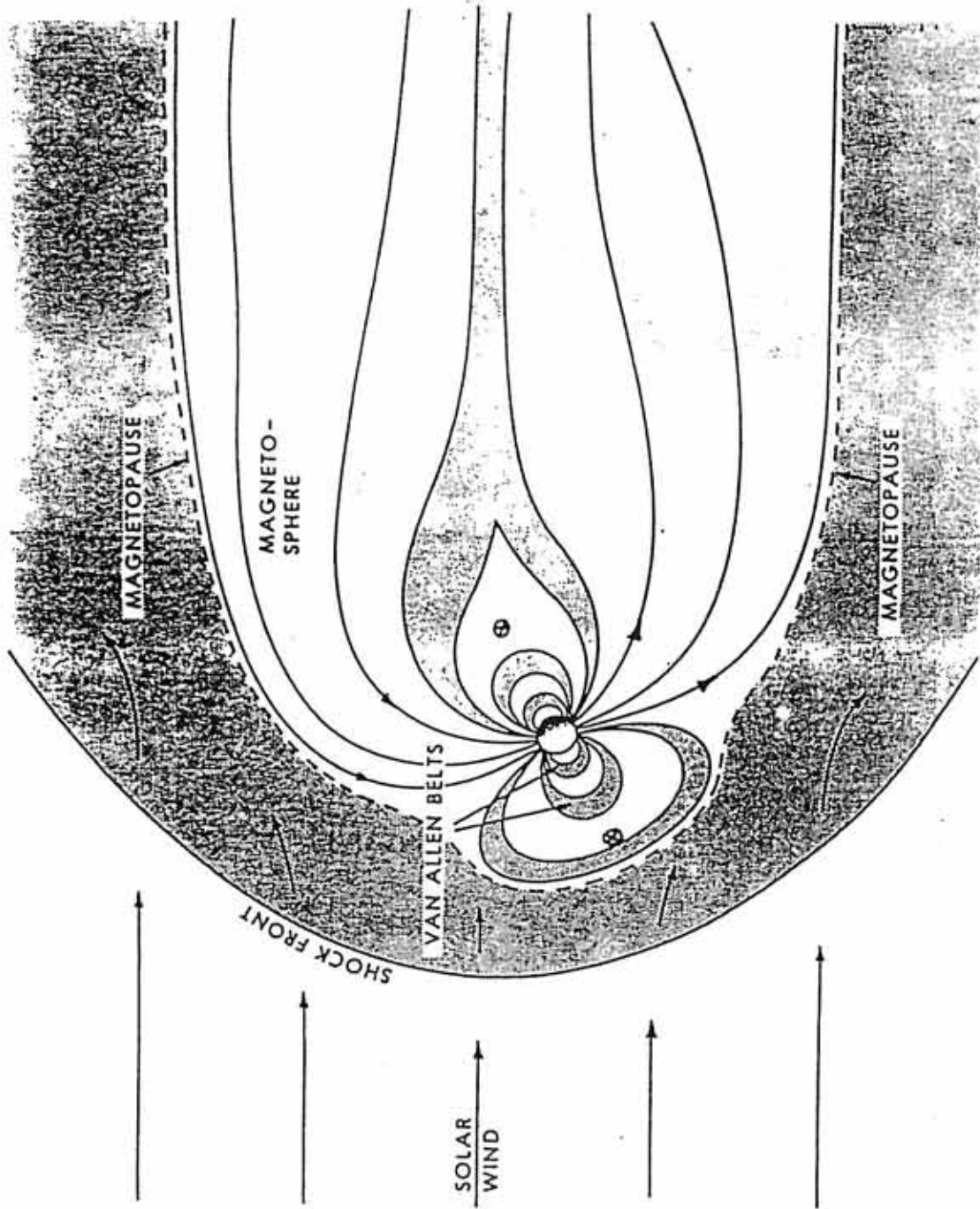


Figure 4. A more detailed cartoon of the Earth's magnetosphere. This diagram shows electric currents, and generalized plasma flow through the system. From Tascione [1988].

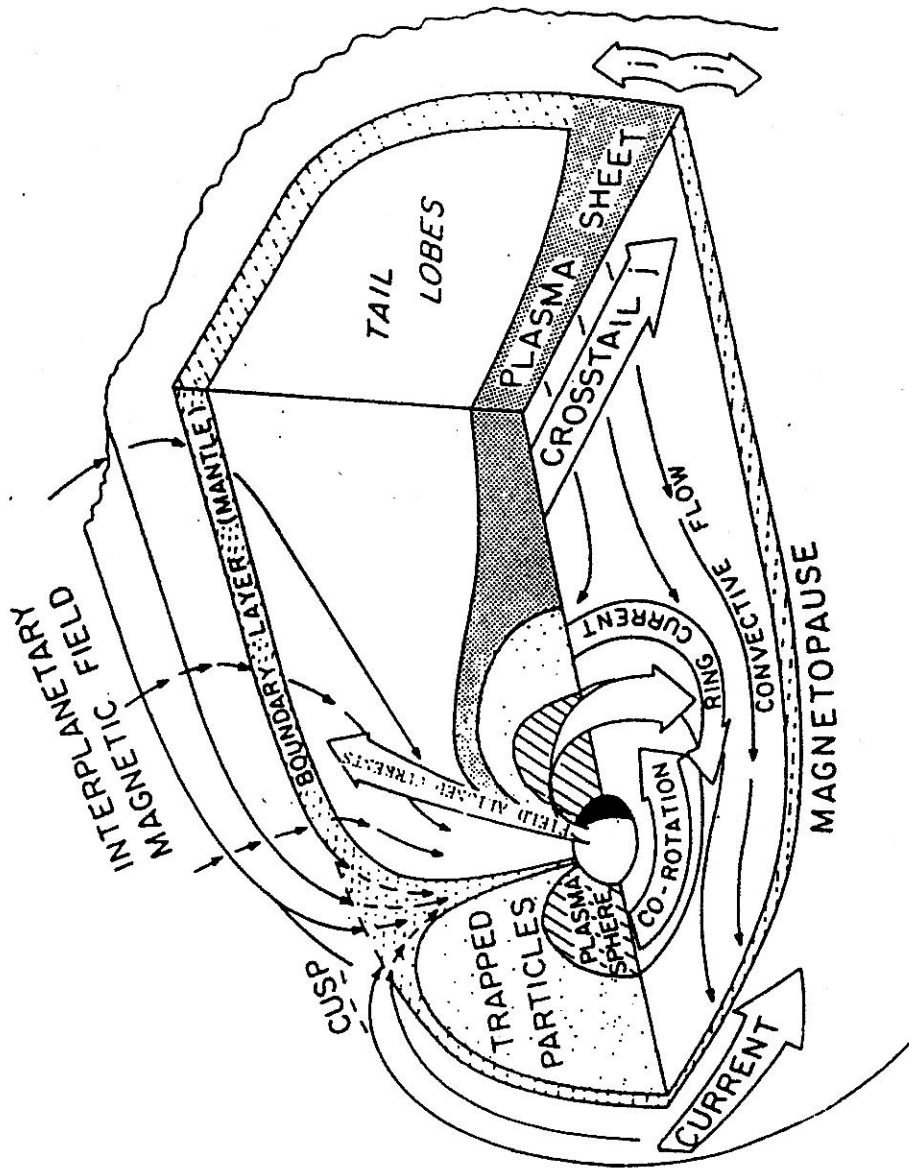


Figure 5. A general picture of plasma convection at the Earth. Plasma moves primarily sunward in the inner magnetosphere, and close to the equator. Plasma flows generally anti-sunward closer to the magnetopause, and in the distant tail. A substorm occurs when magnetic field lines in the tail merge. From Tascione [1988].

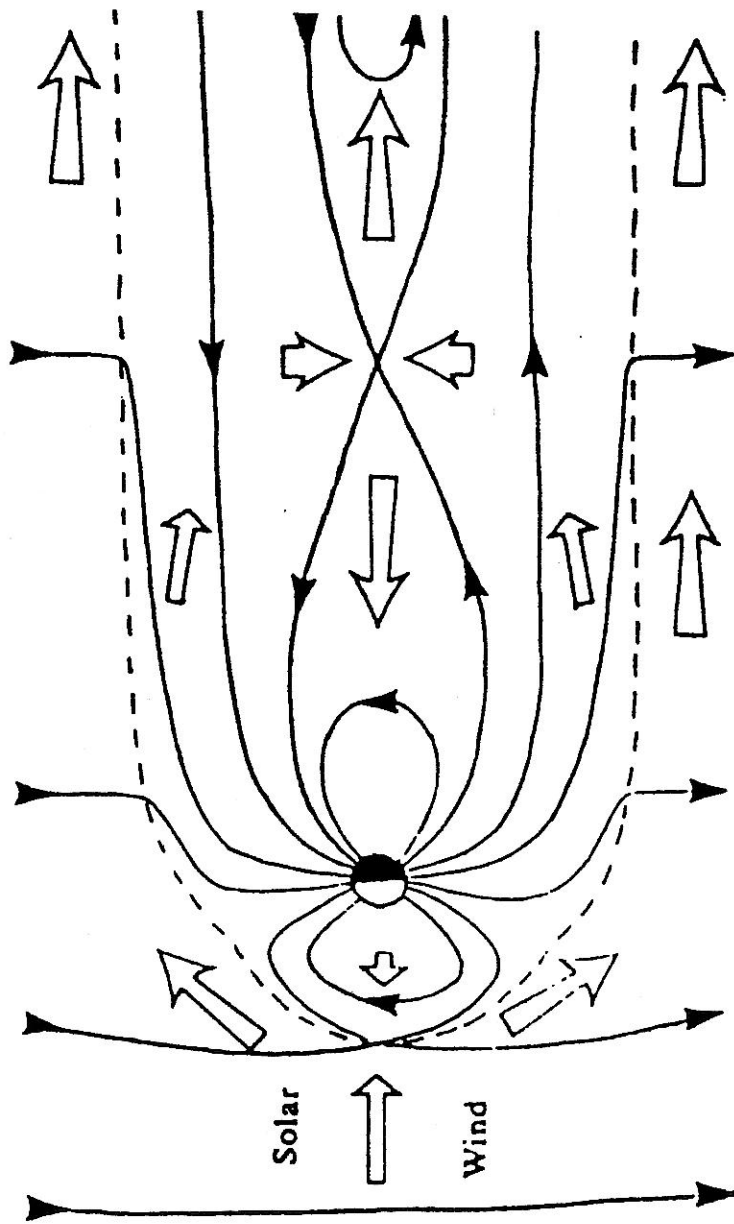


Figure 6. A comparison of magnetic field lines. This cartoon shows field lines in the closed (top) and open (bottom) models of the magnetosphere. In the open model, the interplanetary magnetic field merges with the Earth's field at an "x-line" near the nose of the magnetosphere. From Tascione [1988].

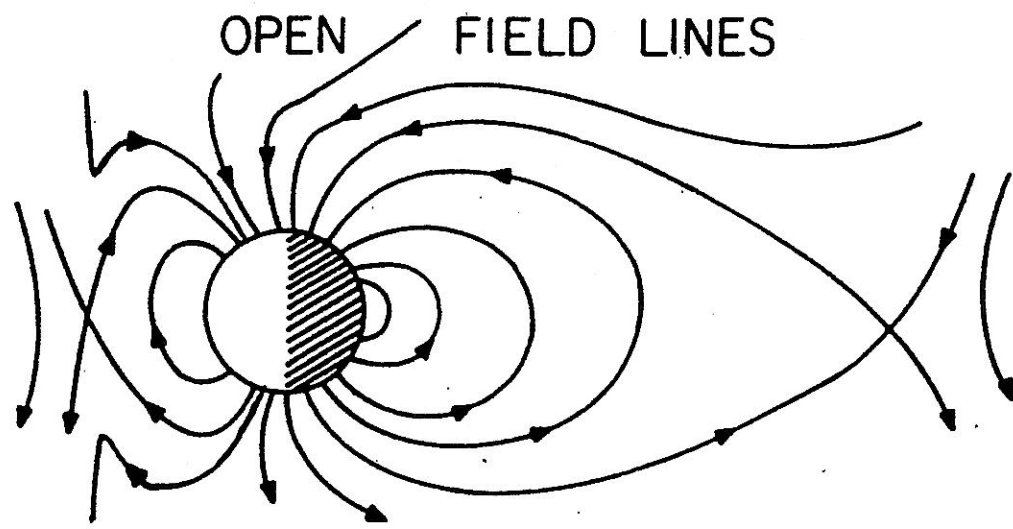
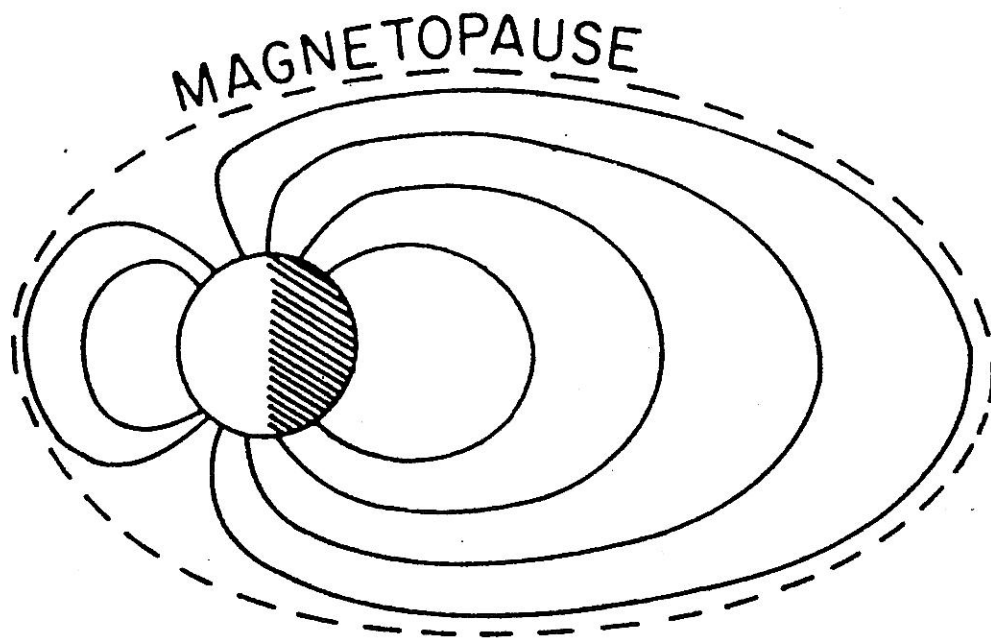


Figure 7. The disc model of the Jovian magnetosphere. An observer at "o" in this time sequence of four diagrams would "cross" the magnetodisc twice in the ten-hour rotation period depicted. The disc would sweep past the observer once from north to south, and once from south to north. The rotational axis of the planet is vertical, and the magnetic dipole axis is tilted, and indicated by an "M". From Dessler [1983].

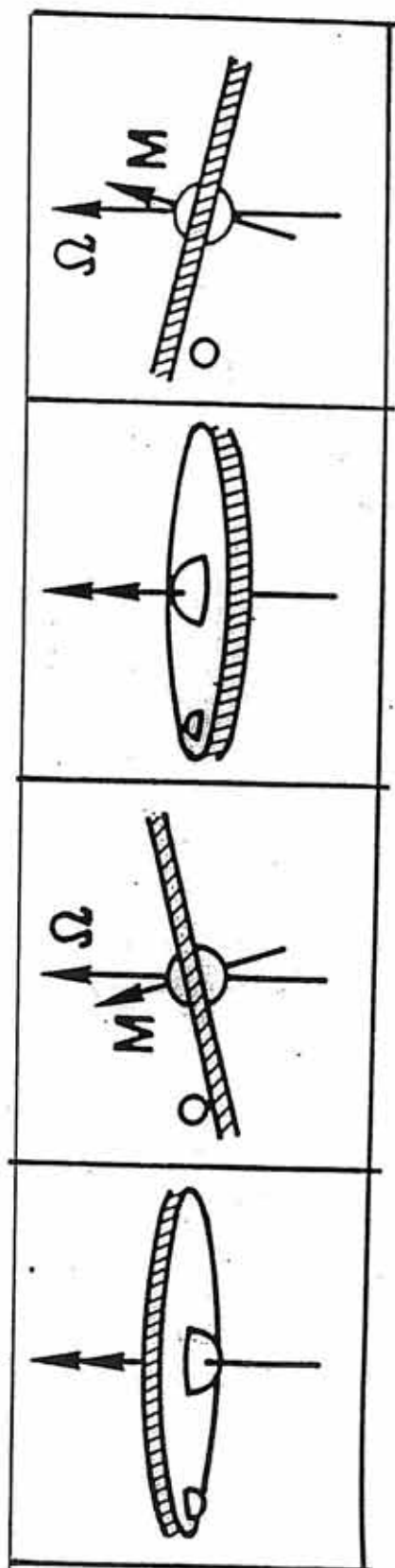


Figure 8. The co-rotating active sector model. In this model of the Jovian magnetosphere, an observer at "o" in each diagram would only encounter the active sector (shaded) once per ten-hour rotation period. From Dessler [1983].

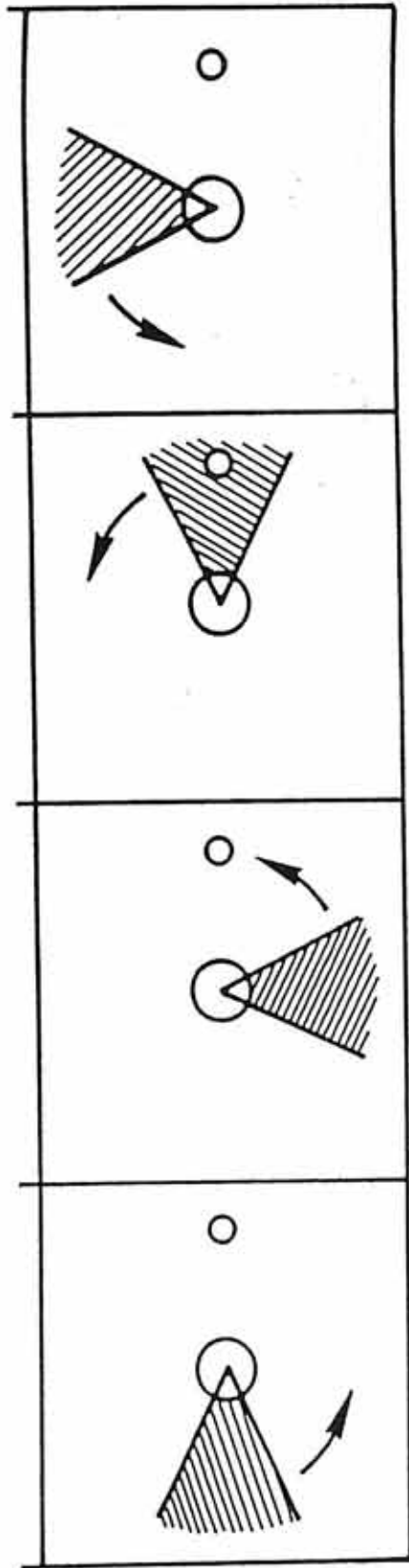


Figure 9. The co-rotating convection model. This is a model of plasma flow at Jupiter. As the denser active sector co-rotates with Jupiter, the plasma outflow is enhanced in this sector, while a return flow occurs at other longitudes. From Hill and Dessler [1991].

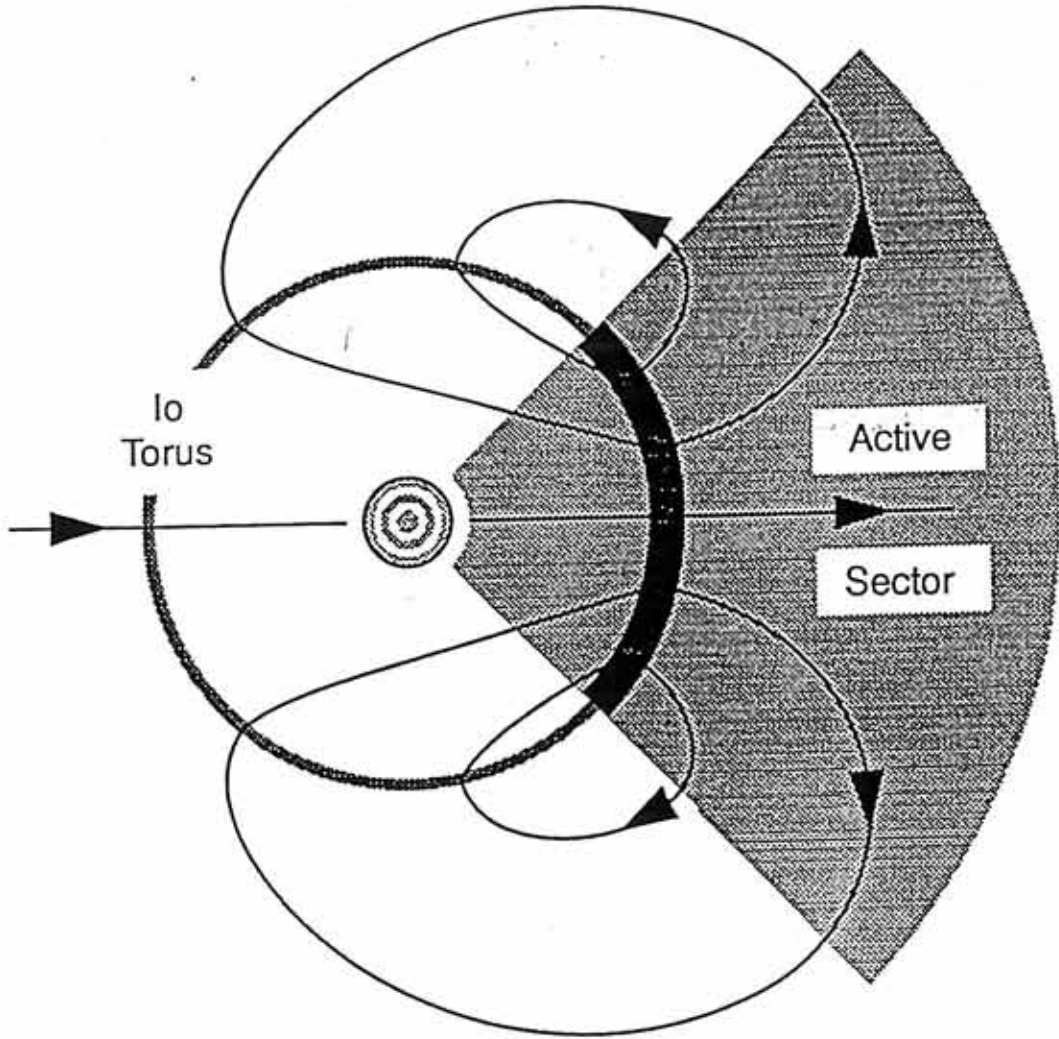


Figure 10. The transient convection model. This is another model of plasma flow at Jupiter. Higher density blobs of plasma break off from the Io torus and flow outward through a less dense medium. The blobs are limited in radial and longitudinal extent. From Hill, [1994].

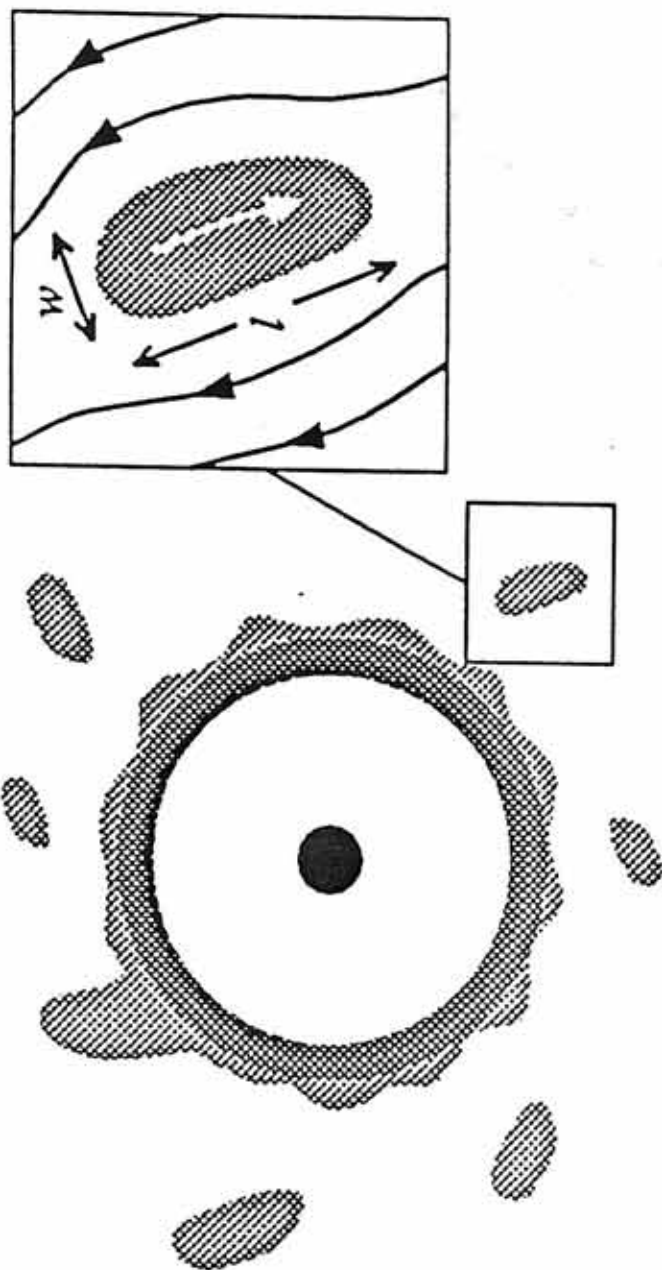


Figure 11. Fingers of dense plasma. This figure shows blobs of plasma breaking away from the dense Io plasma torus as shown in a numerical computer simulation.

From Hill, [1994].

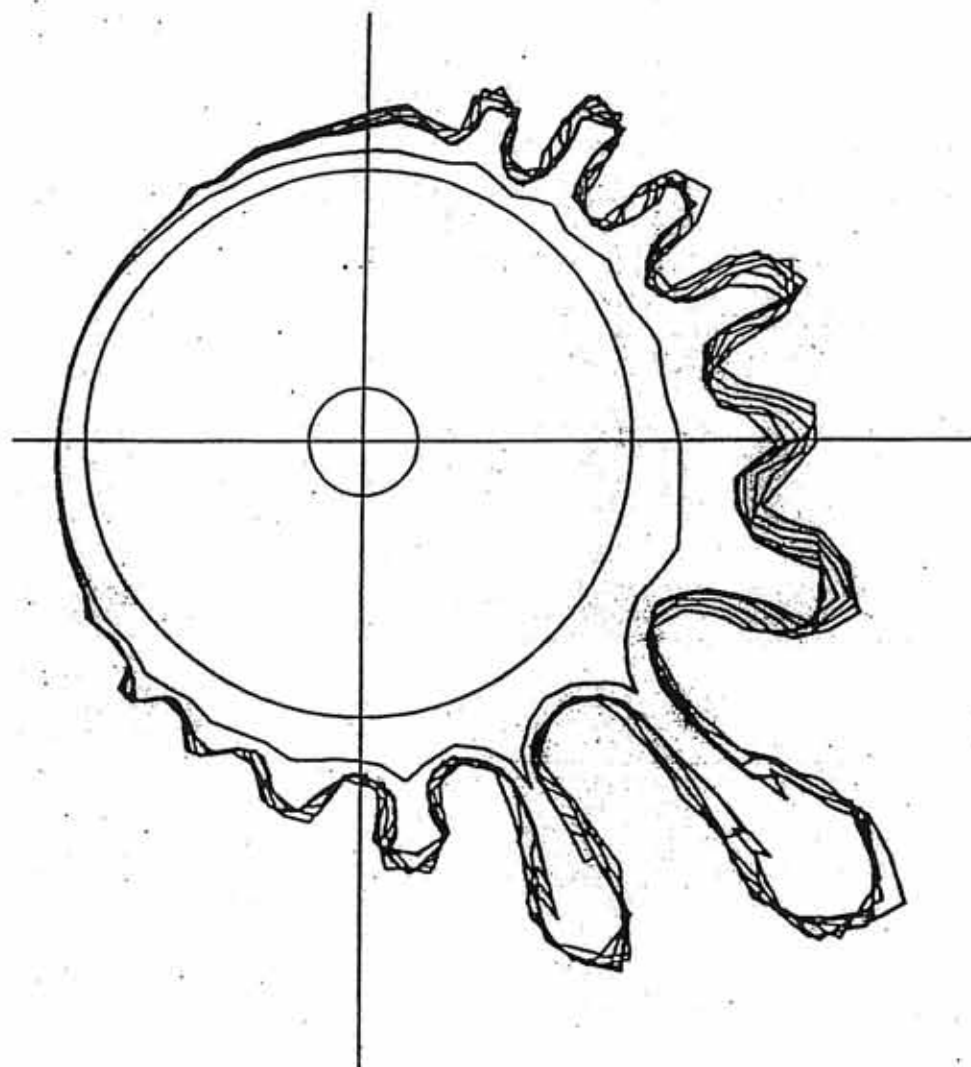
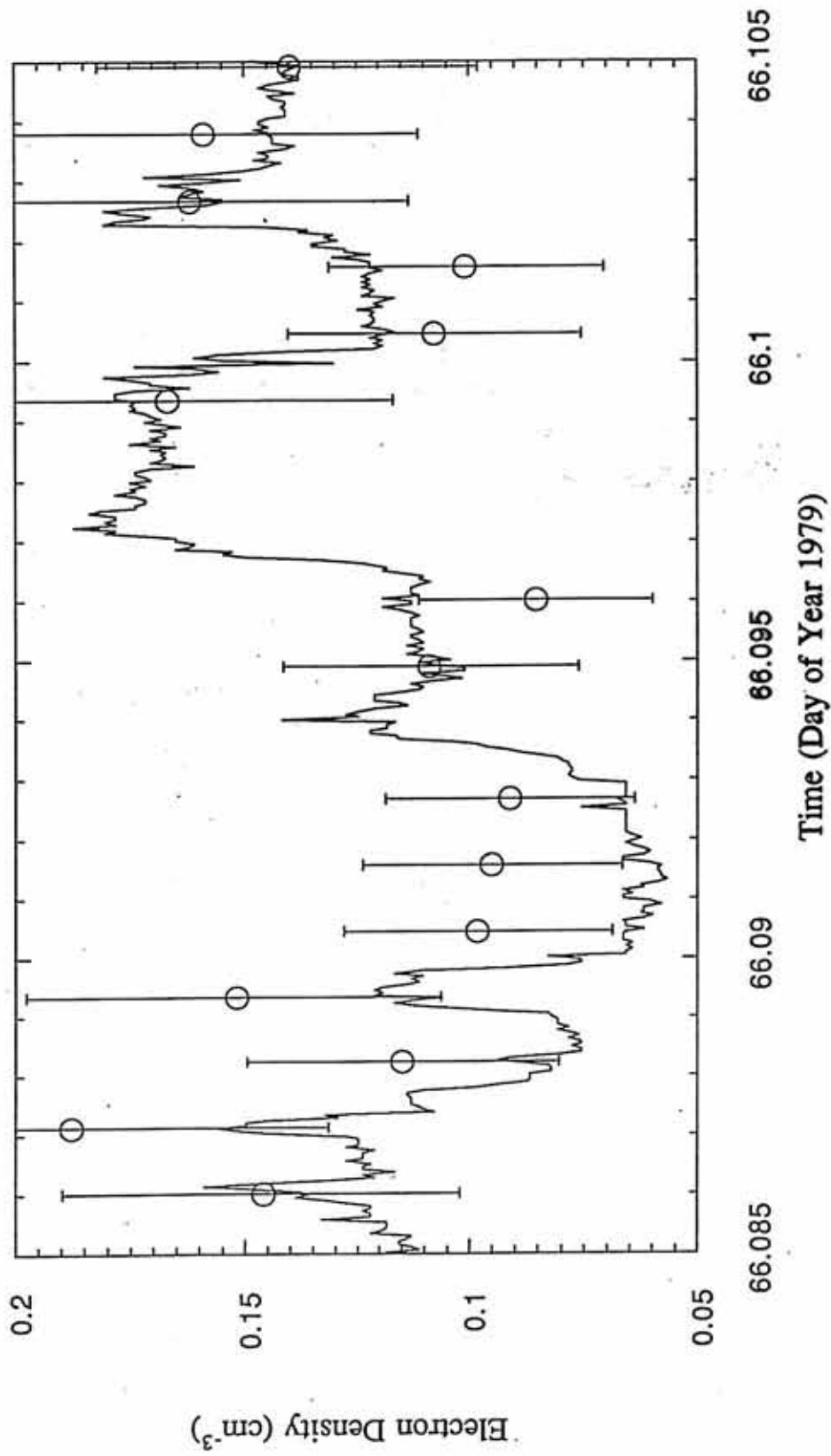


Figure 12. Electron density at Jupiter. These values are derived from Voyager 1 plasma wave data using the same technique employed in this project. The other data points with error bars are the actual density data measured by the plasma science instrument on board the spacecraft. From Ansher et al. [1992].

Voyager 1 PWS Processed Data with PLS Comparison



CHAPTER III: CONTINUUM RADIATION CUTOFF TECHNIQUE

The Role of Continuum Radiation

The technique used for determining electron density with the Galileo plasma wave instrument is a variation on a procedure used at the Earth [Gurnett and Shaw, 1973; Gurnett and Frank, 1974; Gurnett, 1975], and also at Jupiter with Voyager plasma wave data [Gurnett et al., 1981; Ansher et al., 1992; Ansher 1994]. The procedure involves using the individual spectra from the Galileo plasma wave instrument to observe a particular type of radio emission from Jupiter called continuum radiation. The plasma wave instrument's dipole electric antenna samples the frequency range 5.62 Hz to 5.65 MHz once every 37.33 seconds. The magnetic component of plasma waves is also measured between 5.62 Hz and 160 kHz using two search coil magnetic antennas. Using both electric and magnetic measurements together determines whether the detected waves are electromagnetic or electrostatic. These waveform data are then Fourier transformed and displayed on a color plot such as the one in Figure 13. This frequency-time spectrogram shows the frequency scale on the vertical, and the power or intensity of the emission on a relative color scale where red is the most intense emission, and dark blue is the least intense. The time is indicated on the horizontal scale. For this plot, 24 hours of data are displayed. The broadband feature that persists across the entire 24 hours of data shown between about 1 kHz and 10 kHz is known as continuum radiation.

Continuum radiation consists of a mixture of ordinary (L-O) and extraordinary (R-X) mode radiation. The shaded regions in Figure 14 show the frequencies and indices of refraction at which these (and two other) electromagnetic wave modes can propagate

in a magnetized plasma. The solid and dashed curves correspond to directional propagation limits from 0 (parallel to) to 90 degrees away from (perpendicular to) the direction of the local magnetic field. Different modes have propagation cutoffs at different frequencies, as seen along the horizontal axis. The ordinary mode has a low-frequency propagation cutoff at the electron plasma frequency, denoted by ω_p . Although there is also an extraordinary mode component to planetary continuum radiation, the cutoff for that mode, $\omega_{R=0}$, is slightly higher than for the ordinary mode. Therefore, the low frequency cutoff of the continuum radiation is at the plasma frequency.

Continuum radiation has been commonly observed in the magnetospheres of Earth and Jupiter [Gurnett and Shaw, 1973; Gurnett, 1975; Scarf et al., 1979] as well as the other outer planets. This radiation exists in the radio region of the electromagnetic spectrum and usually consists of two components. A trapped component propagates in the magnetospheric cavity at frequencies below the solar wind plasma frequency, and an escaping component propagates away from the planet at frequencies above the solar wind plasma frequency. The trapped radiation is reflected at the magnetopause because the solar wind density is too high for the trapped component to propagate out into that medium. The trapped component has a sharp low-frequency cutoff at the electron plasma frequency, which can be used to determine the local electron density using the relation:

$$f_p = \frac{1}{2\pi} \left(\frac{n_e e^2}{\epsilon_0 m_e} \right)^{1/2} . \quad (2)$$

In this expression, n_e is the electron density, e is the electronic charge, ϵ_0 is the permittivity of free space, and m_e is the mass of the electron. When each of these constant values is substituted into the formula, it can be expressed as:

$$f_p = 8.98 \sqrt{n_e} \text{ kHz} \quad (3)$$

where n_e is the electron density in cm^{-3} . The frequency, f_p in these expressions is related to the angular frequency, ω_p by a factor of 2π . For the free space mode in question, only waves with frequencies greater than f_p are valid solutions to the formula for refractive index:

$$n^2 = 1 - \frac{f_p^2}{f^2} \quad (4)$$

Waves at frequencies lower than f_p would result in an imaginary index of refraction and cannot propagate in the plasma. The experimental manifestation of this theoretical cutoff is a sharp drop-off in intensity of the continuum radiation detected by the Galileo plasma wave instrument. The sharp edge seen in the plasma wave data will usually be referred to as the plasma frequency, but it should be noted that a difference could exist between the theoretical cutoff and the experimental cutoff seen in the data, due to measurement errors. In addition, the few cases where the low frequency cutoff is not perfectly sharp may indicate that the density is not perfectly local. Based on agreement with independent density measurements, there is good evidence that the calculated density is probably local.

The Voyager plasma wave receiver experiment [c f. Scarf and Gurnett, 1977], hereafter PWS, first discovered continuum radiation at Jupiter [Scarf et al., 1979] where it dominates the low-frequency radio spectrum. Gurnett et al. [1979, 1981] first used data from the PWS receivers on board Voyager 1 and 2 to determine the electron density profile there. The same technique has been modified for use in this study. With the Galileo plasma wave receiver, multiple frequency filters are used to sample the spectrum from 5.62 Hz to 5.62 MHz. These frequency channels overlap some, in order to cover the entire spectrum of interest, however, because of finite channel widths, some waves

may be indicated in a particular channel that does not correspond exactly to the wave frequency. For this reason, there is approximately a 5 or 6% uncertainty in the determination of the plasma frequency using this continuum cutoff technique.

Continuum radiation is detected by the Galileo plasma wave instrument inside the magnetosphere of Jupiter at all radial distances beyond about $20 R_J$. The reason it cannot be detected inside of $20 R_J$ is that the plasma density closer to the planet is higher, and continuum radiation cannot propagate into that region. Since trapped continuum radiation does not propagate above the solar wind plasma frequency, the radiation is reflected at the magnetopause, where the density approaches the solar wind density. It is similarly reflected at high-density regions close to the planet. The continuum radiation makes multiple reflections inside the magnetospheric cavity much like microwaves in a microwave oven. This phenomenon is demonstrated in Figures 15 and 16. In Figure 15, the noon-midnight meridian plane of a cartoon magnetosphere is shown with the magnetopause and plasma sheet (high density boundaries) reflecting the trapped radiation multiple times, while it freely propagates through the low-density magnetospheric lobes. Figure 16 shows continuum radiation on a hypothetical graph of frequency and density versus distance from Jupiter inside the magnetosphere. There is often an escaping component of the continuum radiation that propagates at frequencies higher than the plasma frequency in the magnetosheath. It can escape the magnetosphere and propagate through the magnetosheath and out into the solar wind. This escaping component can be seen on some of the frequency-time spectrograms, at frequencies slightly higher than those of the trapped continuum.

Electron Density From Galileo Plasma Wave Data

An examination of all of the plasma wave data from the Galileo primary mission has been made. Out of 350 days of available data from the primary mission, a substantial

fraction (over 85%) of the days contain continuum radiation features of sufficient clarity that the electron density can be calculated. The remaining days of data either contain no continuum radiation, or they exhibit interference from other radio emission at frequencies near the low-frequency edge of the continuum radiation, making it difficult to accurately determine the cutoff. Time periods where the cutoff is not clearly determined are given a quality flag that indicates this uncertainty. This visual inspection of the plasma wave data, though time-consuming, has provided an overview of the entire data set. It has also prompted questions and revealed features that formed the basis for the projects and analyses pursued herein.

A semi-automated processing procedure was developed and implemented to calculate the density whenever a well-defined low frequency cutoff exists in the continuum radiation spectrum. This processing has been carried out primarily by ten student hourly employees who were trained to locate the continuum radiation feature on both a color (frequency-time) spectrogram (Figure 13), and on an individual line spectrum, which relates frequency and intensity of emission (Figure 17). After locating the continuum feature, the students would choose the low-frequency cutoff of that feature by using a semi-automated computer program that displays individual power spectra and a movable cursor. The value of plasma frequency was chosen to be the steepest portion of the sharp cutoff. Earlier work with Voyager plasma wave data [Ansher et. al, 1992] indicated that the bottom point of each cutoff produced a density that was systematically slightly lower than density measured by the other Voyager instruments. It was decided that the steepest portion of the cutoff slope provided the best identification of the plasma frequency. The steepness of the cutoff in most cases and the fact that the continuum radiation seems to "fill in" all the small density cavities (evidenced on the color spectrograms by the small variations of the low frequency cutoff), we have a high degree

of confidence that the cutoff does indeed occur at the plasma frequency. Each plasma frequency value chosen in this way is assigned a data quality flag based upon the appearance of the continuum feature on the power spectrum. A description of the criteria used in assigning this quality flag can be found in Table 1. The quality flag also characterizes the sharpness of the cutoff. The steeper the cutoff is, the more likely it represents the plasma frequency local to the spacecraft, and not some region along the propagation path to the spacecraft. Only the best 2 quality indices have been used in the analysis of the density data.

A numerical study was carried out to assess the consistency of the students' work. Multiple students were given the same data to process. After processing, the frequency values chosen as the cutoff were compared. There is typically a 5 - 6% difference between plasma frequency values chosen by multiple students working on the same data. This is of the same order as the uncertainty associated with the frequency channel widths of the plasma wave instrument. Based upon this comparison of the data processed by the students, it is believed that the processing procedure as implemented by the different students yielded consistent results with an accuracy for determining the cutoff at the plasma frequency of about $\pm 6\%$.

For thoroughness, a comparison of this technique was made by applying the same procedure to selected time periods where high rate plasma wave data were available. The instrument operates in a high rate mode for a small fraction of the mission. In this mode, it provides waveforms, which are then Fourier analyzed. More high-rate mode operation of the instrument was expected, but telemetry issues related to the failure of the high-gain antenna to completely deploy prevented frequent use of the instrument in this mode. In the high rate mode the instrument records more data in a smaller time and has significantly larger telemetry requirements. The plasma frequencies recorded using the

high rate data, were compared to those recorded using the same time period in the low rate data. Aside from the differing time resolutions, the two data sets agreed with each other to within the same 5 - 6% as when different operators processed the same low-rate time period. The use of high rate data did not improve the ability to locate the low frequency cutoff of the continuum radiation, as it is subject to the same user-dependent uncertainties. It was determined that using the continuum cutoff technique with the low rate data was sufficiently accurate and adequate for identifying the continuum cutoff on the color spectrograms. Combining the 6% uncertainty in determining the frequency from the instrument and the 6% uncertainty due to the user's choice of the cutoff on the power spectra, it can be calculated that there is an overall uncertainty of about 8.5% in determining the value of the plasma frequency.

Additional software tools have been used to validate the accuracy of the plasma frequency values chosen. One tool plots the plasma frequency values returned by the user, as a white trace on top of the color spectrograms (Figure 18). This tool helps to visually determine if the frequency variations produced by the user match the variations in the low-frequency cutoff of the continuum radiation visible on the spectrograms. It also provides a simple check for accuracy in the recorded frequency values, and they can be displayed efficiently using any desired time interval. If there are discrepancies, they can be quickly noticed, and if necessary, corrected. All of the data in the data set has been appropriately inspected in this manner, and where necessary, corrected by a second round of processing. This thorough treatment combined with the data quality flag gives us high confidence in the accuracy of the plasma frequency values, and hence, the density measurements presented. This accuracy is necessary before the data set can be offered to the general research community.

Some of the time periods demonstrate multiple wave mode signatures in the frequency range of interest, such as Z-mode, or whistler mode waves. One such time period is shown in Figure 19. Some different techniques have been applied to try to decipher the overlapping and intermixing of these different wave modes, and the manner in which they are displayed in the color spectrograms and on the power spectra. This is done so that the continuum radiation (the wave mode that is the source for our density determination technique) can be distinguished from other wave modes present at the same frequencies. If the multiple wave modes cannot be distinguished from one another, the low-frequency edge of the mode we are interested in is difficult to determine. The overlap of these modes occurs when the low frequency cutoff of the continuum (the electron plasma frequency) drops below the upper cutoff of the whistler mode radiation (the electron cyclotron frequency). This problem affects approximately 10% to 15% of the entire data set. It is therefore a significant concern. The electron cyclotron frequency is given by:

$$f_{ce} = \frac{1}{2\pi} \left| \frac{eB}{m_e} \right| \quad (5)$$

where e is the electronic charge, B is the magnetic field magnitude, and m_e is the electron mass. Because of differing opinions as to the interpretation of the location of different cutoffs in the data when such overlapping of modes exists, it is difficult to accurately determine the density in these regions. The data in these cases have been assigned a quality flag appropriate to the level of uncertainty in determining the plasma frequency. If the quality flag indicates high uncertainty (a flag of 2 or 3, as described in Table 1), then these data are not used in the analyses. Additionally, if the plasma frequency is known to be less than the cyclotron frequency (or if the cyclotron frequency is unavailable), these data are also omitted from the analyses. These precautions ensure that

only the highest quality data in the data set are analyzed. Because of the relationship between electron density and plasma frequency expressed in equation (3), propagation of errors indicates an uncertainty in the calculated density values of about 17%.

Initial analysis of some of the more interesting time periods in the data set show clear indications in the color spectrograms of familiar, identifiable magnetospheric features. Plasma sheet crossings are most clearly evident in the middle magnetosphere, though they frequently occur less conspicuously throughout the data set. They are identified by a rapid (a fraction of an hour) increase and subsequent rapid decrease in the low frequency cutoff of continuum radiation as seen in the color spectrograms. These changes in plasma frequency are related to the change in density as the spacecraft encounters the higher density plasma sheet. Clear examples of plasma sheet encounters can be seen in Figure 20 at 07:00, 10:00, 16:30, and 20:30. Other features such as entries of the spacecraft into the tail lobes of the magnetosphere are found throughout the data set, and are characterized by the overlap of different wave modes as described previously. This overlap is likely due to the fact that the electron density is very low in the lobes, and therefore, the plasma frequency is dropping below the electron cyclotron frequency. When this happens, whistler mode waves, which have their upper cutoff at the cyclotron frequency, enter the frequency bands occupied by the continuum radiation.

Quality Flag	Confidence in Plasma Frequency Identification	Description of Criteria Used to Identify Plasma Frequency from Cutoff of Continuum Radiation
0	Excellent	Clear, sharp cutoff
1	Good	Clear, slightly less sharp cutoff
2	Fair	Cutoff apparent, but clear identification hindered by waves, interference, or data gaps near plasma frequency
3	Poor	No identifiable cutoff

Table 1. Data Quality Flags




Figure 13. A sample 24-hour color spectrogram. This plot shows data from Galileo's plasma wave instrument. The broadband feature between 800 and 10000 Hz is continuum radiation. The color indicates relative intensity. This plot shows time on the horizontal axis.

Galileo PWS

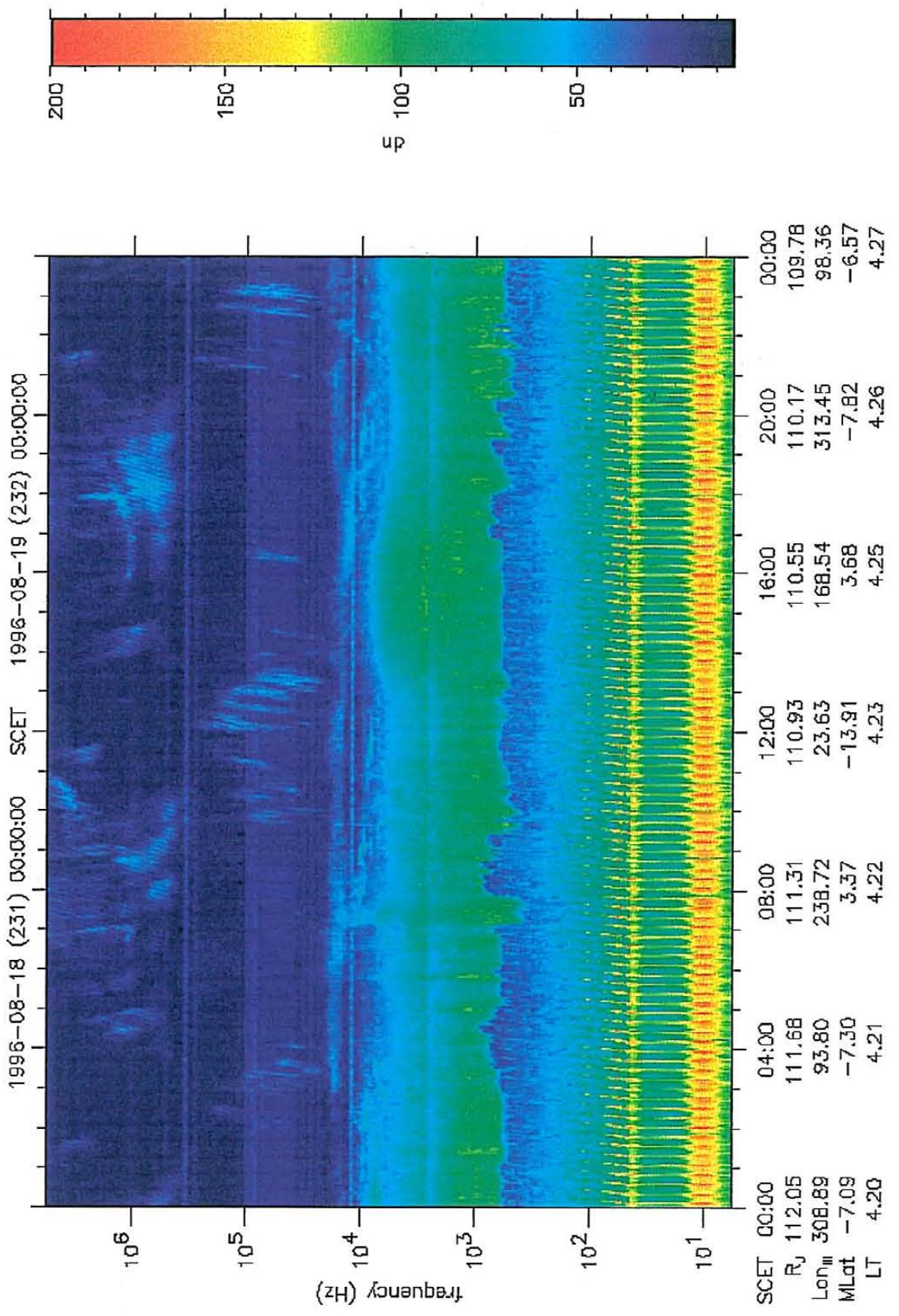
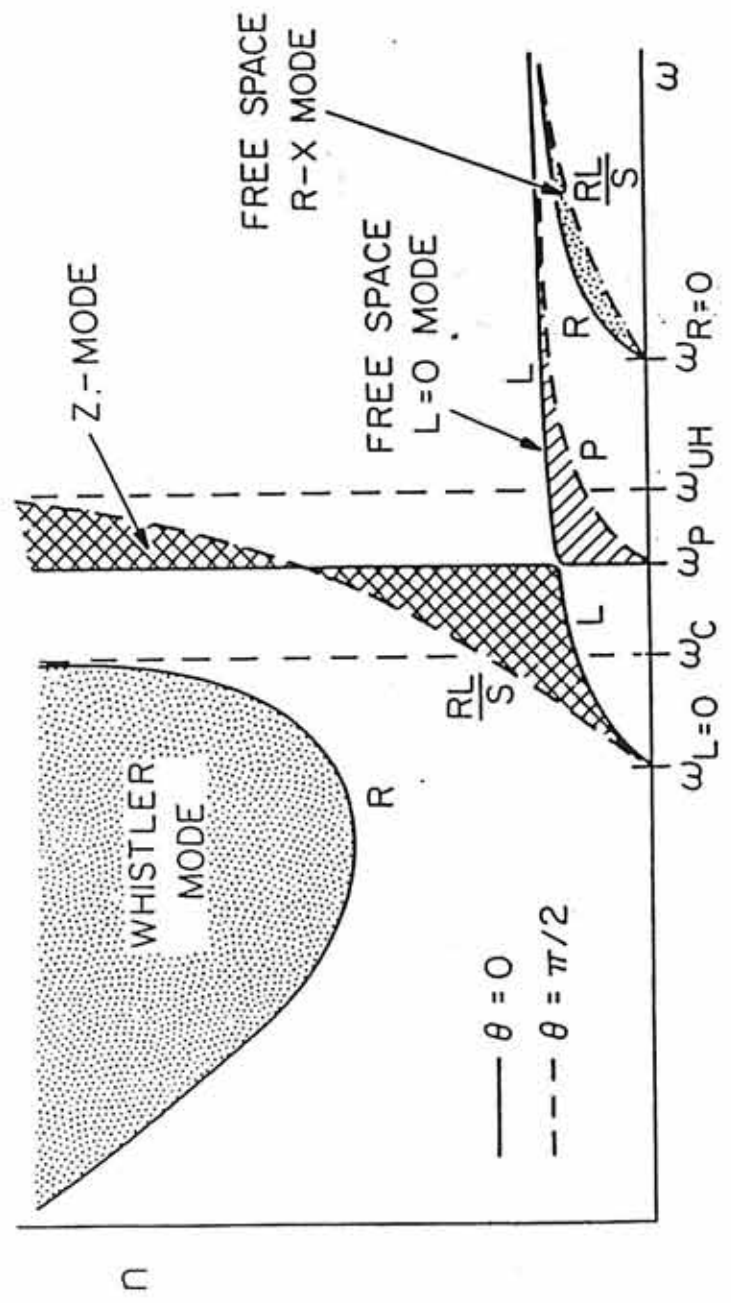


Figure 14. A diagram of index of refraction versus frequency. The shaded regions correspond to the four electromagnetic wave modes that can propagate in a magnetized plasma. The free space L-0 mode has a lower cutoff at the plasma frequency, allowing the electron density to be calculated.

A-G83-882




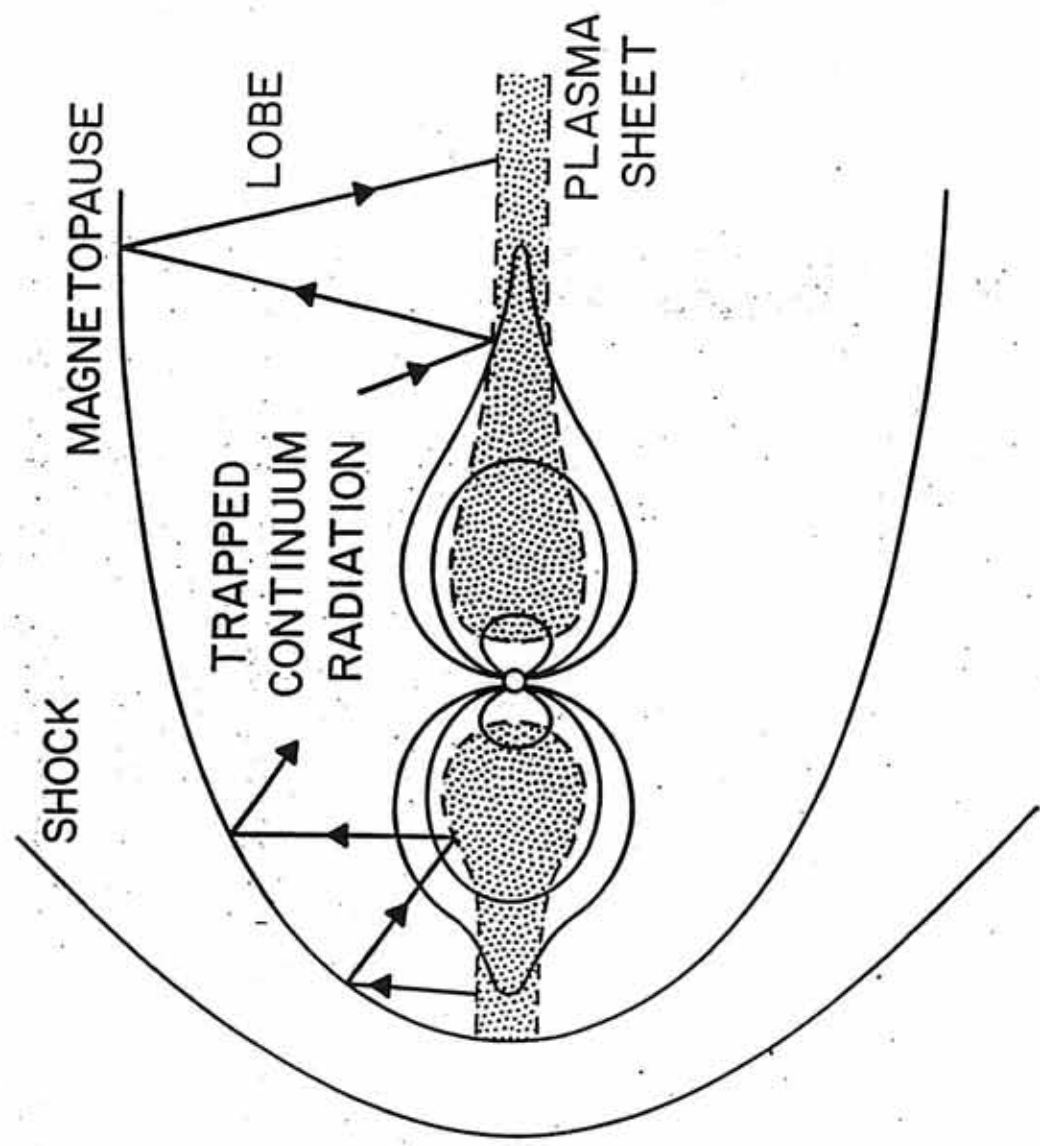


Figure 15. A simple cartoon of continuum radiation. This diagram shows a magnetospheric cavity and the continuum radiation trapped inside. This continuum radiation is reflected multiple times at the cavity walls, as well as the higher density interior regions, and is detected by the plasma wave receiver as broadband radio waves.

A-G97-237




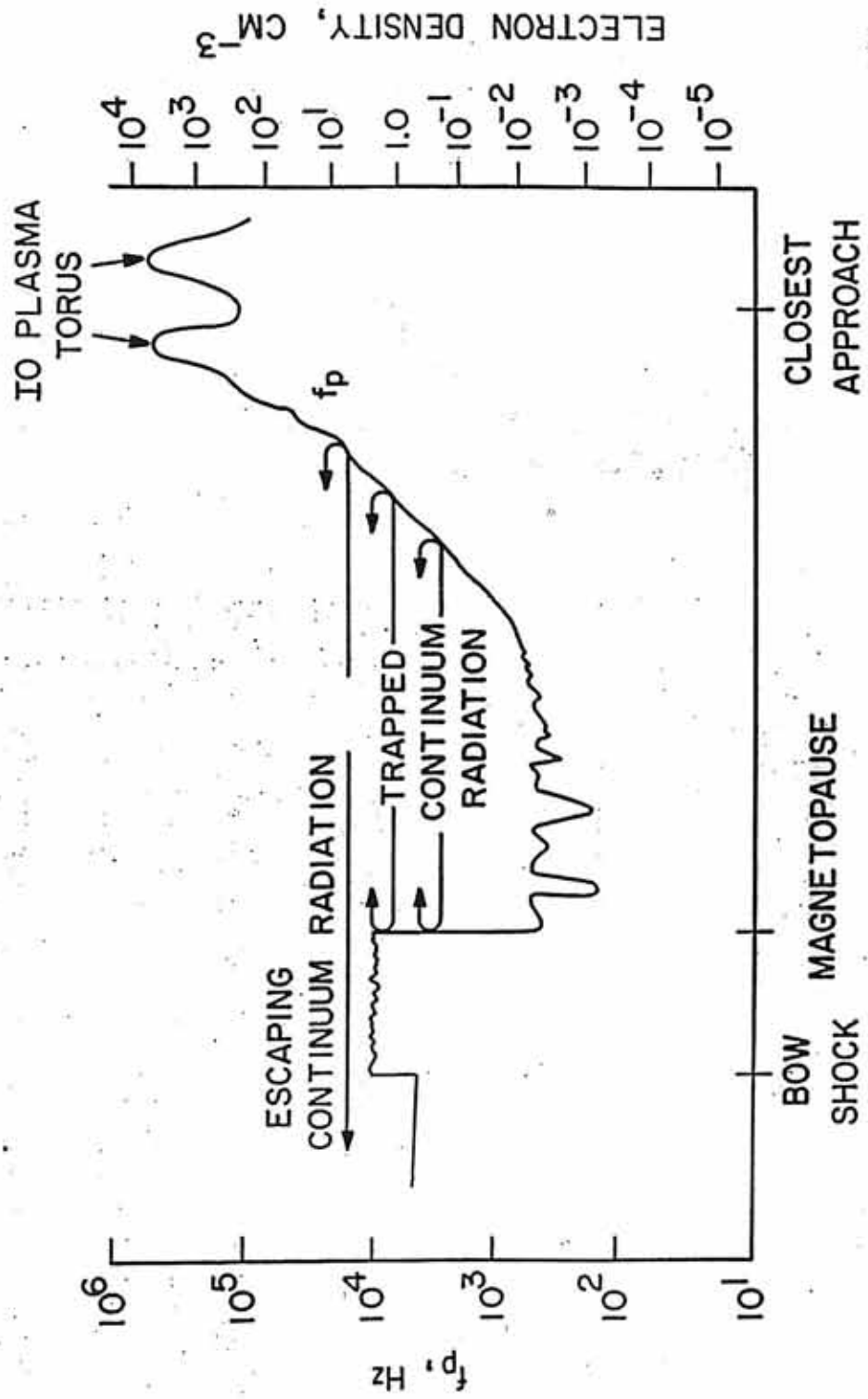


Figure 16. The electron plasma frequency at Jupiter. This plots the plasma frequency as a function of radial distance in the Jovian magnetosphere. The trapped continuum is indicated inside the magnetopause. It remains inside the magnetosphere because it cannot propagate into the higher density solar wind.

A-G79-358




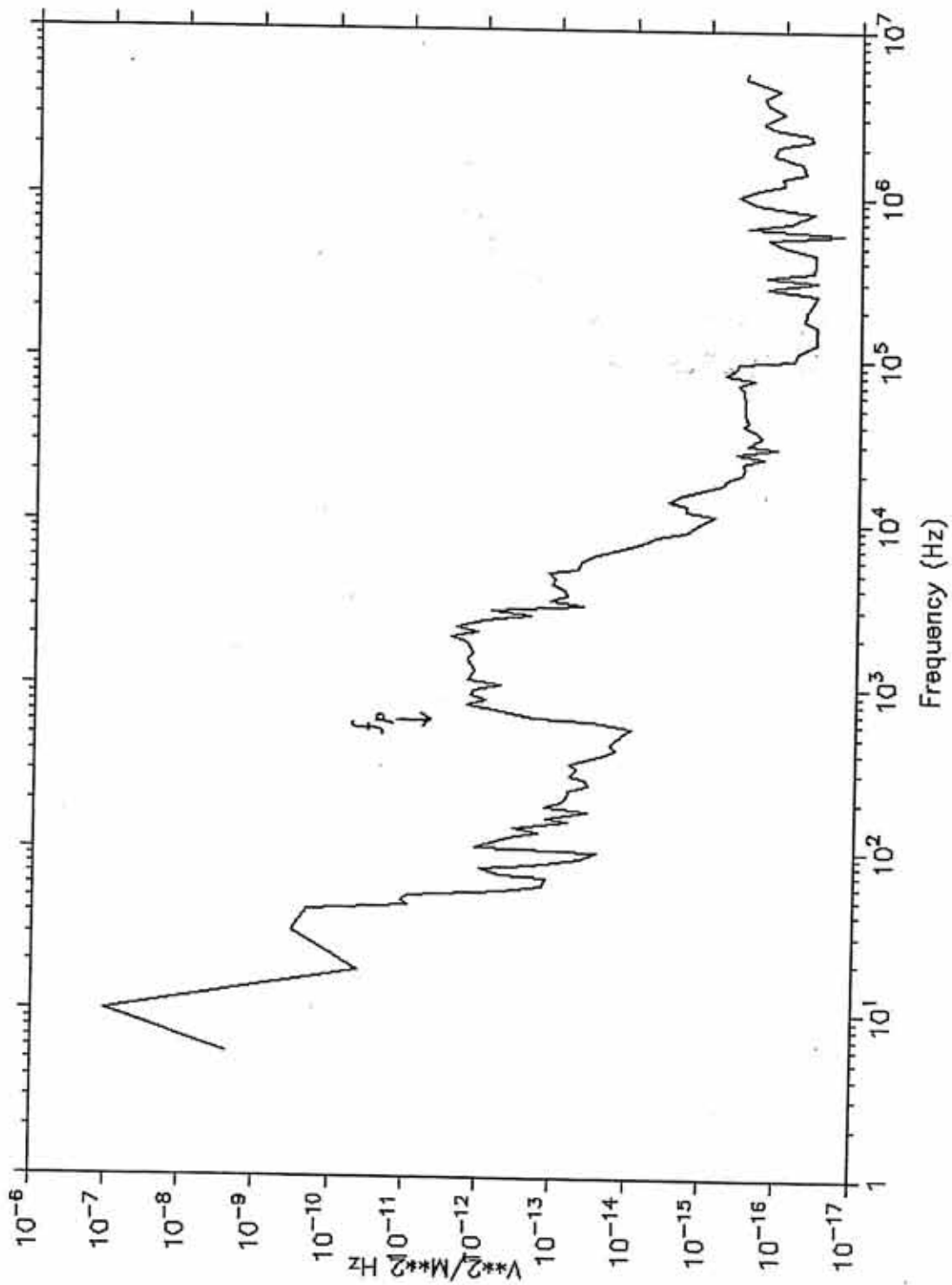


Figure 17. A sample power spectrum from Galileo. This data is from the same day as Figure 13. The tall, broadband feature between about 600 and 9000 Hz is the continuum radiation. The arrow indicates where the plasma frequency is. One of these spectra is produced every 37.33 seconds.

1996 231 (August 18) 16:11:03
Galileo PWS - Electric




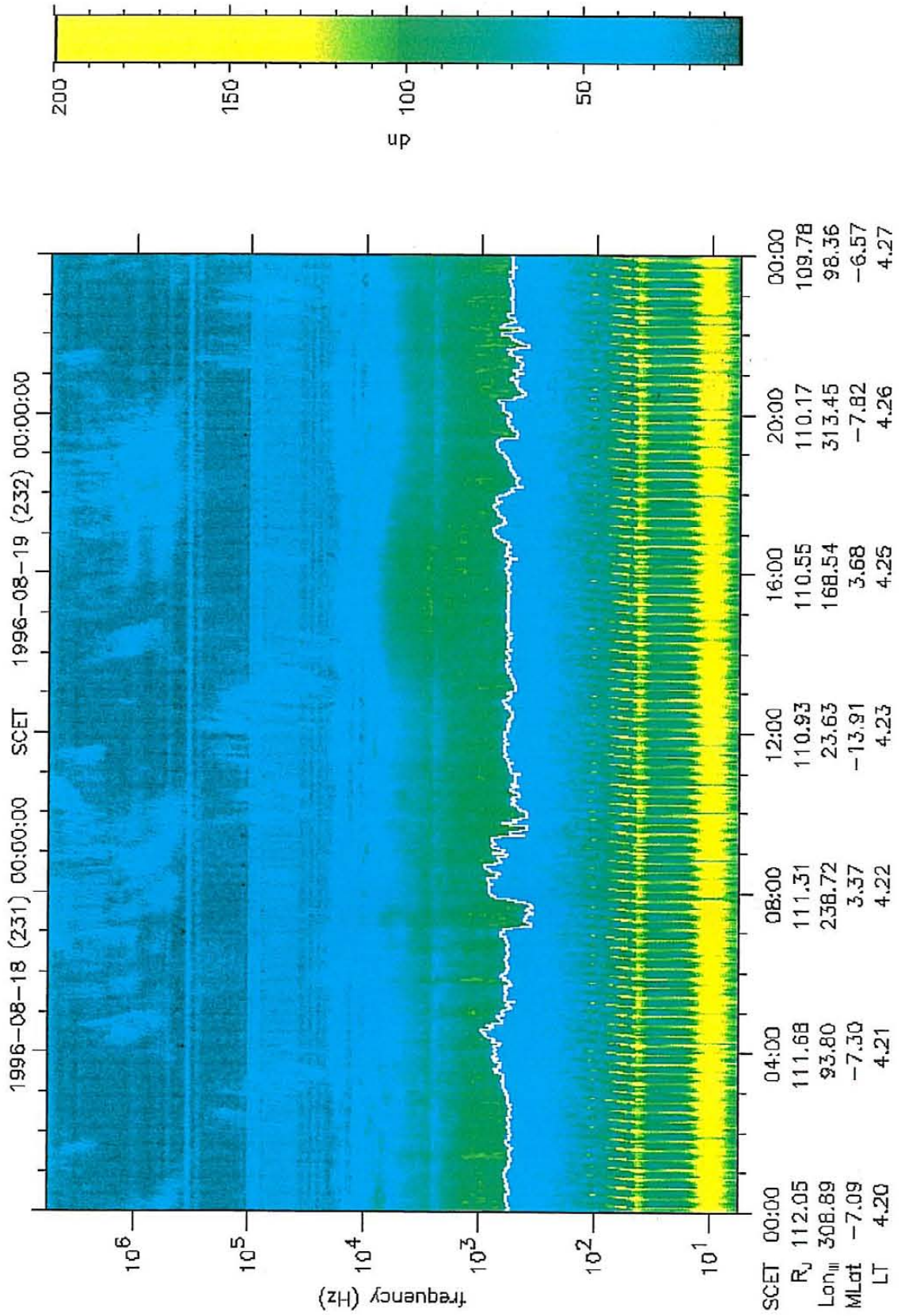


Figure 18. A spectrogram with the plasma frequency. This is the same 24-hour color spectrogram as in Figure 13, with the overlaid plasma frequency in white. The plasma frequency is chosen by looking at spectra like the one shown in Figure 17.

Galileo PWS




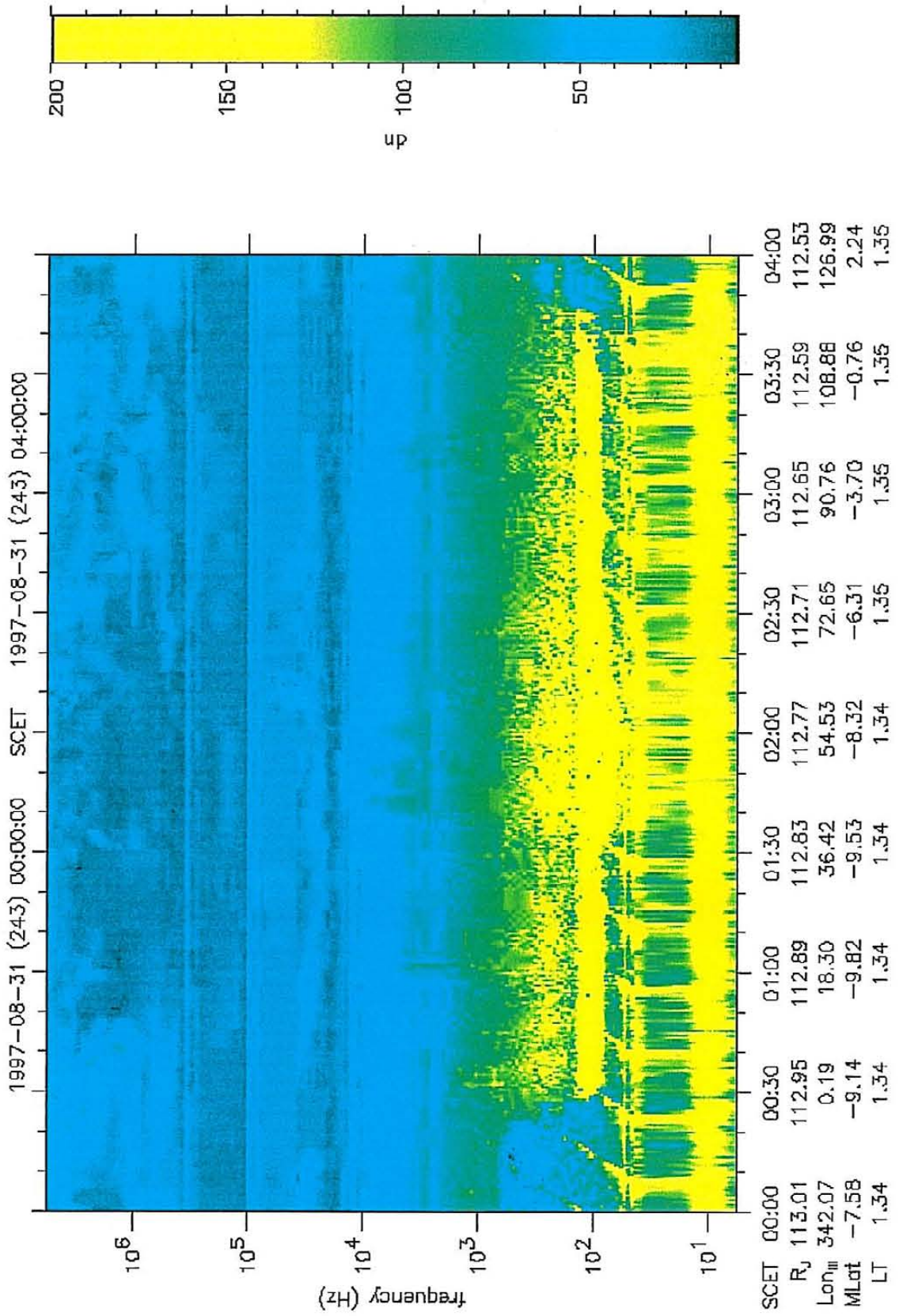


Figure 19. An example of wave superposition. This shows a 4-hour spectrogram in which there are several radio wave modes superimposed near the low frequency edge of the continuum radiation. Note that this intensity drop-off marking the plasma frequency (near 800 Hz, seen between 00:00 and 00:30), is soon masked by high intensity (yellow) emission at several hundred Hz, and higher intensity (red) emission near 100 Hz. This extra emission is likely Z-mode or whistler mode waves.

Gaileo PWS




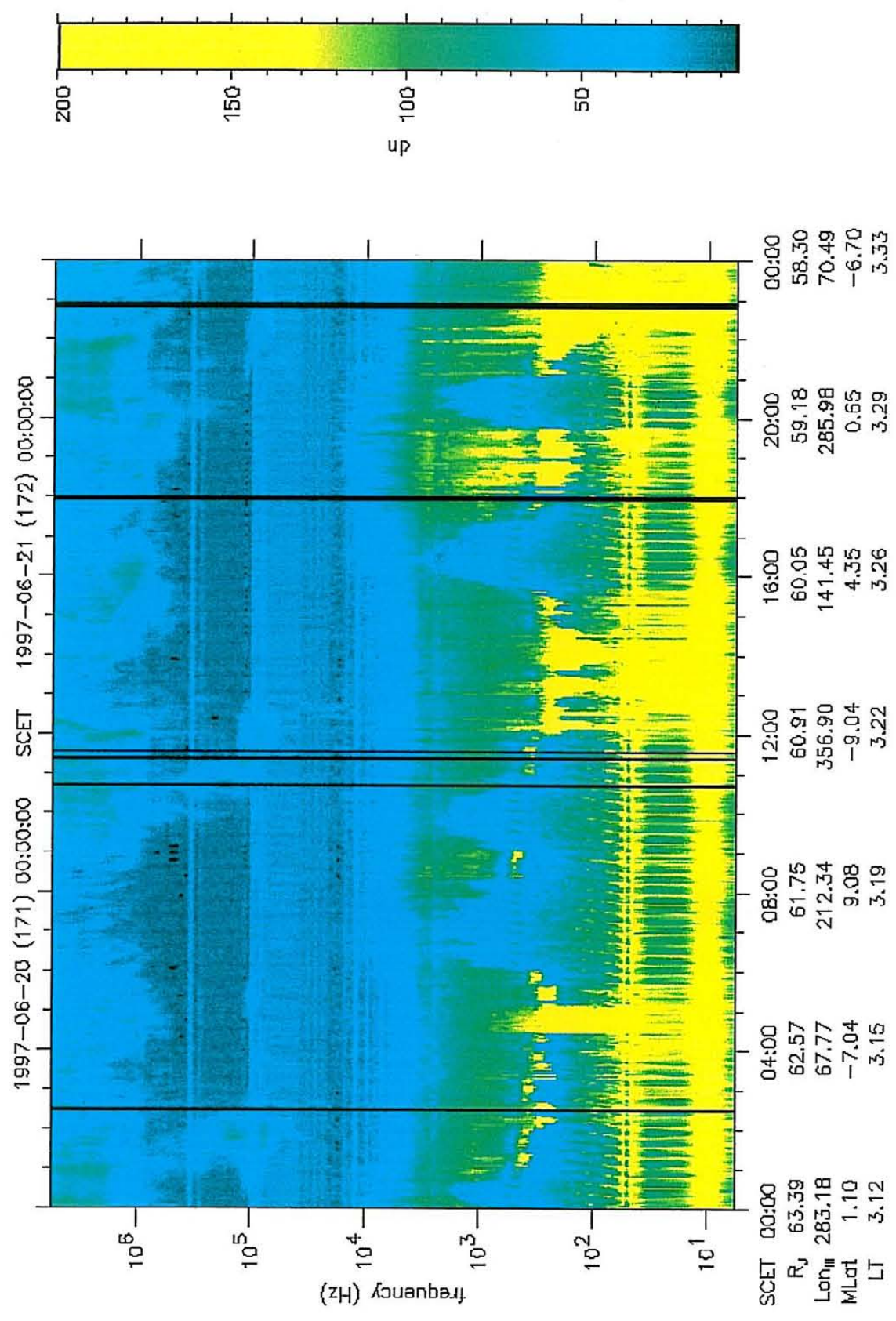


Figure 20. Plasma sheet crossings. This 24-hour color spectrogram shows Galileo's path through the plasma sheet. The plasma sheet is crossed several times in this plot, most notably at 07:00, 10:00, 16:30, and 20:30. As seen by the plasma wave instrument, the plasma sheet is characterized by a rise in the plasma frequency, indicating a higher plasma density. Even from this basic survey plot, aspects of some magnetospheric models are apparent. For example, the plasma sheet is crossed twice in each ten-hour period, as predicted by the disc model (depicted in Figure 7).

Galileo PWS



CHAPTER IV: ELECTRON DENSITY PROFILE AND SURVEY

Radial Density Profile of the Plasma Sheet

Two analysis tools, the radial profile tool and the global density display tool have been developed to observe the electron density at Jupiter in specific contexts. The first global view of the electron density profile at Jupiter involved plotting the data as a function of radial distance from the planet. This type of a plot confirms the behavior of the plasma frequency exhibited in Figure 16. The first radial profile of density produced from this data set exhibited that there is indeed a wide range of densities found in Jupiter's magnetosphere (Figure 21). This was expected, as electron density is known to vary over seven orders of magnitude between the Io torus and the outer magnetosphere. In order to make the data set easier to work with, the following reduction procedures were applied. First, as with all the data discussed in this document, only the two highest quality indices were used, and only data for which the plasma frequency is higher than the electron cyclotron frequency were used. Next, the data were subjected to ten-minute averages. The highest ten-minute average value for each Jovian rotation (every ten hours) was then recorded and displayed on the plot. The reason for this "rotation selection" criterion was to identify the peak electron density in the plasma sheet. Since the density is expected to be much higher near the center of the plasma sheet than the northern or southern lobes, this method ensures that density values characteristic of the central plasma sheet are selected and plotted as a function of radial distance. A least-squares best fit to all of the data (Figure 22) shows a decrease of the electron density in Jupiter's plasma sheet beyond about $20 R_J$ proportional to $(1/r)^{2.14 \pm 0.01}$. A discussion of the error associated with this

fit, as well as comments about the quality of the power law fit is included at the end of this section. Although the technique of using continuum radiation to determine the plasma frequency does not usually work for $r < 20 R_J$, electron density can be determined at smaller radial distances using the upper hybrid frequency. The upper hybrid frequency is related to the plasma frequency and the cyclotron frequency by the relation:

$$f_{UH}^2 = f_p^2 + f_c^2 \quad (6)$$

When $f_p \gg f_c$ (close to Jupiter), the f_c term can be neglected, $f_{UH} \approx f_p$, and electron density can be calculated as before. Because Galileo went as close as $5 R_J$ to Jupiter on its closest pass, the upper hybrid method can provide density measurements all the way in to the Io tours. This technique, carried out as part of a different study, produced additional density values, which can be added to the density values from the continuum study. When density values computed using the upper hybrid frequency from $r < 30 R_J$ are added, the entire profile looks like Figure 23. The best fit power law to the upper hybrid data (Figure 24) scales as $(1/r)^{6.55 \pm 0.05}$. It is uncertain what causes this $(1/r)^{6.55}$ dependence, but it is known that the dipole magnetic field magnitude decreases as $(1/r)^3$. If the density were related to B^2 in some way in that inner region of the magnetosphere, then this would produce a similar dependence of $(1/r)^6$.

Note the difference in slopes between the density data profile calculated from the upper hybrid frequency and the density data profile from the plasma frequency. The power law seems to change at about $20 - 25 R_J$. This may be for several reasons. First, at about 25 or 30 Jovian radii from the planet, co-rotation is known to begin to break down. It takes a finite amount of time for information about the rotation of Jupiter to be transmitted via Alfvén waves to the distant plasma. Beyond about 25 or 30 R_J , the plasma begins to lag behind co-rotation speed [Hill, 1979]. Also, just beyond this distance, there is believed to be a "hinge" or bend in the plasma sheet or magnetodisc. At

this distance, too, the dipolar nature of Jupiter's magnetic field begins to stretch into a more tail-like radial configuration. Each of these factors may have some influence on the density profile changing its appearance here. Because the data used in this profile were taken over the course of multiple orbits, it is likely that this break in the power law is a persistent global feature in the density profile, and describes a long-term trend.

With regard to the quality of the power law fits to the density data, there are clearly discernable trends in the density over radial distance. The best-fit curves were determined by applying a linear regression analysis in logarithmic space, where a power law appears as a linear relationship. A careful statistical analysis, using the proper errors to weight the data, show that the Pearson's R values for linear correlation were high in both cases, indicating a high probability of correlation between the density and radial distance. However, the large minimum χ^2 values indicated that there is a low probability that the density values, when taken together, are described by the specific power law that was the best fit to the data. The density values are seen to vary by a factor of 2 or more above and below the power law best fit. As a result, the standard deviation (the +/- error) in the value for each power law slope is not particularly valuable because of the large scatter in the data. The physical interpretation we draw from this analysis is that while there is a high degree of correlation between the density and the radial distance, the likelihood is small that any given snapshot of the density profile at Jupiter would reproduce the specific best-fit power law. Our data are an aggregate representation of the global trend of density at Jupiter, taken during multiple orbits, and over a time exceeding 2 years. The variability in the system at Jupiter due to solar wind influence and plasma production at Io (which both occur on much shorter time scales) make it difficult to accurately fit our data to a specific functional form. Nevertheless, we report the best-fit values as indicative of general average trends in Jupiter's magnetosphere. The R-values

for both fits of density vs. radial distance indicate a higher than 99.9% confidence that the quantities are correlated (i.e. they are not random). The power law exponents, along with values of R and reduced χ^2 are all summarized in Table 3 at the end of this document.

Global Density Display

Another useful programming tool was developed, called a "global density display". This tool plots the PWS derived electron density in color onto a spatial two-dimensional space representing Jupiter's magnetosphere. The horizontal coordinate used in these plots is the distance from Jupiter along the x-axis in Jupiter-centered solar magnetospheric coordinates (+x points toward the sun, +z is north out of the ecliptic plane, and +y completes the right-handed system). The vertical axis shows the distance above or below a model predicted plasma sheet center, located at z=0. The model that predicts the location of the center of the plasma sheet is the Khurana 1998 Current Sheet Model.

The Khurana model (Figure 25) is more elegant than a simple rigid disc, and can be described by the equation:

$$Z_{cs} = r \left\{ \tan(9.6^\circ) \left[\frac{x_0}{x} \tanh\left(\frac{x}{x_0}\right) \right] \cos(\lambda - \delta) \right\} \quad (7)$$

where

$$\delta = 22^\circ + \frac{\Omega_J r}{v_0} \ln \left[\cosh\left(\frac{r}{r_0}\right) \right]. \quad (8)$$

Z_{cs} is the distance of the center of the current sheet from the jovigraphic equator (distance of the current sheet away from the Z=0 plane shown in Figure 25). The variable r is the radial distance of the spacecraft away from Jupiter (in the Z=0 plane), x is the spacecraft distance from Jupiter along the Jupiter-Sun line (the X-axis in Figure 25), λ is the System-III longitude of the spacecraft, and Ω_J is the rotational velocity of Jupiter. The model includes three parameters. X_0 represents the "hinge distance" in the midnight

sector of the magnetosphere. This hinge in the magnetodisc changes the plane of the disc from one coinciding approximately with the magnetic equator to one (about 9.6 degrees away) coinciding more with Jupiter's spin equatorial plane. The hinging is evident in Figure 25 at about $X = -30 R_J$. The model also includes a corotation delay of the distant current sheet due to the finite propagation speed (v_0) of information (at the Alfvén speed) from the inner magnetosphere to the outer magnetosphere. The parameter r_0 represents the distance at which the propagation delay becomes important.

An example of the global density display, using the entire PWS density data set is shown in Figure 26. The axes indicate radial distance along the Jupiter-Sun line on the x -axis, and Δz , the distance between the spacecraft and the predicted magnetic equator (the current sheet). This Δz is just the perpendicular distance between the location of the current sheet (Z_{cs} from the Khurana model) and the location of the spacecraft. The data is limited in Δz by the trajectory of the Galileo spacecraft. The tilt of the magnetic field with respect to the equatorial plane, and the resulting "wobble" of the plasma sheet about that plane, translates to the spacecraft appearing to be a large "height" above or below the predicted location of the magnetic equator. In actuality, the spacecraft was never very far away from the rotational equator of Jupiter. The magnetic equator just rocks back and forth over the spacecraft, exposing it to a range of about 20 degrees in magnetic latitude. Depending on Galileo's distance from Jupiter, and its System III longitude, the spacecraft can reach no higher than about $20 R_J$ above or below the plasma sheet center.

The data in Figure 26 indicates the higher density plasma sheet clearly. The highest densities are confined to the area close to the predicted magnetic equator (a complicated surface in real space, but in this plot, the $z=0$ axis). The farther away (above or below) from the magnetic equator (Δz), the lower the electron density is. Also, as was seen in the radial density profile, at larger radial distances away from Jupiter, the

electron density decreases. Note also that the extreme low density of the tail lobe regions and the variations thereof are also evident on the plot. The higher density in the southern lobe at large radial distances is due to the spacecraft's encounter with the magnetosheath described earlier.

The coherence of the plasma sheet as a well-defined structure also decreases with increasing radial distance from the planet. The plasma sheet as a unit is not as easily recognizable beyond about $50 R_J$. This phenomenon is noted in the collection of frequency-time spectrograms as well. In the middle magnetosphere, the variation in the low frequency edge of the continuum radiation due to plasma sheet traversal is clearly identifiable, but at large radial distances from the planet, this variation is absent. The transition is different for each orbit, but the change occurs somewhere between 50 and 70 Jovian radii from the planet. As seen in Figure 26, the plasma sheet loses its identity as a denser plasma region at radial distances beyond about $50 R_J$. This may have something to do with plasma transport in this region of the magnetosphere, or may be due to a boundary layer, as described by Gurnett, et al. [1980]. The aspect ratio has been stretched in Figure 27 to make the plasma sheet easier to see. The expanded scale allows clearer identification of the location of the plasma sheet boundary. At small radial distances, the inner plasma sheet and extended Io torus can be more clearly seen in red and orange.

The overlay of actual crossings of the central plasma sheet can be added to the global density displays. These plasma sheet crossings are shown as black points in Figure 28. These actual crossings are determined by the reversal of the radial component of the magnetic field, as measured by the magnetometer onboard Galileo. Since the magnetic field lines in Jupiter's middle magnetosphere are highly stretched, above the center of the plasma sheet, the field lines are pointing nearly radial outward, and below

the sheet, nearly radial inward. The change in sign of this radial component signifies the crossing of the center of the plasma sheet. Using the actual crossings of the central plasma sheet on such a plot can assess the accuracy of the Khurana model.

One potential application of this global density display (beyond the scope of this work) is that individual orbits or passes through the magnetosphere can be observed and compared to one another. For example, a single inbound pass in the pre-dawn sector may be compared to the inbound pass on the subsequent orbit (in the same general region of the magnetosphere). If there has been any significant change in the configuration of the plasma sheet (thickening, thinning, shift north or south, etc.), such a change would be clear in these plots.

Magnetopause Encounters

Although the dynamics of Jupiter's magnetosphere are dominated by the rapid rotation of the planet, and the strong plasma source in the vicinity of Io, solar wind variations are known to affect the size and shape of Jupiter's bow shock and magnetopause. Data from the Voyager 1 and Voyager 2 spacecraft indicated when each of those spacecraft encountered these boundaries. From that data, models of the magnetopause and bow shock were developed [Acuña et al., 1983].

In the process of examining the electron density data set, several clusters of data points were noticed to have unusually large density values at large radial distances from Jupiter. It is known that higher density plasma is found closer to Jupiter, near the Io plasma torus, but the large density values discussed here were located at about $120 R_J$ from the planet, when the spacecraft was believed to be in the low density lobes of the magnetosphere. It was hypothesized that these data were attributable to the Galileo spacecraft encountering the magnetopause on the dawn side of Jupiter's magnetosphere, and traversing into the higher density magnetosheath.

To test this hypothesis the time and spacecraft location for each of the large density values was determined. It was noticed that the data points clustered together in two seven-day time periods. Color spectrograms of these time periods were inspected to find the exact times where the plasma frequency rose to near the solar wind plasma frequency (about 10 kHz). An example of one of these time periods is shown in Figure 29. The times when the large density values were observed correspond to the times that the plasma frequency increases to nearly the solar wind plasma frequency, and the continuum radiation is no longer observable by the plasma wave instrument. If the spacecraft were close to Jupiter, an explanation for this would be that the electron density is too high, and the continuum cannot propagate inward to Galileo's location. However, during the time periods in question, the spacecraft is over 100 R_J from Jupiter. In these cases, it is suspected that the density has risen (as evidenced by the increase in the plasma frequency at the lower boundary of the continuum) because the spacecraft has crossed into the higher density magnetosheath, and the continuum radiation vanishes.

This magnetosheath hypothesis is confirmed by comparing the spacecraft position to the Voyager based models of the magnetopause, and by magnetometer team determinations of the magnetopause location. In Figure 30, the model magnetopause boundaries are displayed in the jovigraphic equatorial plane, along with the locations where the spacecraft detected the large electron density values.

Further evidence comes from identification of magnetopause boundary crossings by the Galileo magnetometer instrument. Although the magnetopause is sometimes difficult to determine from magnetic field data on the flanks of Jupiter [Joy, 2000], the magnetometer data showed that the spacecraft was in the magnetosheath during the same time intervals that the continuum radiation vanished from the plasma wave instrument spectrograms. The magnetosheath is identified as a region in which the magnetic field

magnitude exhibits higher wave power as compared with data inside the magnetosphere. This is due to the turbulent nature of the magnetosheath, where shocked solar wind plasma is decelerated and heated. Other features of the magnetic field components also indicated that the spacecraft was in the magnetosheath during these time periods [Joy, 2000].


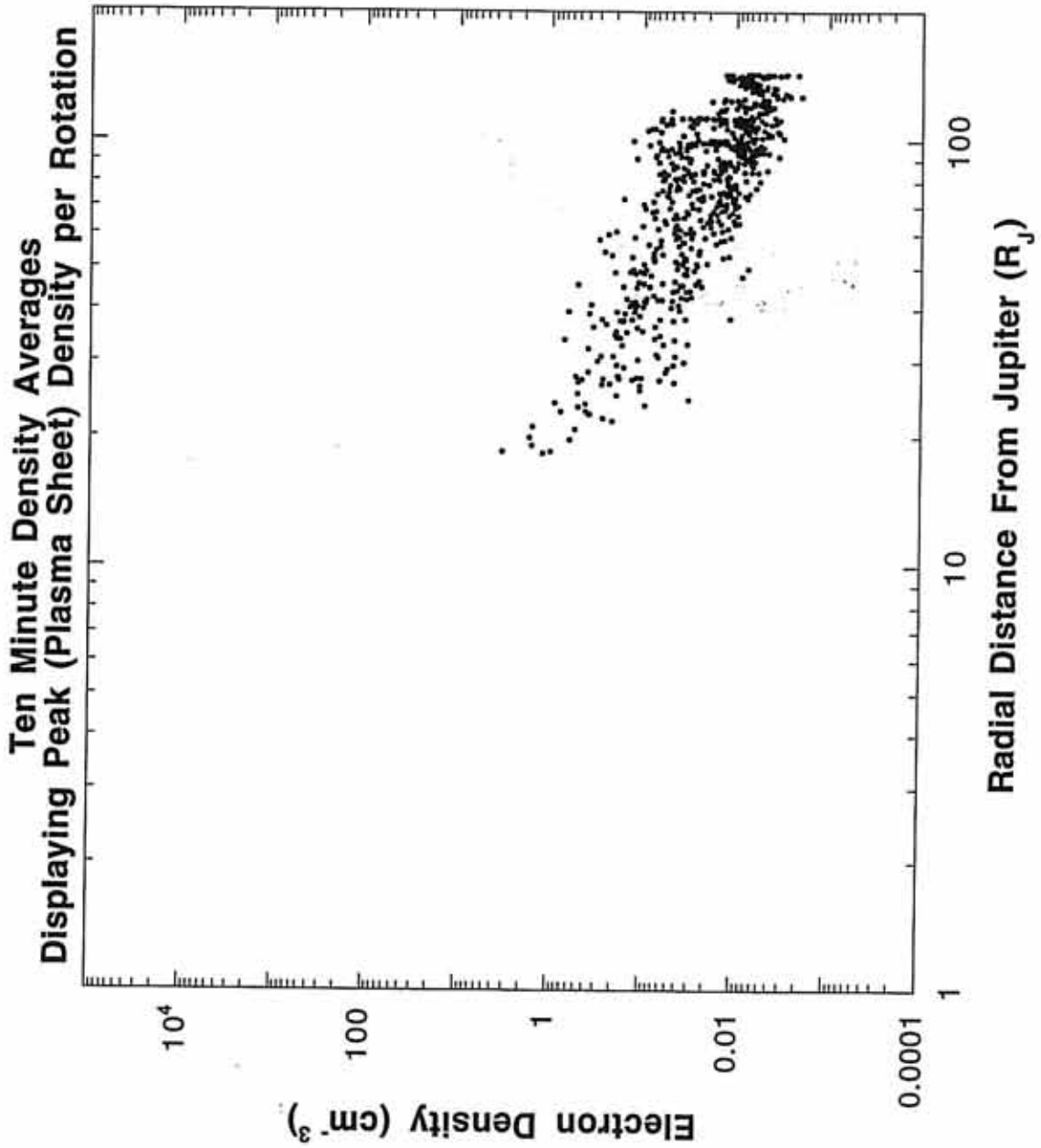


Figure 21. Plasma sheet density. This plot displays ten-minute averages of density data from the Galileo PWS derived data set. After the density was averaged over ten-minute intervals, the peak value per ten-hour rotation was plotted on this plot. This ensures that the plasma sheet (peak density) values are displayed. Plasma sheet density can be seen to decrease with radial distance from Jupiter.






Figure 22. Fitted plasma sheet density. The same plot as shown in Figure 21, but with a best-fit power law added to the data. Despite the large scatter about the fit, a trend shows the average electron density in the plasma sheet decreasing as $(1/r)^{2.14 \pm 0.01}$.

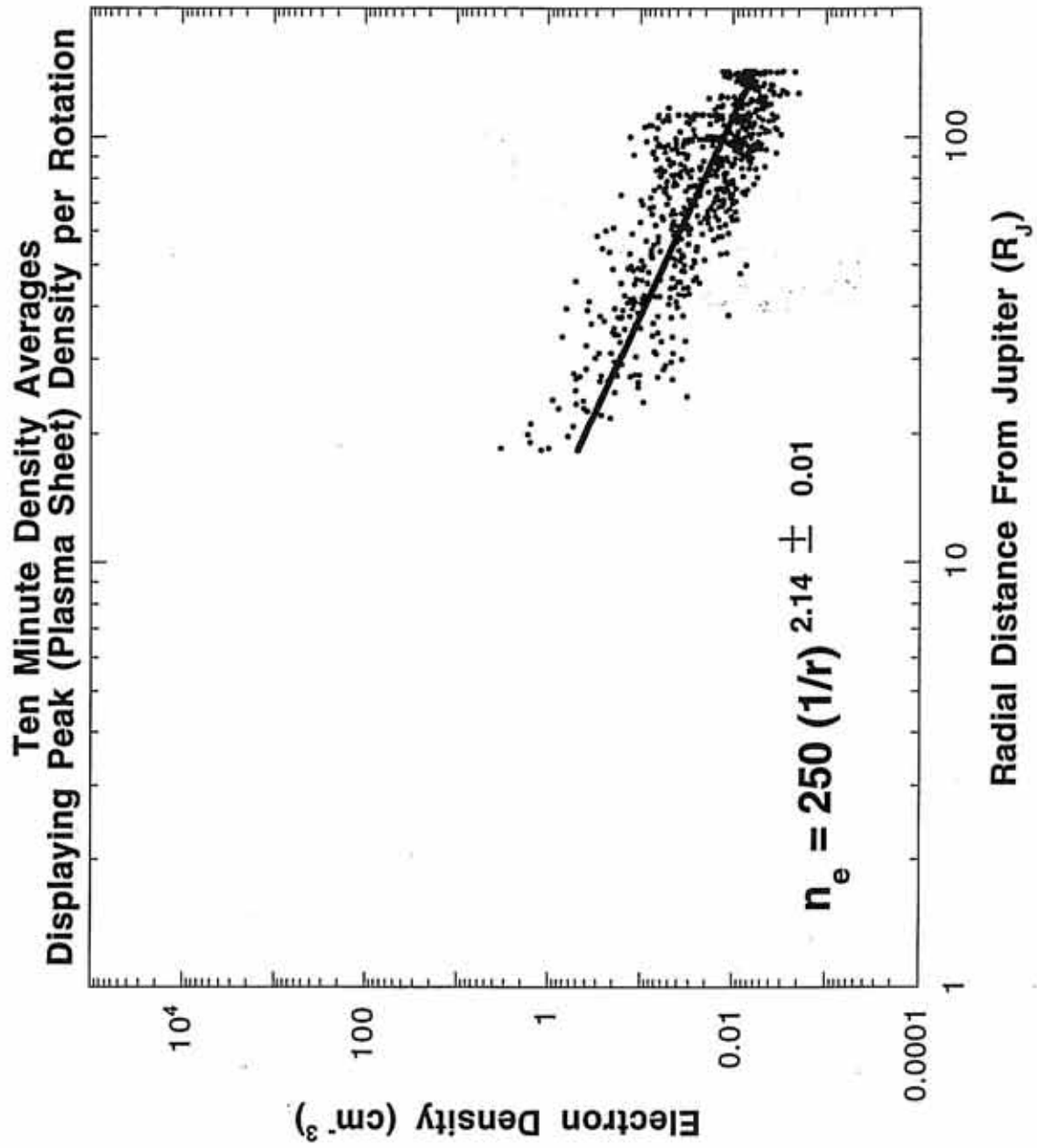
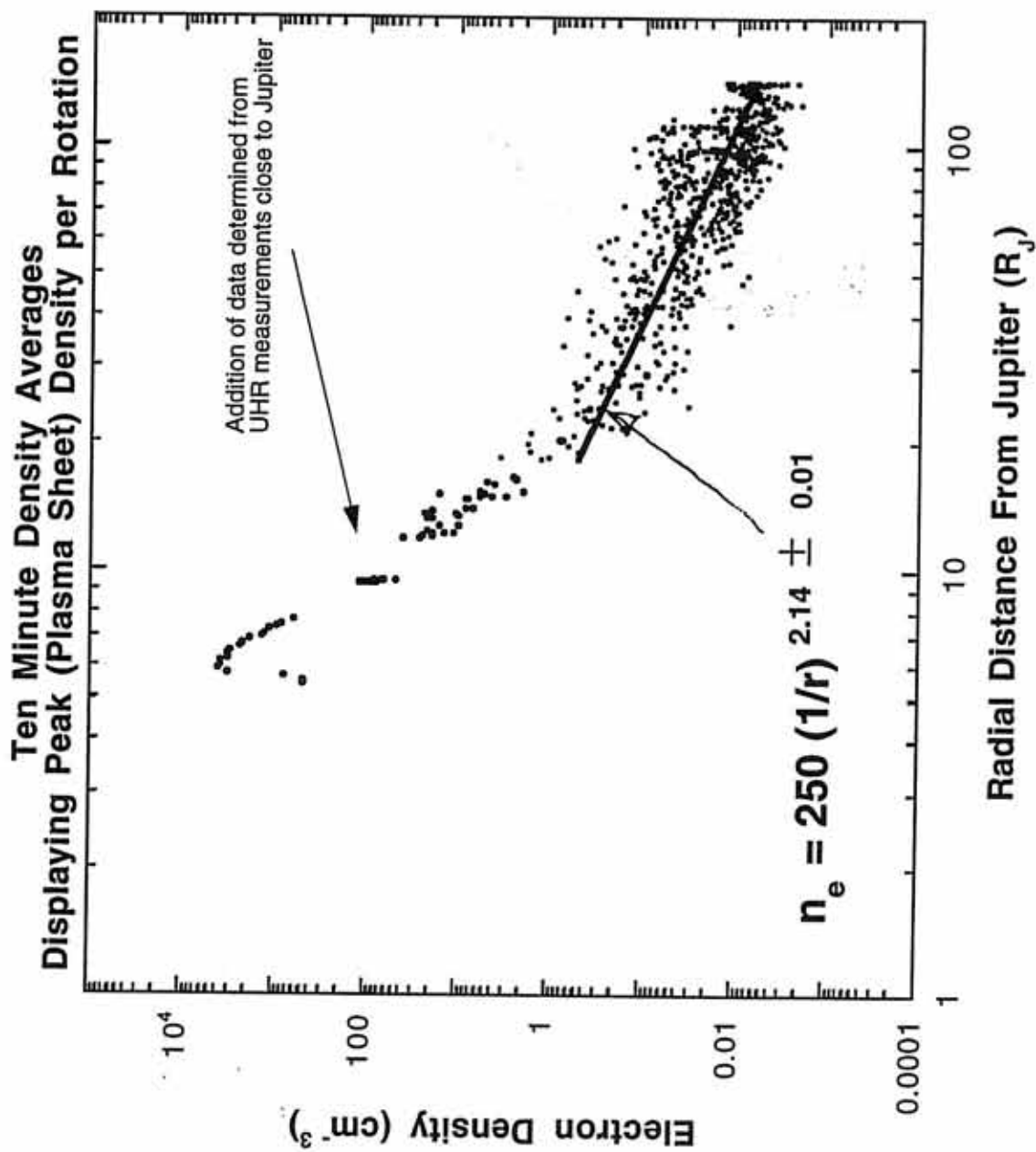


Figure 23. Jupiter's electron density profile. A profile of electron density throughout the entire Jovian system, calculated using the PWS continuum cutoff technique. Additional density measurements from another study (upper hybrid frequency measurements) were added to show the higher densities close to the Io plasma torus at about $6 R_J$. These measurements are closer to Jupiter than the continuum radiation study is able to obtain. Notice the deviation from the previous power law in the middle and outer magnetosphere ($>20 R_J$). Possible explanations for this are discussed in the text.




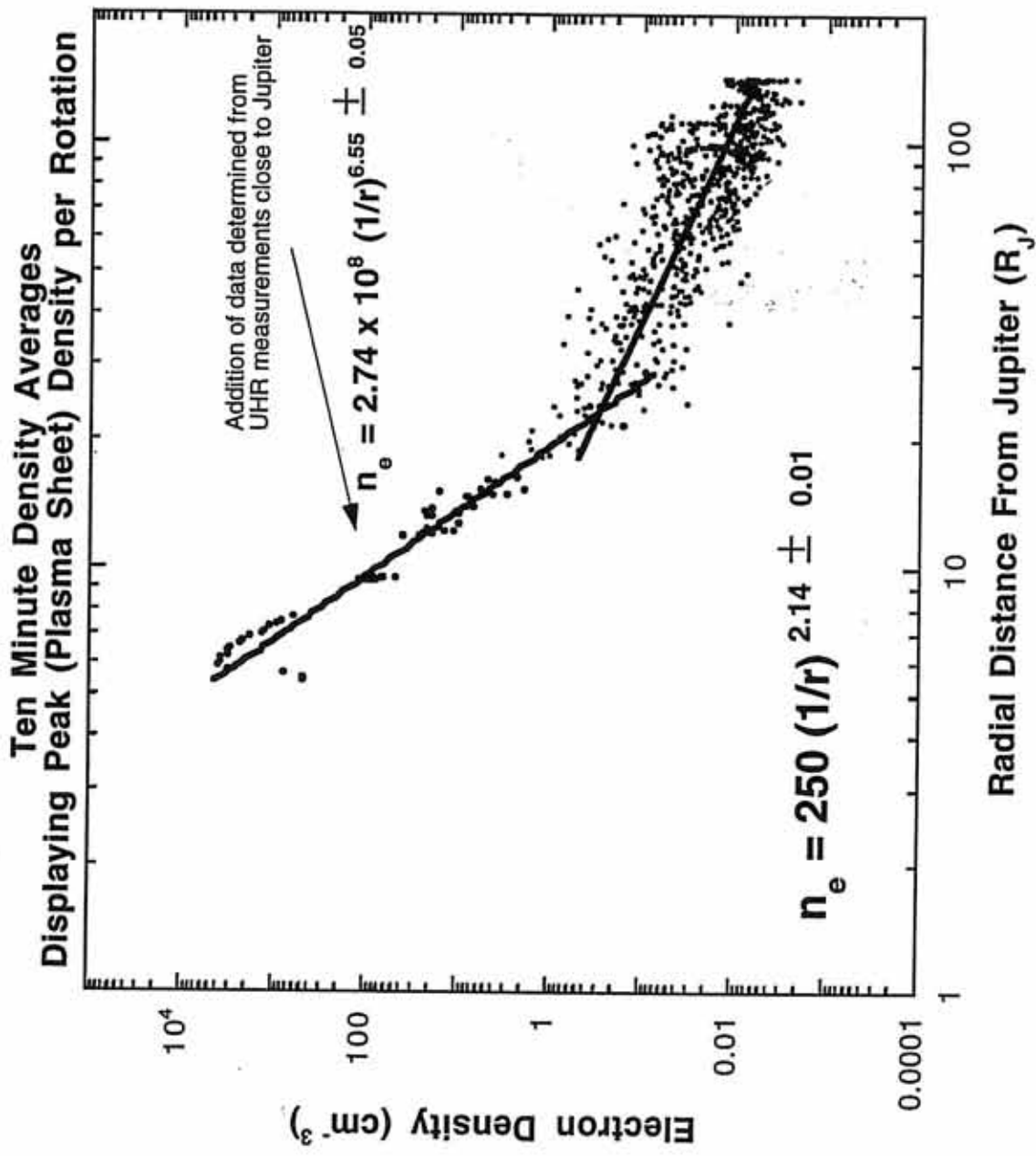


Figure 24. Two different power laws. The same figure as Figure 23, with a power law added to the upper hybrid density data. The power law is much steeper for the density measurements made closer to Jupiter. Again, there is a large statistical scatter of the values about the fit, but the clear trend in the data is evident.






Figure 25. The Khurana model. This shows a diagram of the Khurana hinged-magnetodisc magnetic field model. The +X direction (to the left) is in the direction of the sun. Note the dipolar configuration at small radial distances, the hinge point at about $X = -30$, and the more extended tail-like structure beyond $X = -30$.

Khurana's Jovian Magnetic Field Model

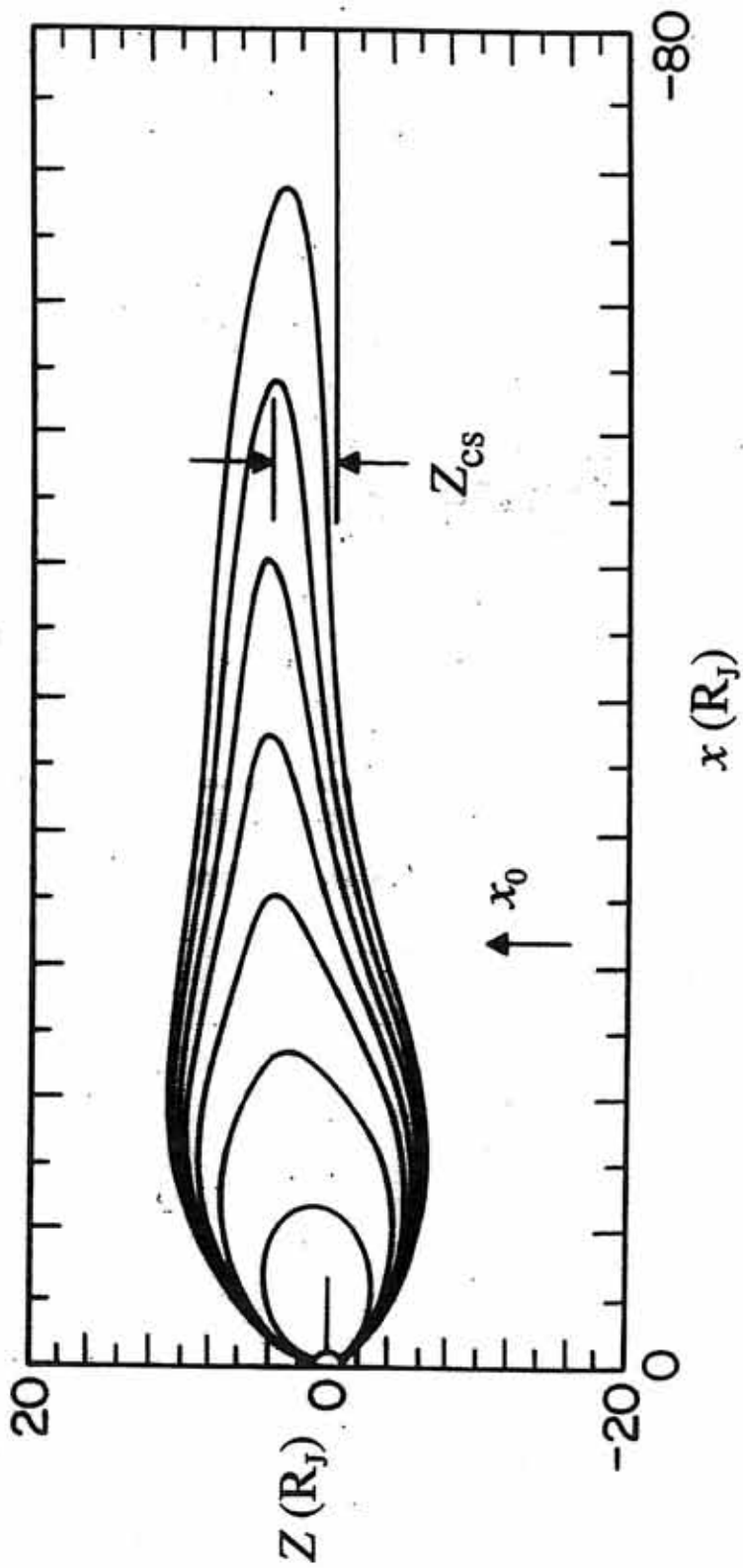
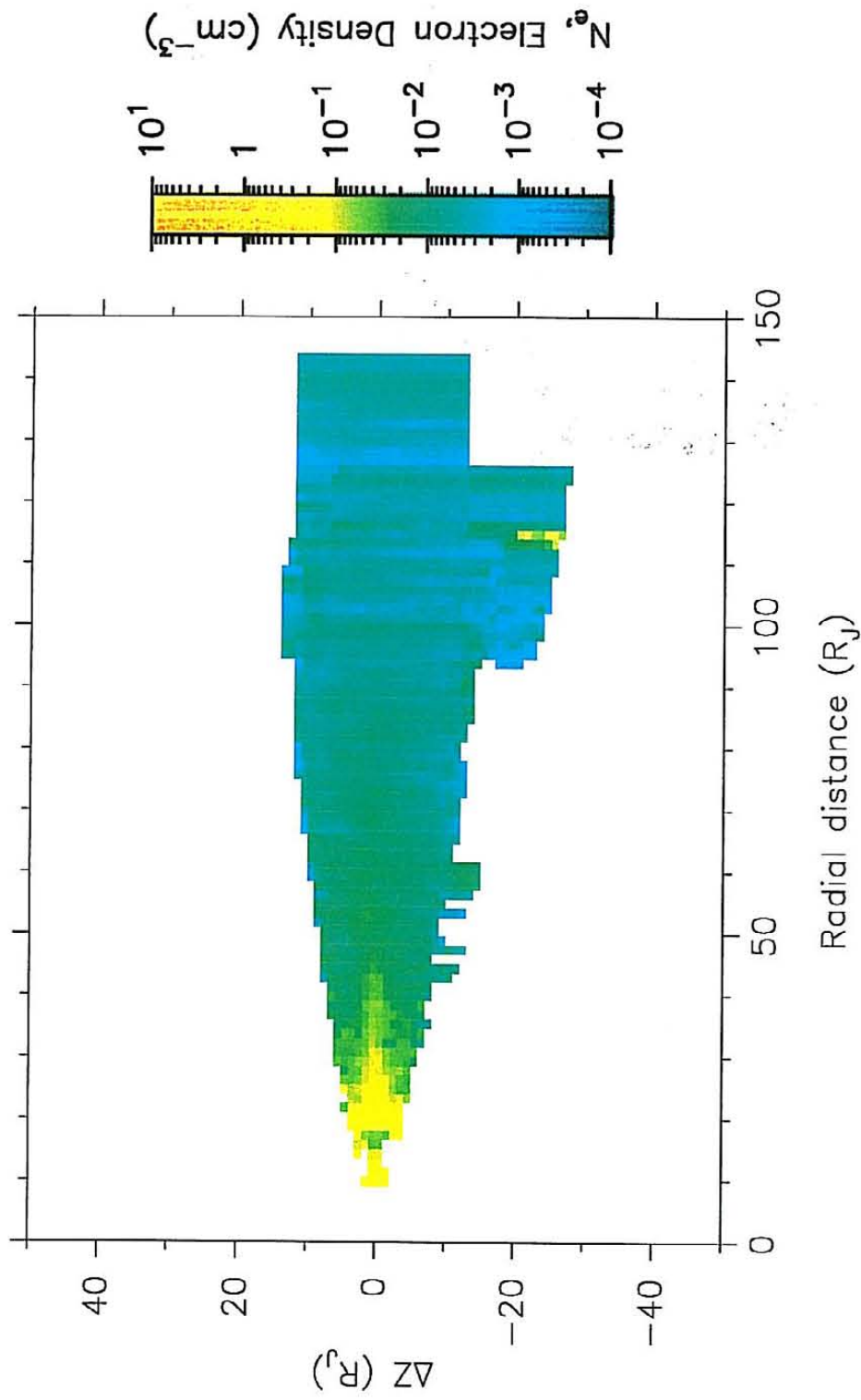


Figure 26. A global density display. This plot shows electron density above and below the predicted model location of the current sheet. The predicted location (vertical axis) is determined by the Khurana 1998 current sheet model. Radial distance from Jupiter is indicated on the horizontal axis, and PWS-derived electron density on the color scale. Red is the densest plasma, while dark blue is the least dense. The plasma sheet is clearly evident close to Jupiter, and confined about the model $\Delta z=0$ plane (x-axis). The high density values around $115 R_J$ and at about $\Delta z = -20$ are due to spacecraft encounters with the magnetosheath on an early orbit. This plot represents all the data in the Galileo primary mission.

1996 144 (May 23) 00:00:00 - 1997 314 (November 10) 00:00:00




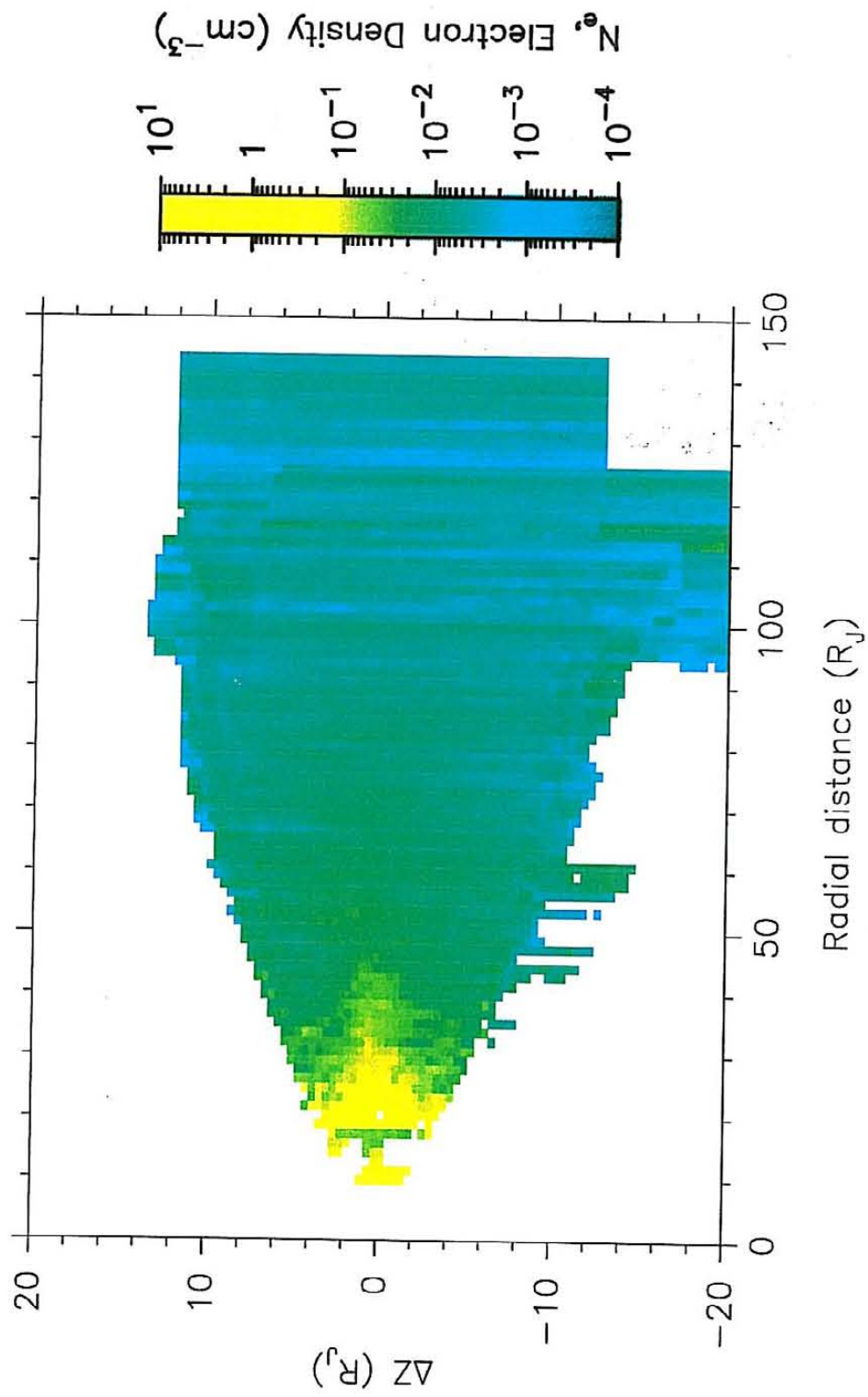


Figure 27. Stretched density display. The same global density display as Figure 26 is shown here with a stretched vertical scale. The higher density plasma sheet is now expanded and it can be seen more clearly.

1996 144 (May 23) 00:00:00 - 1997 314 (November 10) 00:00:00




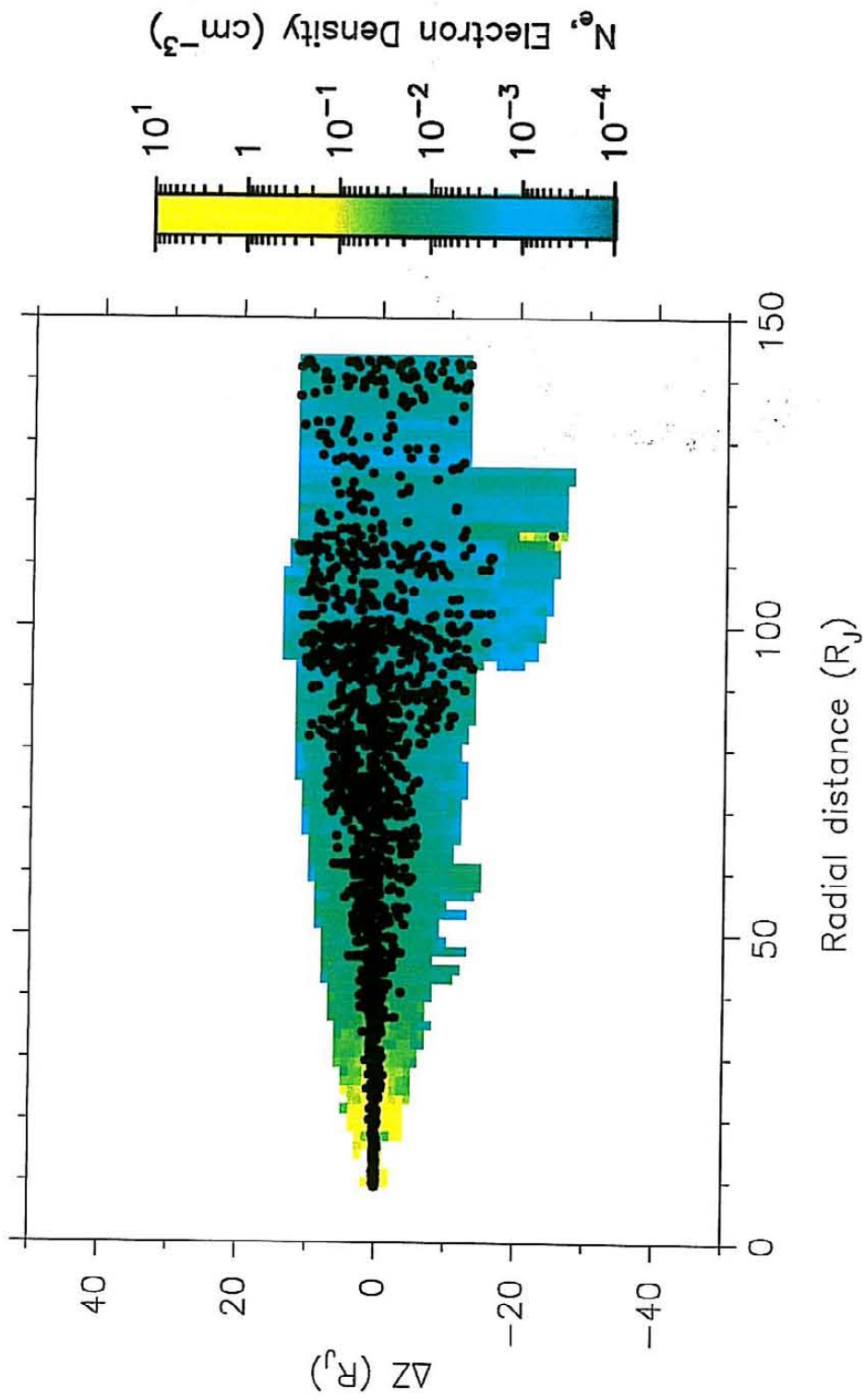


Figure 28. Global density display with crossings. The same figure as Figure 26, with the addition of actual crossings of the center of the plasma sheet. These crossing locations were determined from the radial component of the magnetic field using data from the Galileo magnetometer. The spread of actual crossings away from $\Delta z=0$ is a result of the Khurana model. It is more accurate in predicting the center of the plasma sheet at smaller radial distances.

1996 144 (May 23) 00:00:00 - 1997 314 (November 10) 00:00:00



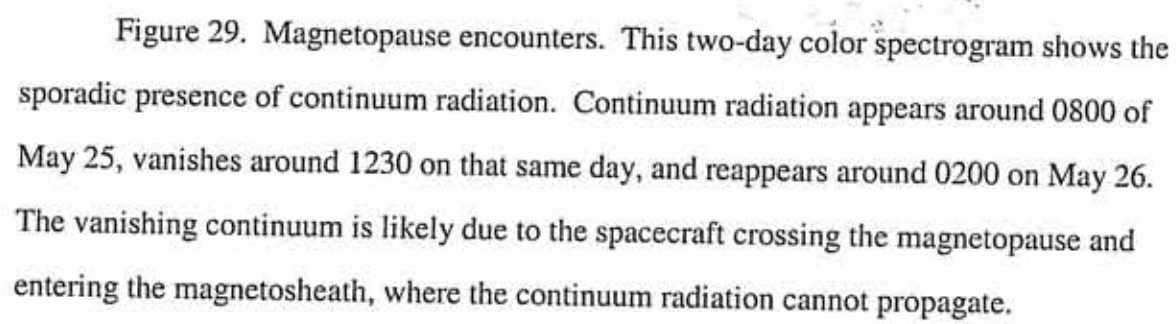
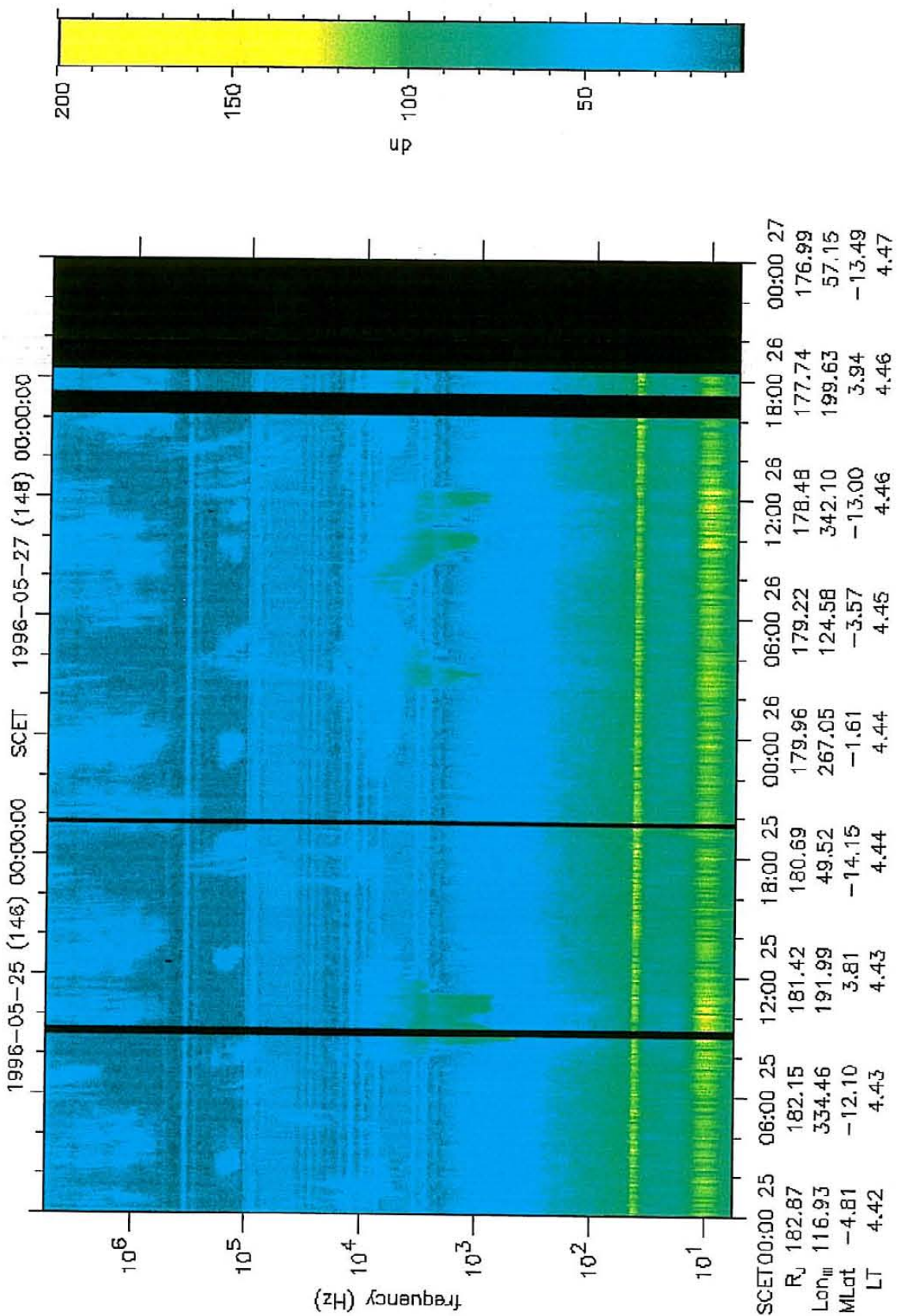


Figure 29. Magnetopause encounters. This two-day color spectrogram shows the sporadic presence of continuum radiation. Continuum radiation appears around 0800 of May 25, vanishes around 1230 on that same day, and reappears around 0200 on May 26. The vanishing continuum is likely due to the spacecraft crossing the magnetopause and entering the magnetosheath, where the continuum radiation cannot propagate.

Galileo PWS



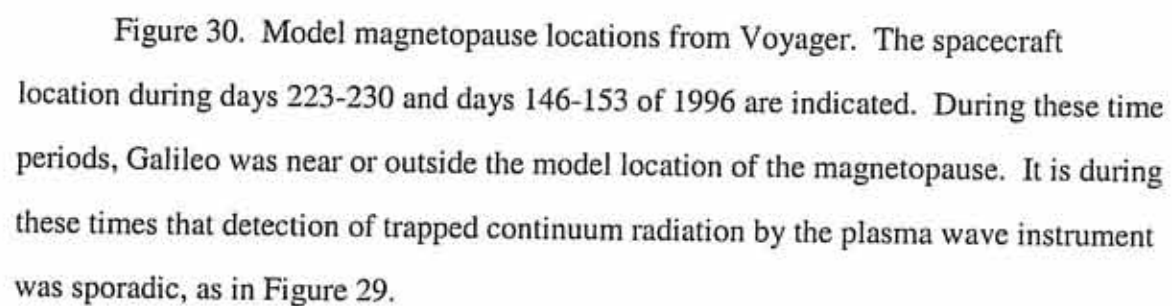
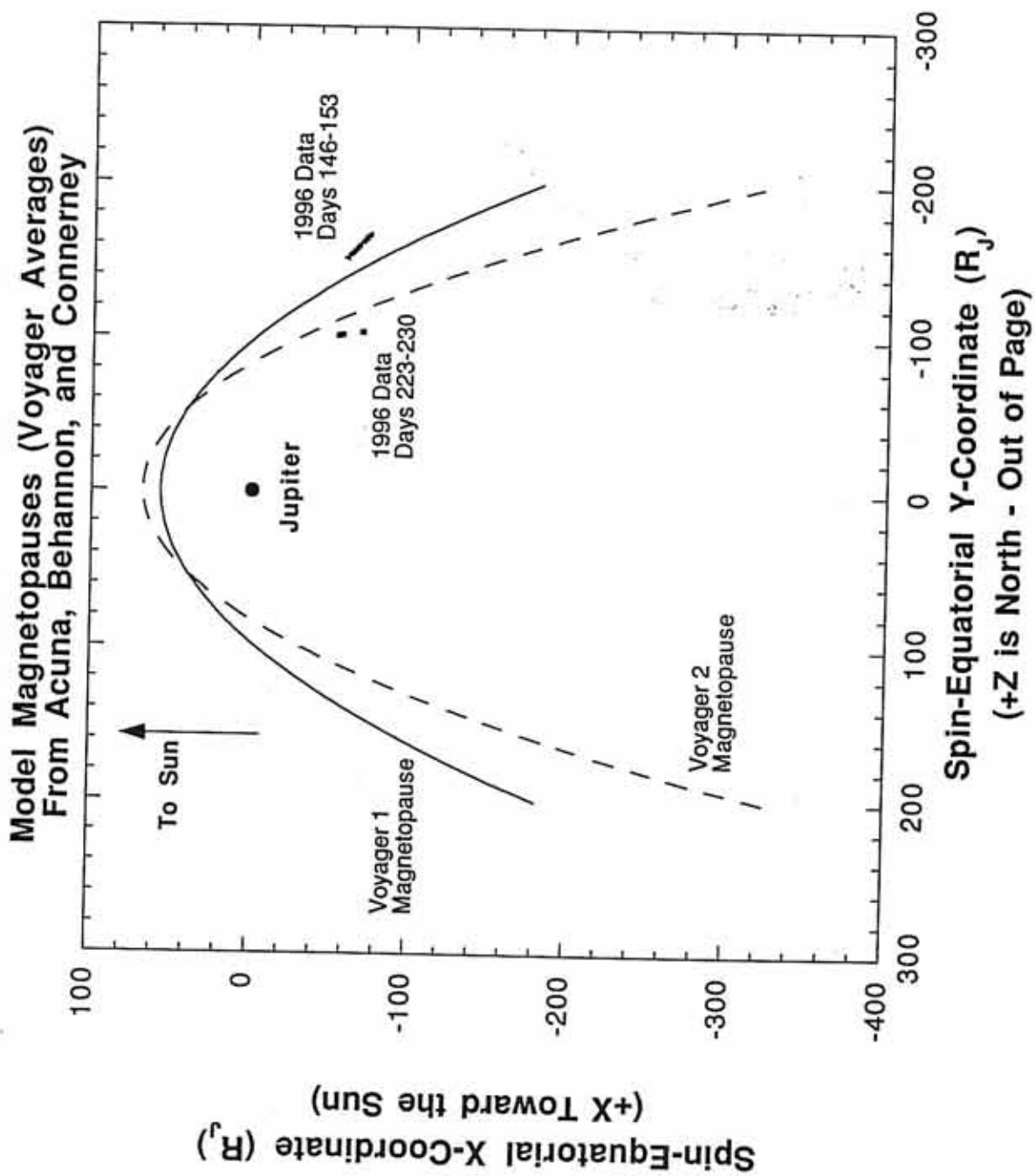


Figure 30. Model magnetopause locations from Voyager. The spacecraft location during days 223-230 and days 146-153 of 1996 are indicated. During these time periods, Galileo was near or outside the model location of the magnetopause. It is during these times that detection of trapped continuum radiation by the plasma wave instrument was sporadic, as in Figure 29.



CHAPTER V: PLASMA SHEET MODELS

Jupiter's magnetosphere has a source of plasma deep inside it (the volcanic moon, Io). Because the plasma source is in the plane of Jupiter's rotational equator, most of the material starts out confined there. Upon ionization, however, electromagnetic forces play a large role in the subsequent motion. The tilt of Jupiter's magnetic field with respect to the spin axis can alter particle orbits, and change the latitudinal distributions of plasma.

Plasma Sheet and Magnetodisc Models

The first in-situ descriptions of Jupiter's nightside magnetotail, and a structured magnetodisc come from Pioneer 10 and Pioneer 11 measurements of energetic particles in the magnetosphere [Northrop, et al., 1974; Van Allen, et al., 1974; Van Allen, 1976; Goertz, et al., 1976; Van Allen, 1979; and Goertz, et al., 1979]. Additional data were provided by Voyager 1 and Voyager 2, in 1979 as each spacecraft flew past Jupiter [Barbosa, et al., 1979; Ness, et al., 1979; Gurnett, et al., 1980]. The disc model, or offset tilted dipole model describes a plasma disc that is centered along the magnetic equatorial plane, and therefore tilted 10 degrees from the spin equatorial plane. As a result, this disc of plasma wobbles up and down, and an observer in the spin equatorial plane would encounter the so-called magnetodisc twice per rotation period: once as the disc sweeps past from north to south, and once from south to north [Hill et al., 1983]. There is some dispute among more detailed models as to whether this magnetodisc is rigid, bent, warped, or wavy. Several of these possible magnetodisc configurations are depicted in Figure 31.

It is this basic disc model that is best represented in the PWS density data, especially in the middle portion of the magnetosphere. It is evident from the color spectrograms and the density data set that the magnetosphere can be described by three major subdivisions. Other descriptions subdivide the magnetosphere differently, but also into three regions [Dessler, 1983]. Based on the PWS measurements, the inner magnetosphere (less than about 20 R_J) is characterized by higher density, and lacks any evident modulation of the continuum radiation (in fact, it often lacks any continuum emission at all). In this inner portion of the magnetosphere, the field is roughly dipolar:

$$\vec{B}_{dipole} = \frac{3(\vec{m} \cdot \vec{r})\hat{r} - \vec{m}}{r^3}. \quad (9)$$

The middle portion of the magnetosphere (between 20 and about 60 R_J) is highlighted in the color spectrograms by very regular plasma sheet crossings. These crossings occur twice per Jovian rotation period, or about twice every ten hours. The plasma frequency (and therefore the electron density) increases very sharply at the onset of these crossing events, and peaks near the center of the plasma sheet.

The 60 R_J outer boundary of the middle magnetosphere is somewhat variable from orbit to orbit, but represents an average distance for the transition to the outer magnetosphere. In the outer part of the magnetosphere (greater than about 60 R_J), some plasma sheet crossings are still evident in the PWS data, but the regularity and classic appearance of the crossings in the data are no longer present. In their place are unpredictable, more disorganized density variations. There are still sharp density gradients, as with the plasma sheet crossings, but they do not appear as symmetrical, and are rarely bounded by entries of the spacecraft into the tail lobes. This implies that the plasma sheet may be thicker, more diffuse, or less well confined to the magnetic equator

at larger radial distances. As the quasi-dipolar magnetic field weakens with larger radial distance from Jupiter, it is reasonable to assume that the confining nature of the tail field configuration (nearly radial) is less effective, and thermal motions, as well as the rotational effects will be more important in governing the plasma motions:

$$|F_{centrifugal}| = mr\Omega_J^2. \quad (10)$$

The centrifugal effects already dominate gravitational effects outside of $2.2 R_J$, but magnetic effects continue to dominate out to at least about $25 R_J$, where co-rotation begins to break down.

For the purposes of the next section, I intend to proceed under the assumption that, at least in the middle magnetosphere, a disc model is the correct picture. Some of the other models discussed earlier (the magnetic anomaly model and the corotating convection model [Dessler and Hill, 1975; Hill and Dessler, 1991; Hill et al., 1981]) may be useful in describing particular aspects of the data that have not yet been studied in detail. However, based on the data examined, the disc model best describes the density data set.

Identification of the Plasma Sheet in the Data

It is important to be able to accurately identify the places in the data set where the spacecraft is encountering the plasma sheet. Several criteria were used to locate the plasma sheet crossings in the PWS density data set. A visual identification from the color spectrograms was used to preliminarily locate the plasma sheet. In the middle magnetosphere the central plasma sheet is marked by the significant increase in the plasma frequency. The boundaries of the plasma sheet are often marked by a sudden sharp increase in the plasma frequency, or by a diminishment of the intense wave activity often detected in the tail lobes. As the spacecraft passes from a lower density region (the lobes) into the plasma sheet, the plasma frequency becomes greater than the electron

cyclotron frequency, and the continuum emission is easily distinguished from other wave modes detected in the low-density regions. The density generally reaches a peak near the center of the plasma sheet, and drops off near the edges or boundaries, just as the behavior of the plasma frequency is observed to do.

After a visual identification of candidate plasma sheet encounters is made, further verification can be achieved using the magnetic field data. In a quasi-dipolar geometry, the magnetic field magnitude will approach a local minimum as the spacecraft crosses the magnetic equator. In addition, the radial component of Jupiter's magnetic field as measured at Galileo will reverse itself. A set of typical plasma sheet crossings along with the magnetic field data (displayed as the electron cyclotron frequency in black on the plot) can be seen in Figure 32. The peak density occurs close to the time of the radial field reversal, and close to the minimum of the field magnitude. The boundaries of the plasma sheet are also evident by observing the times where the magnetic field changes from its nearly constant, steady configuration to a more disturbed state.

Use of the Khurana Current Sheet Model

The use of an existing model has proven to be perhaps the most substantially useful step in this project's progress. A recent model using Jupiter's intrinsic magnetic field along with other characteristics of a generalized magnetodisc was chosen to help organize and compare the density data. The Khurana [1992] model used information about Jupiter's plasma sheet from the Voyager and Pioneer spacecraft flybys to predict where along the spacecraft's trajectory, it should encounter the current sheet. The central portion of the plasma sheet, where most of the current is flowing (due to near-corotation of the denser plasma) is often referred to as the current sheet. It is a very thin structure, and is marked by the reversal of the radial component of the magnetic field. Recall that equations (7) and (8) are used to describe the Khurana 1992 model.

The Khurana 1998 model is a modification of the 1992 version, but uses Galileo magnetic field data to refine the model from its Voyager/Pioneer bias. An additional change in the 1998 model makes the location of the current sheet dependent upon the relative tilt between Jupiter's magnetic axis and the solar wind direction. This modification implies that the solar wind plays a small but significant role in shaping the current sheet.

As this model is well suited for comparison with the PWS density data, the computer code has been obtained from the author and incorporated into a computer program to plot the electron density from any chosen time interval. The program can output the times, relevant trajectory information, the PWS density values, and the predicted distances away from either the 1992 or 1998 model current sheet. In addition, the user can choose to have the program plot the density values in a spatial coordinate system based upon the model current sheet, or to output the data to a text file for other analysis. An example of the plot output of this program is shown in Figure 33.

The results of this computer program have been very helpful in analyzing the density data. In most cases, the 1998 model predictions are superior to the 1992 model predictions in locating the central part of the plasma sheet. The 1998 model uses Galileo magnetic field observations and includes information about the angle between Jupiter's magnetic field and the solar wind direction. For this reason, the 1998 model results are used in analyzing the density data. If there are individual cases where the 1998 model does not adequately represent the data, studying the 1992 model may be useful.

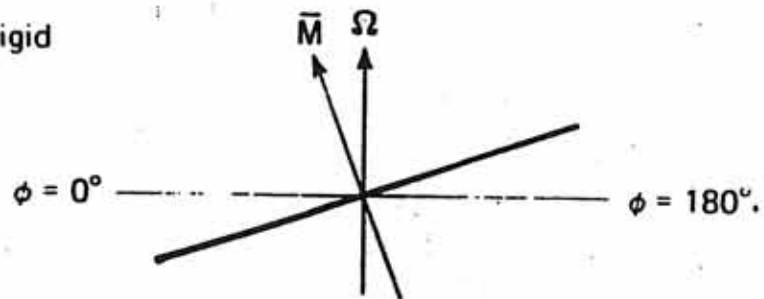
Two of the most useful characteristics that can be determined using the Khurana models are the plasma sheet thickness, and the shift of the plasma sheet away from its predicted location. The thickness of the plasma sheet is measured in multiples of Jupiter's radius, and is easily determined from the conveniently chosen geometry of the

model's cylindrical coordinate system. The perceived shift of the plasma sheet can be measured in two convenient ways. The shift can be measured physically in Jovian radii corresponding to the plasma sheet lying either above or below the predicted location. In the cylindrical system, the predicted location is placed at $z=0$. Temporally, the shift can be quantified by describing the plasma sheet encounter as occurring either before or after its predicted time. The geometry of the magnetodisc's rotation past the spacecraft is such that the two views are equivalent, and both descriptions of plasma sheet "position" are used commonly in the literature.

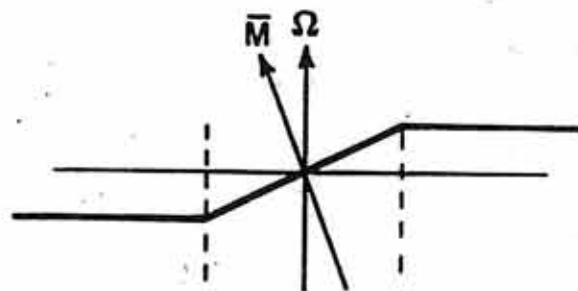
Because of the time resolution of the PWS density data set, the location of the thin current sheet can be fairly accurately identified. The reliability of the PWS density data are proving useful to the model author, just as his model proved useful to this project. The peak densities from the PWS data set are good indicators of the actual location of the current sheet. With knowledge of deviations of peak density from the predicted location of the current sheet, future versions of this current sheet model may be refined further. Presently, the model works well to predict the location of the current sheet relative to the spacecraft in the inner magnetosphere. It contains all the major features described by a hinged magnetodisc and has a good basis in physical reality. It can be simply described with three variable parameters. The specific predictions by the model regarding where and when the spacecraft is expected to encounter the center of the plasma sheet have been very easily applied to the electron density data set. The biggest drawback to the Khurana model is that it is preferentially accurate closer to Jupiter. At larger radial distances, current sheet crossings do not occur when the model predicts. Further understanding of the plasma dynamics farther from Jupiter, plus a more elegant solar wind interaction term may improve the model's accuracy.

Figure 31. Four different magnetodisc models. Each describes a different shape and orientation of the magnetodisc. The model that is best represented by the density data presented here is probably the bent (or hinged) magnetodisc model.

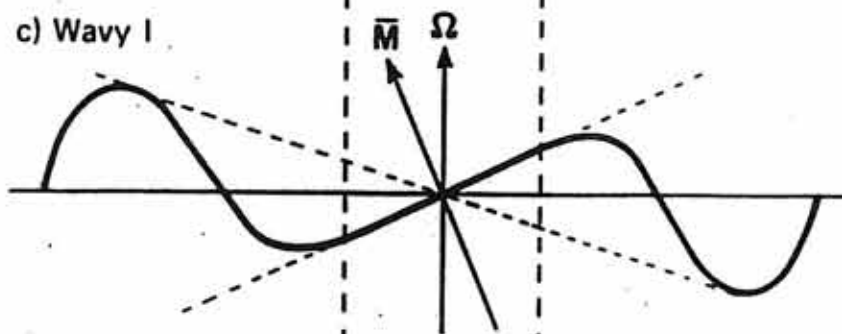
a) Rigid



b) Bent



c) Wavy I



d) Wavy II

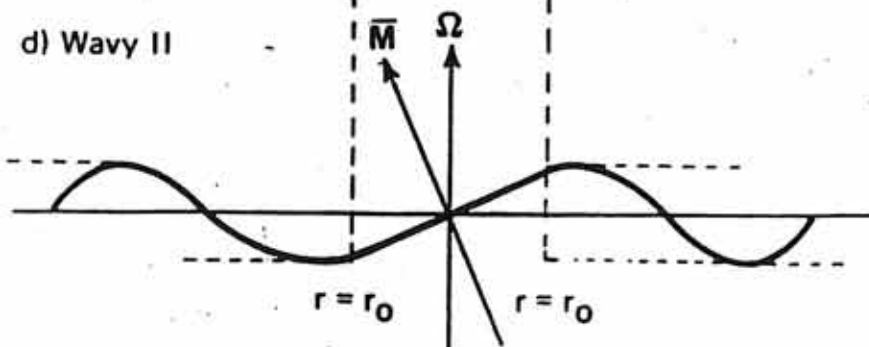
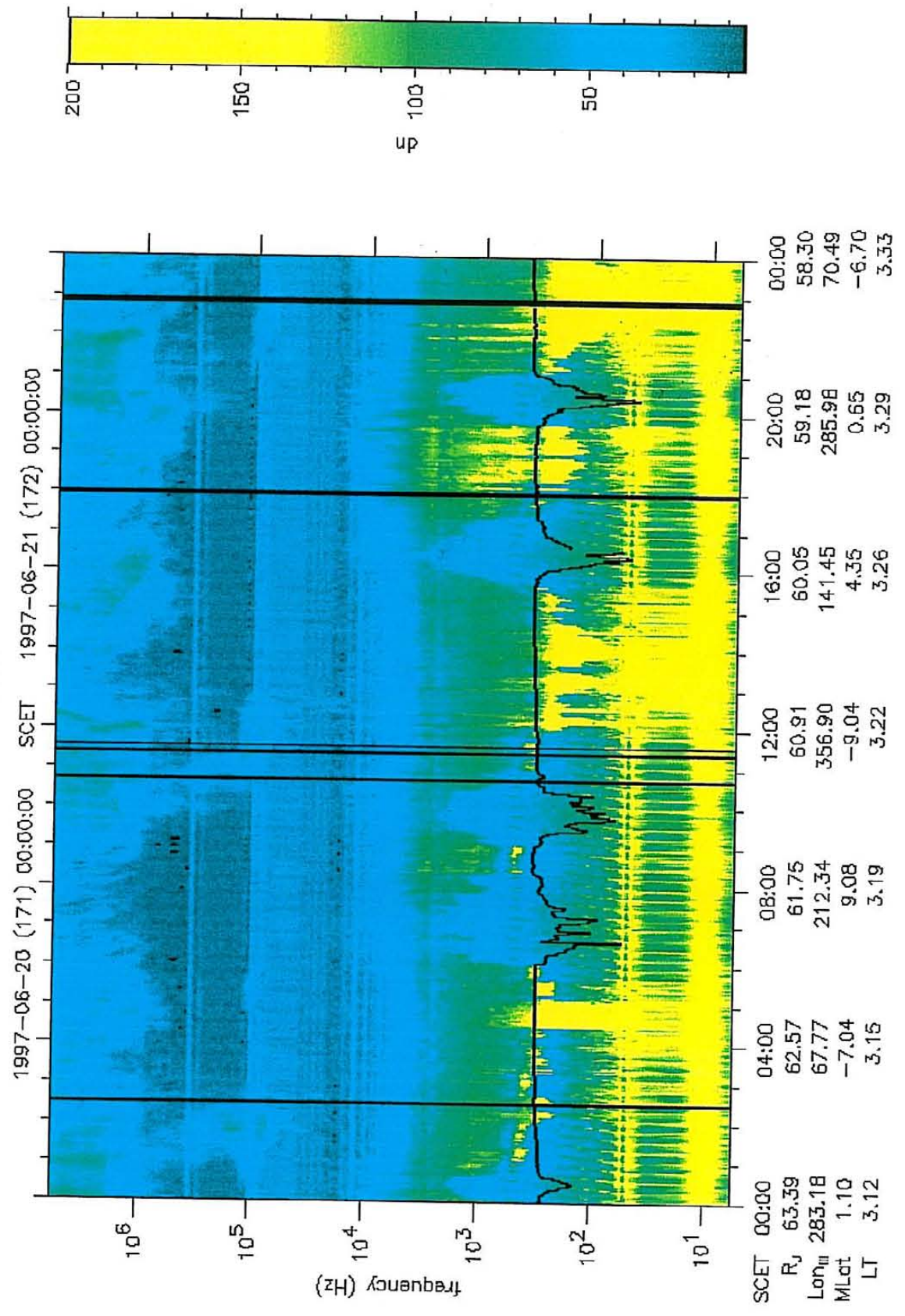


Figure 32. Density and magnetic field strength. The same figure as Figure 20, only with the addition of the electron cyclotron frequency as a black curve on the plot. This cyclotron frequency is directly proportional to the magnetic field magnitude (provided by the Galileo magnetometer team). Note that as the plasma frequency rises (as the density increases) entering the plasma sheet, there is a corresponding decrease in magnetic field strength. This diamagnetic effect allows for the computation of an effective temperature in the plasma sheet.

Galileo PWS




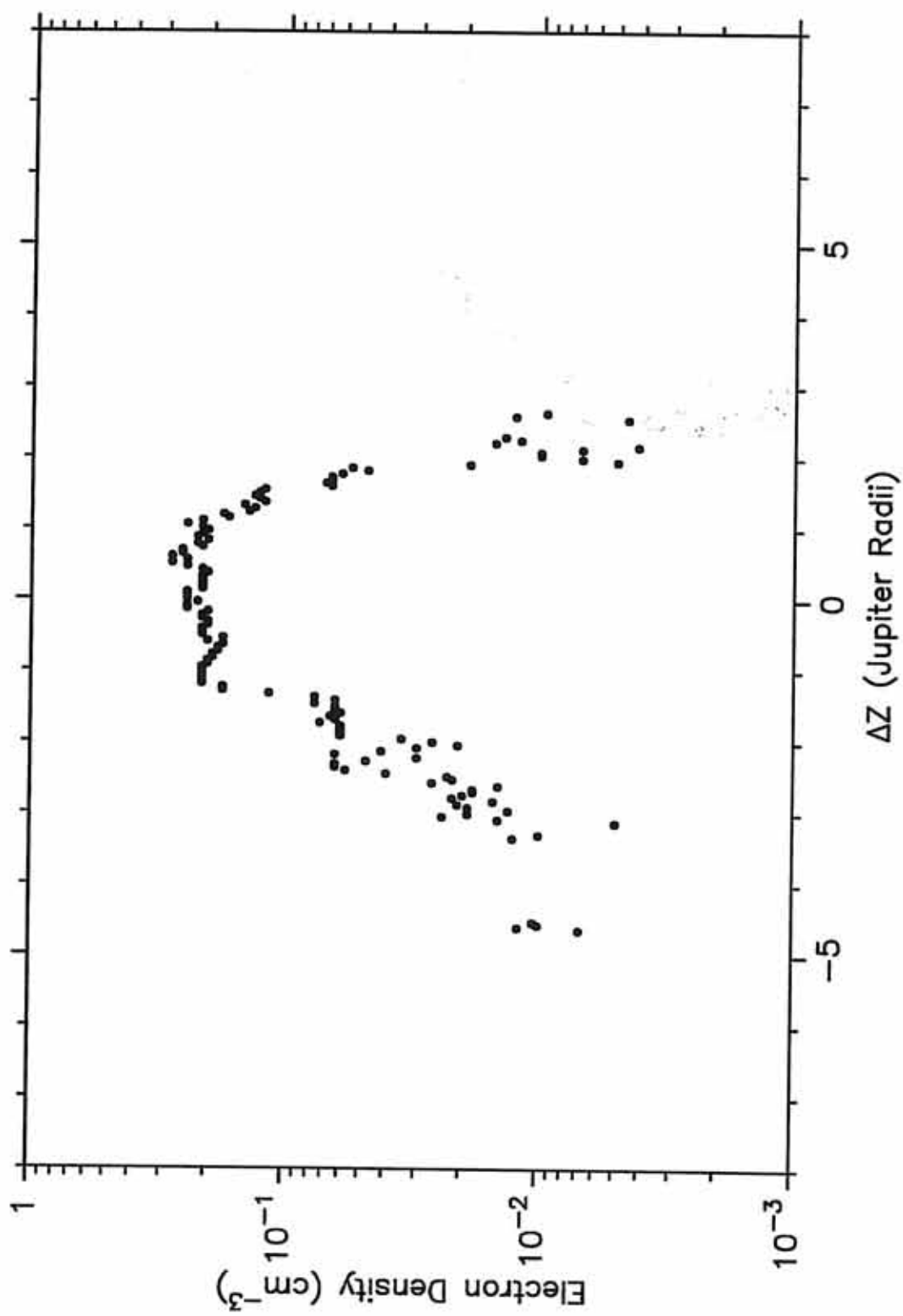


Figure 33. One plasma sheet crossing. A display of electron density from a single plasma sheet crossing (about 2 hours of data) shown in the coordinate system of the Khurana 1998 current sheet model. The horizontal axis indicates spacecraft distance (measured in Jovian radii) above or below the predicted location for the current sheet. Note that the peak density occurs exactly at the location of the current sheet, as predicted by the model ($\Delta z=0$).

1997 174 (June 23) 12:10:00 - 14:10:00



CHAPTER VI: PRESSURE BALANCE ACROSS THE PLASMA SHEET

Magneto-hydrodynamic Pressure Balance

Plasma sheet crossings, as shown in Figure 20, commonly occur throughout the Galileo mission. As the plasma rotates past the spacecraft at near the co-rotation speed, the spacecraft makes pairs of crossings through the plasma sheet (and the current sheet at its center) from north to south and then again from south to north each rotation of Jupiter. This is because of the ten-degree tilt of Jupiter's magnetic axis with respect to its rotation axis. If the spacecraft is located above or below the actual spin equatorial plane, encounters with the plasma sheet will not be exactly periodic but rather, pairs of crossings will occur closer together than the symmetric five-hour period expected if the spacecraft were exactly located in the spin equatorial plane. For example, if the spacecraft were located north of the equatorial plane, the plasma sheet, on its north-moving pass, would sweep past the observer near its northernmost position, and very quickly sweep past the observer a second time as it wobbles back toward the south. If the observer is in the equatorial plane, the crossings will be spaced apart equally in time.

With the addition of the Khurana 1998 current sheet model, a plan was developed to study pressure balance during crossings of the plasma sheet using the electron density data from this project, and the magnetic field data from the Galileo magnetometer instrument. The results of displaying numerous plasma sheet crossings in the density data have yielded a variety of different types of crossings. Most of the time segments analyzed are five-hour segments bounded by the maximum separation of the spacecraft from the location of the current sheet, as predicted by Khurana's 1998 magnetic field

model. From magneto-hydrodynamics (MHD), a relationship can be written down that expresses all the forces acting on a magnetized plasma:

$$\rho_m \left(\frac{d\vec{U}}{dt} \right) = -\vec{\nabla}p - \vec{\nabla} \left(\frac{B^2}{2\mu_0} \right) + \frac{1}{\mu_0} (\vec{B} \cdot \vec{\nabla}) \vec{B} \quad (11)$$

The above relationship is essentially $F=ma$ as it applies to a magnetized plasma. Time dependent mass flow (the acceleration term) is expressed on the left-hand side of equation (11), and is the result of pressure and magnetic forces. This term is sometimes referred to as the convective derivative and written as:

$$\rho_m \left(\frac{d\vec{U}}{dt} \right) = \rho_m \left[\frac{\partial \vec{U}}{\partial t} + (\vec{U} \cdot \vec{\nabla}) \vec{U} \right] \quad (12)$$

The terms on the right hand side of equation (11) represent a particle pressure gradient, the gradient in magnetic pressure (or energy density of the magnetic field), and a term describing the tension due to curvature in the magnetic field lines.

It is sometimes the case that there are no time dependent flows in the region of interest, or these flows may change on time scales much longer than those which are required for the spacecraft to encounter the plasma sheet (a few hours). If this assumption is true, and the acceleration term $(\vec{U} \cdot \vec{\nabla}) \vec{U}$ is also negligible, then the time derivative on the left-hand side of equation (11) will vanish. If it is also assumed that there is little curvature to the magnetic field lines then the $(\vec{B} \cdot \vec{\nabla}) \vec{B}$ term on the right hand side also vanishes. This assumption of minimal field line curvature is probably valid for most locations close to the magnetic equator and in the vicinity of the current sheet in Jupiter's magnetotail due to the highly stretched and nature of the magnetic field lines there. This stretched configuration, as contrasted with the near dipolar shape of the field closer to the planet is due in part to the mass loading of field lines with dense plasma from Io. As this plasma is centrifugally slung outward by the rapid spin of the planet, the

field lines become stretched into a long magnetotail. Jupiter's tail magnetic field generally points radially inward toward the planet north of the current sheet and radially outward south of the current sheet. As long as the spacecraft is not close to a magnetic merging region, frequently called an "x-line", or a region where the field lines are significantly curved, the field will be generally antiparallel and the field lines straight. With these simplifying assumptions, equation (11) reduces to

$$\vec{\nabla} \left(nkT + \frac{B^2}{2\mu_0} \right) = 0. \quad (13)$$

Integrating this equation gives

$$nkT + \frac{B^2}{2\mu_0} = \text{constant} \quad (14)$$

where n is the electron density, k is Boltzmann's constant, and T is the particle temperature. B is the magnetic field magnitude and μ_0 is the permeability of free space. The constant on the right-hand side of equation (14) has units of pressure. This equation indicates that total pressure across the plasma sheet (more rigorously, the total pressure directed normal to the plasma sheet) should stay constant across the plasma sheet. A hypothetical idealized graph depicting this relationship is shown in Figure 34.

Because the density data set provides values for n and the magnetic field data provides field magnitudes for B , there are two free parameters in the equation. The variable T and the undetermined constant can be subjected to a least squares fitting program to calculate the best pairs of values that fit the data.

The Least-squares Fitting Program

The first thing in accomplishing this was to convert both the magnetic field data set and the density data set to identical time resolutions in order to add the corresponding pressures together point by point. This was accomplished by averaging the 24 second resolution magnetic field data and the 36.67 second resolution density data over one minute intervals. Once a given value of T is chosen, the values from each data set can be used in equation (14) above, to get a total pressure. A least squares fitting program was developed to choose the value of T and then calculate the corresponding total pressure. For a given T , a best-fit constant straight line was fit to the total pressure curve and the chi-squared value was recorded. The program then steps through differing values of T , and calculates corresponding total pressures, homing in on the value of T that gives the minimum chi-squared for the best-fit constant pressure. The range of values for T used by the program was determined ahead of time by studying numerous crossings in the density and magnetic field data. Based upon the magnetic pressure maximum values outside the plasma sheet, and maximum densities inside the plasma sheet, an inclusive range for T was chosen.

An example of the program output can be seen in Figure 35. The plot window shows a time period of approximately five hours, or one-half of a Jupiter rotation period. Pressure is indicated on vertical scale. The red curve represents the pressure due to the particles, and is at every point equal to the product nkT . The blue curve on the plot indicates the magnetic pressure computed from the magnitude of the magnetic field. The black curve indicates the arithmetic sum of the red and blue curves (point by point) and the straight line in black represents the best constant value fit to the total pressure. The temperature T that provides this best fit for the total pressure is recorded in a data file along with the total pressure itself, and the relevant orbital parameters for each time

segment. The black triangle at the bottom of the plot indicates the actual location of the current sheet as determined by the radial component of the magnetic field. The magnetic field strength is much higher in the plasma-poor lobes of Jupiter's magnetosphere and reaches a local minimum when the center of the current sheet is encountered. The center of the current sheet is defined by the location where the value of the radial component of the field changes sign. This happens as the spacecraft crosses from the region of radially inward directed magnetic field above the current sheet, to the radially outward directed configuration below the current sheet.

The five-hour time segments were chosen by using Khurana's 1998 current sheet model to predict when the spacecraft would be at its maximum distance from the current sheet. Assuming the model is accurate, a single current sheet crossing should appear at the center of each five-hour plot. Not every five-hour time segment contains a sheet crossing, however. In some cases, the magnetometer registers multiple crossings in a five-hour period. In other cases, there was no evident crossing at all, or there was a complicated variation in the magnetic field that made determination of the plasma sheet crossing difficult. This may have been due to several factors. Availability of both the magnetic field data and the density data sometimes produces gaps in coverage and rendered some five-hour time segments unusable. Jupiter's current sheet location may vary in some cases from the predicted location by the model. There may have been fluctuations in the position of the plasma sheet relative to the spacecraft over the time scale in question. Depending on the radial distance of the spacecraft from Jupiter, a clear plasma sheet crossing is not always evident in the density data. At larger radial distances the identity of the individual plasma sheet crossings seems to vanish. This phenomenon has been noted from observing the entire set of color spectrograms, and from global

density displays of the entire magnetosphere (Figure 27). The significance of this is discussed in Chapter IV.

Analysis of Program Output

Over 1060 of these five-hour time segments were analyzed with the best T and the best-fit total pressure recorded for each. Each run of the fitting program also computes the maximum deviation of the data from the best-fit curve, as well as the average RMS deviation from the best-fit curve. These values can be compared to the maximum variations in the individual pressures as well as to each other in order to get a numerical assessment of the quality of the fit. Before inclusion of the best-fit values in the analysis, a visual inspection of each run of the fit program was made for two main reasons. The first reason for the visual inspection is that it was necessary to determine if the density and the magnetic field varied significantly with an opposite correlation as the spacecraft crosses the plasma sheet. If there is no variation then no valid temperature can be calculated. This is because the relationship expressed in equation (14) for the constant pressure is the result of integrating equation (13). If there is no actual variation in the magnetic or particle pressures, then no useful information regarding T can come from integrating equation (13). If n and B were both constant, then *any* value of T would provide a solution to equation (14). The second reason for the visual inspection was to get a general idea of the quality of curve fits to go along with the numerical chi-squared values. Five separate categories were identified in this visual inspection. The categories are described in Table 2. The first category consisted of plots where the best-fit curve to the total pressure was good everywhere throughout the time period. On these plots there were no significant deviations of the data from the best-fit curve. The data were consistently flat throughout the entire time segment. Category two included data that were fairly consistent with the best-fit curve everywhere in the plot. There were some

minor deviations of the data from the best fit but the data could be best described as variably flat. The third category included data that was variable during much of the time segment. These plots were usually characterized by one or more significant deviations of the data from the best fit, or by extended minor deviations from the best fit. The isolated significant deviations usually occurred near the center of a plot where the magnetic field was at a minimum. Any extended minor deviations usually occurred both above and below the best-fit curve. The single term description of these plots was variable. The fourth category of plots was characterized as a poor fit. These plots exhibited significant deviation of the data from the best-fit line the route the entire plot. The data were often chaotic and bore little resemblance to the best-fit curve at all.

The fifth and final category was a miscellaneous category and consisted of plots that were unusual or difficult to categorize. Some of the problems with these plots included too much missing data or gaps in the data, too short a time periods to be useful (not enough data to properly characterize a plasma sheet crossing), otherwise irregular data, or data that did not resemble plasma a sheet crossing. Some plots included in category five indicated time periods where no fit was readily calculable, or where there was no clear variation in the two curves to reliably compute a temperature. Only density data with the two best confidence quality flags and only data where f_p was known to be greater than f_c were included in the fit program. These category 5 plots represented 24% of the 1063 time segments and were not analyzed.

Many complicated looking sheet crossings were included in categories 1 through 3. For example, many were multiple crossings. Some of the individual data sets were interesting in their own right. Some of the plots despite their flatness or variability indicated that the particle pressure was less than the magnetic pressure consistently through the plot. There were others where the magnetic pressure was consistently less

than the particle pressure. There were also a significant number of plots where the minimum magnetic field strength and/or the peak density were significantly offset from the center of the plot, indicating poor agreement with the plasma sheet model for that particular crossing. Regardless of some of these irregularities, there was a consistent diamagnetic effect seen in most of the plots. Of the 1063 plots approximately 18% were category one, 28% were category two, 24% were category three, and 6% were category four. Approximately half of all of the pressure fits fell in the top two categories and it was these cases that were retained for further examination. Even after all the restrictions, designed to increase the accuracy and validity of the fits, were applied, there were still over 480 cases for which a best fit T , and a best fit total pressure were determined. In each of these cases the RMS deviation from the best fit normalized to the total pressure, was less than 20%. This is indicated in Figure 36.

Pressure and Temperature

The results of the temperature calculation can be seen in Figures 37 and 38. According to the program output, typical temperatures in the plasma sheet are around 10^8 K, corresponding to energy of just less than 10 keV. Ion energies of 0.1 to 10 keV were estimated to make dominant contributions to the plasma pressure by Goertz et al. [1979] based on Pioneer 10 data. The particle energies determined by Voyager instruments ranged from about 1 keV [McNutt et al., 1981], to a range of 20-45 keV [Krimigis et al., 1981; Krimigis and Roelof, 1983]. It is believed that in the middle and outer magnetosphere of Jupiter, the rapid spin of the planet indirectly imparts this energy to the colder outward-moving Io torus plasma. It should be noted that the parameter T , obtained using this computer routine is not the temperature of any individual particle species. In this analysis, it is assumed that the density $n = n_e = n_i$. Since the total pressure is the sum of the electron pressure and the ion pressure, it follows that T is the

arithmetic sum of the ion temperature and the electron temperature. In order to compute the actual temperatures of any given particle species, the ratio of electron temperature to ion temperature would be needed, and more information about ion distributions in the plasma. It should also be realized that the electrons are *not* assumed to account for the entire component of the particle pressure in the best-fit program, despite the use of $n = n_e$ in Equation (14). Van Allen [1979], using Pioneer 10 data, reported that the intensity of energetic electrons was well correlated with the drop in magnetic pressure in the plasma sheet. However, these energetic electrons provide only a small fraction (about 3%) of the total particle pressure in Jupiter's plasma sheet. Ions are believed to make the dominant pressure contribution [Van Allen, 1979; Goertz et al., 1979], as they also do at the Earth. A description of the ion composition and temperature in the plasma sheet at Jupiter is necessary for a complete picture of total pressure balance.

From Figures 37 and 38, it is apparent that the temperature of the plasma sheet is highly variable. The same statistical analysis was done to the temperature and pressure data, this time using the RMS deviation as a basis for evaluating the uncertainty. The reduced χ^2 values are high for each fit because of the large amount of scatter in the data. With the pressure profile, it is visually obvious that a general radial trend exists in the data. In the case of temperature, it is not as clear, but the correlation coefficient, R, for both pressure and temperature fits indicate that there is a radial relationship in the data with a confidence level of 99.9%. The best-fit power law to this data indicates that the average temperature decreases with radial distance from Jupiter as $(1/r)^{0.81 \pm 0.01}$, though actual temperature values vary by a factor of 5 above and below this fit. The clearer trend in the total pressure can be seen in Figures 39 and 40. The average total pressure scales as a power law proportional to $(1/r)^{2.23 \pm 0.01}$, with about a factor of 2 scatter about the fit. In order to satisfy the relationship $P = nkT$ (where P is the total particle pressure),

the exponents on the radial pressure, density, and temperature profiles must satisfy the relation where

$$r^\gamma \propto r^\alpha r^\beta. \quad (15)$$

If density and temperature have a radial dependence, α and β , respectively, then the radial dependence of the pressure, γ , should be the sum of α and β . Because of the high degree of scatter about the specific power law best fits, it is not surprising that they only satisfy this relationship to within about 35%. Again, it should be noted that this is frequently the case with data from Jupiter's magnetosphere. Because our data set covers multiple orbits and a long time scale, it is likely that variable conditions produced by solar wind variations and Io plasma production are responsible for the high degree of scatter in the data. Careful analysis of observations on shorter time scales, supported by other data sets (such as density or speed of the solar wind at Jupiter) may produce better power laws that describe specific variations in pressure or temperature with identifiable causes. However, that is beyond the scope of this work. It is the intent of this work only to identify the average trends in the whole of the density data set.

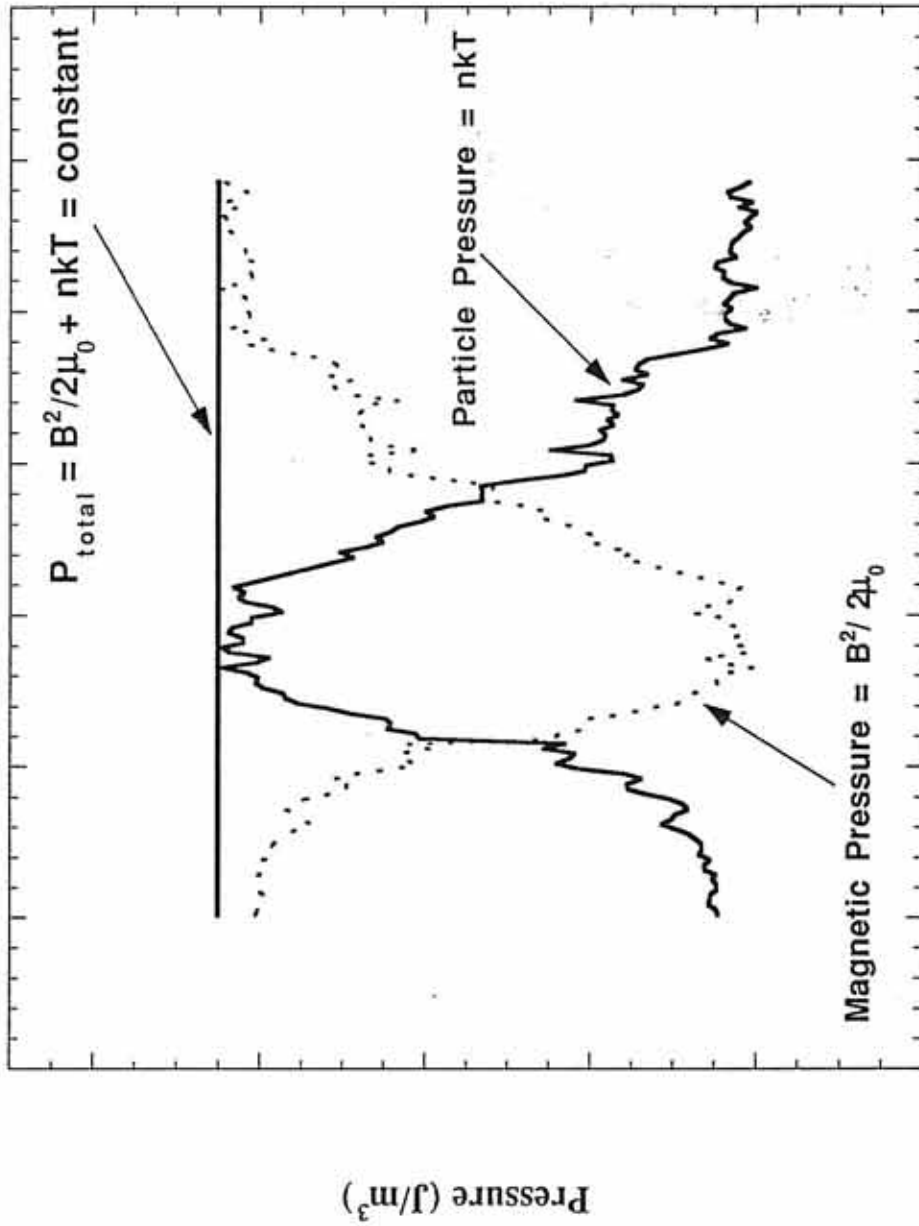
Because the total plasma sheet pressure is dominated by the magnetic field in the high magnetic latitude lobes of the magnetosphere, this pressure trend can be used to describe the magnetic field's influence on the shape of Jupiter's nightside magnetopause. Some limiting cases for the shape of Jupiter's tail magnetopause can be considered to place constraints on the magnetic pressure profile. If the magnetic field had a purely radial configuration in the magnetotail, with a conical magnetopause, as in Figure 41, then the magnetic field would decrease as $(1/r)^2$ with increasing radial distance, and B^2 would scale as $(1/r)^4$. If the magnetic field were purely radially away from the planet, with a cylindrical magnetopause, then the magnetic field lines in the magnetotail would be parallel, and B would remain constant with increasing distance away from Jupiter. As

a result, the magnetic pressure (B^2) would also remain constant with distance from the planet, and would scale as $(1/r)^0$. Because we see that magnetic pressure (which depends on B^2) scales as $(1/r)^{2.23}$, the shape of the tail magnetopause at Jupiter lies somewhere between that of a cylinder and a cone. As this power law seems fairly uniform between 20 and at 140 Jovian radii, it would seem that the flare angle (which determines the shape of the magnetopause) stays fairly constant in this region.

Category	Quality	Description	Deviations from best fit	Often
1	Very Good	Consistently Flat	Only small (< 10%), brief deviations from best fit	18%
2	Good	Variably Flat	Slightly larger (< 20%), perhaps longer deviations from best fit	28%
3	Variable	Some Significant Deviations	Some larger deviations (generally $20\% < d < 50\%$)	24%
4	Poor	Chaotic	Very large (> 50%) deviations or for long duration	6%
5	Unusual	No fit	Unknown	24%

Table 2. Pressure Fit Categories

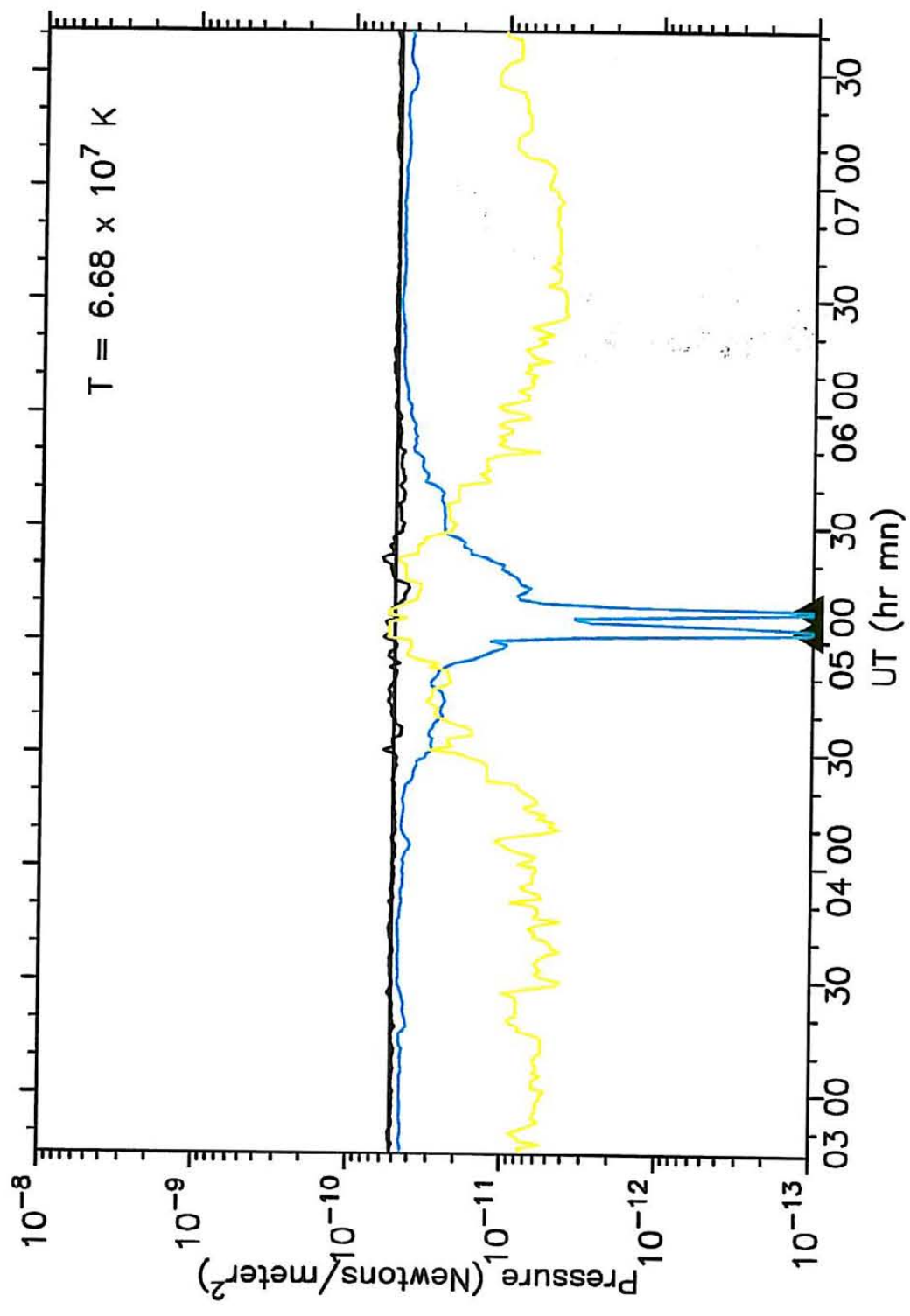
Figure 34. Idealized pressure balance. An idealized situation showing the sum of particle pressure and magnetic pressure during a plasma sheet crossing. If the total pressure is constant, the least squares fit program described in the text is used to get values of T and total pressure.



Spacecraft Time (Hours)

Figure 35. Temperature and pressure. An example of the output of a computer program designed to compute the best-fit temperature for a given plasma sheet crossing (about 5 hours of data). The red curve is the particle pressure calculated using the best-fit temperature, the blue curve is the magnetic pressure, and the black curve is the sum of the red and blue curves. The straight line is the best-fit constant value to the total pressure (black curve). The best-fit temperature is indicated in the upper right corner of the plot window. The black triangles at the bottom of the plot indicate where the magnetometer identifies the actual crossing of the center of the plasma sheet (the current sheet).

1997 170 (June 19) 02:44:16 - 07:41:04



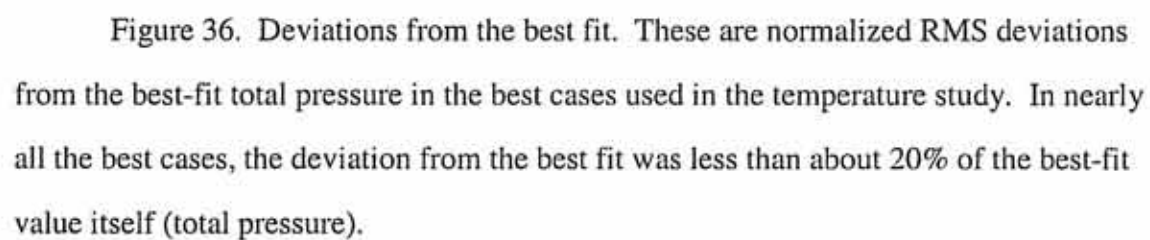


Figure 36. Deviations from the best fit. These are normalized RMS deviations from the best-fit total pressure in the best cases used in the temperature study. In nearly all the best cases, the deviation from the best fit was less than about 20% of the best-fit value itself (total pressure).

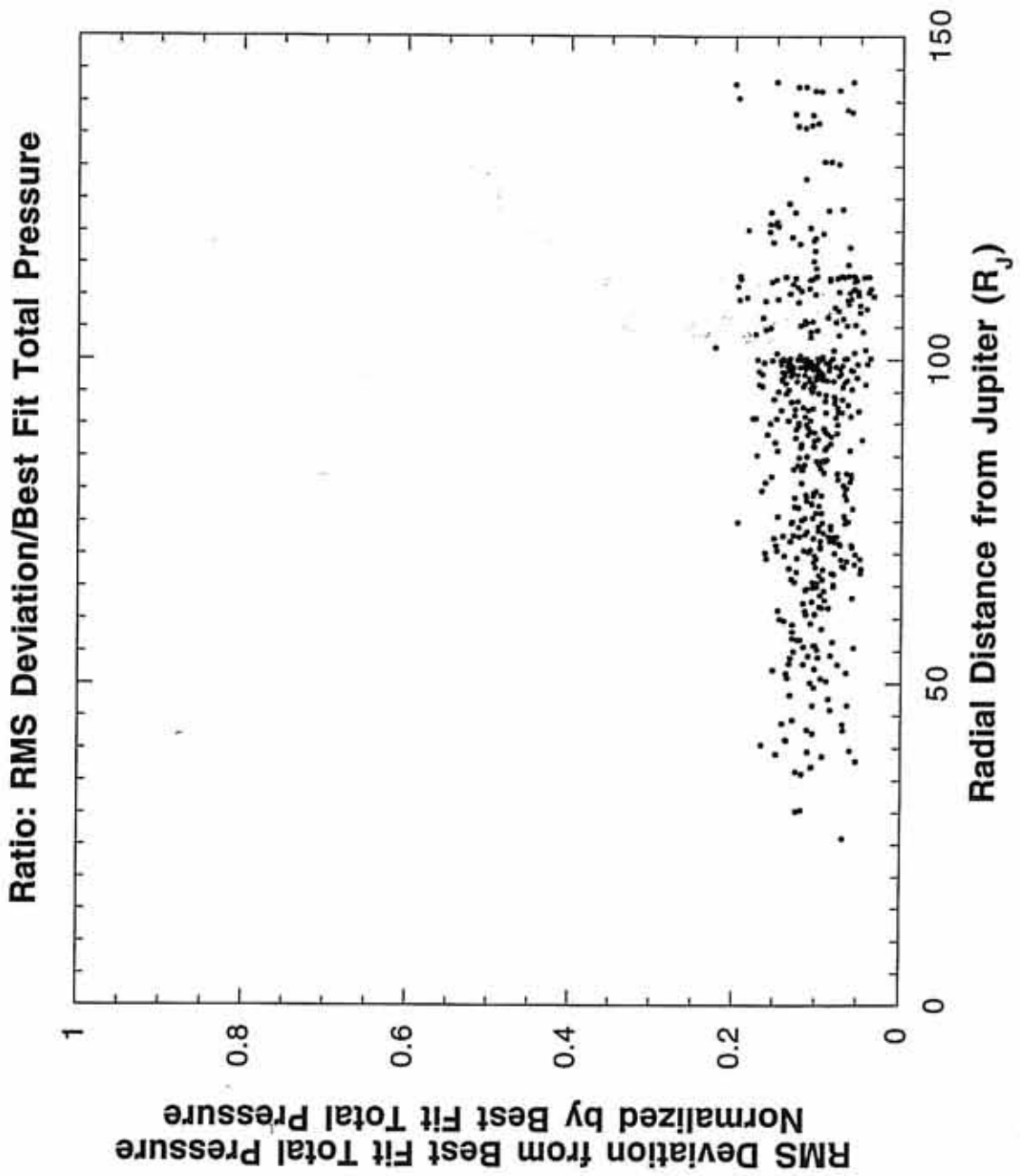
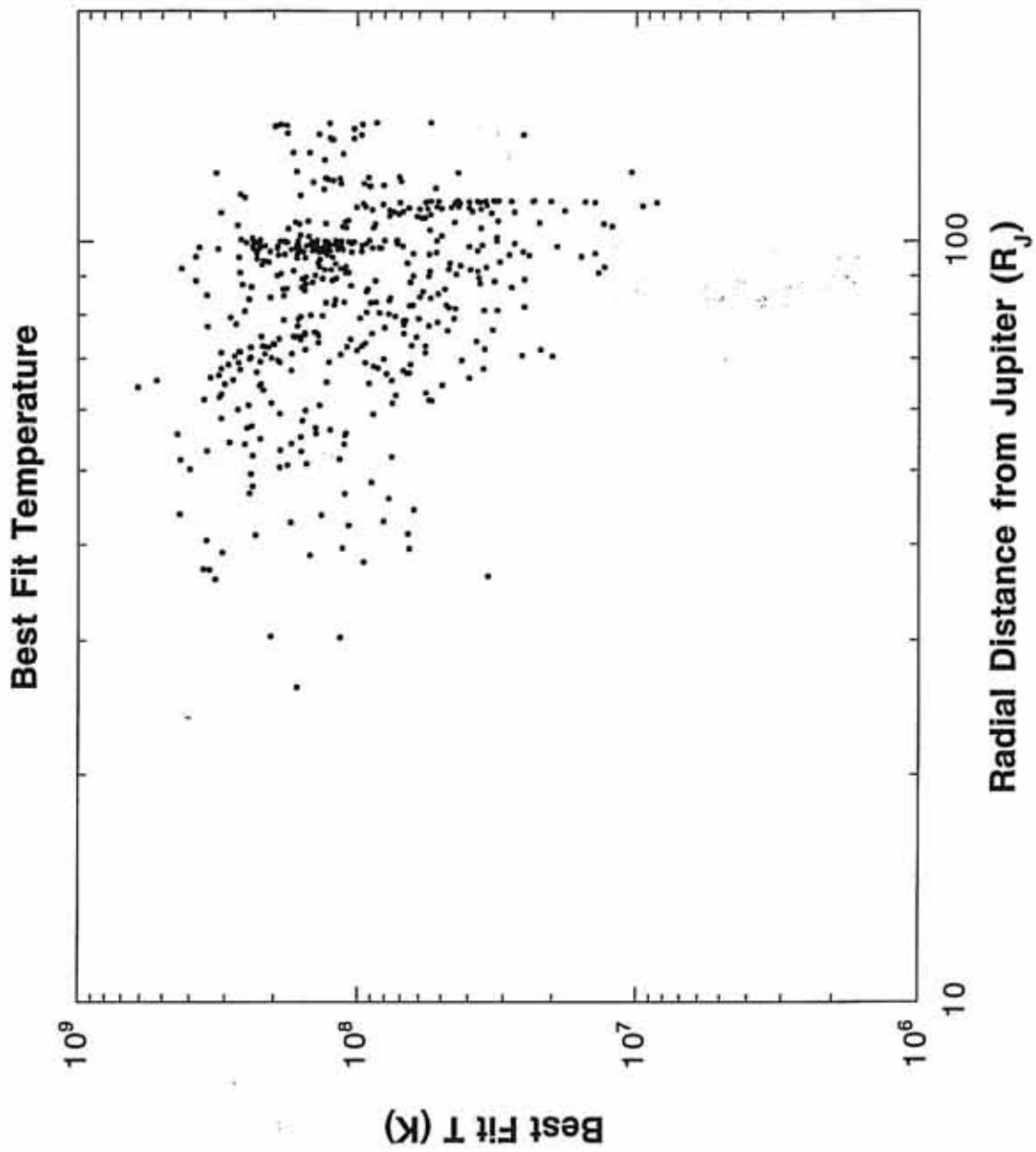


Figure 37. The best fit temperatures. These values of temperature are from the cases described in Figure 36, and plotted as a function of radial distance from Jupiter.




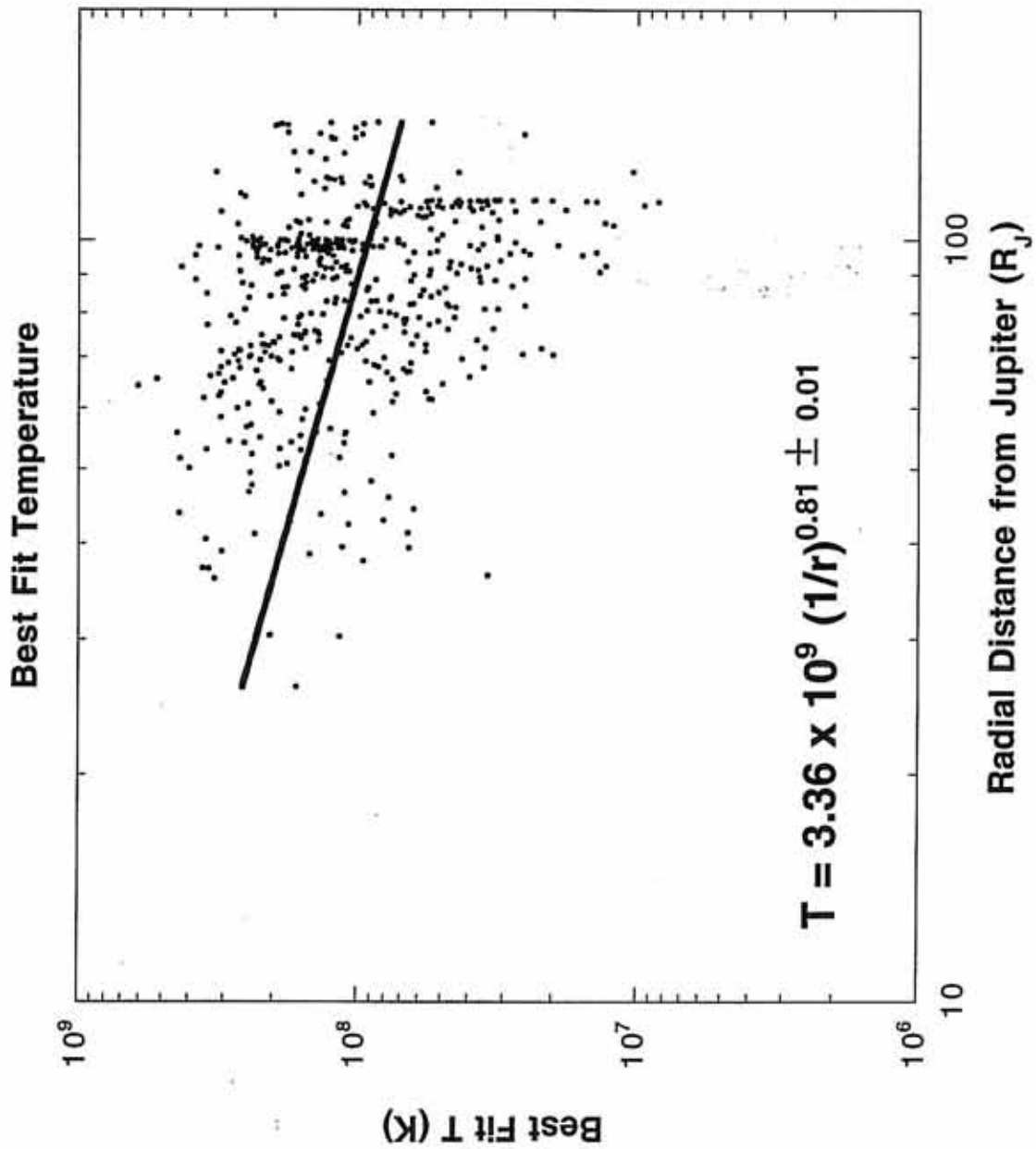


Figure 38. Radial temperature profile. The same data in Figure 37, with a best fit power law to the data. Although there is a great deal of scatter in the data, there is a weak trend toward lower plasma sheet temperatures with increasing radial distance from Jupiter. The power law scales as $(1/r)^{0.81 \pm 0.01}$.




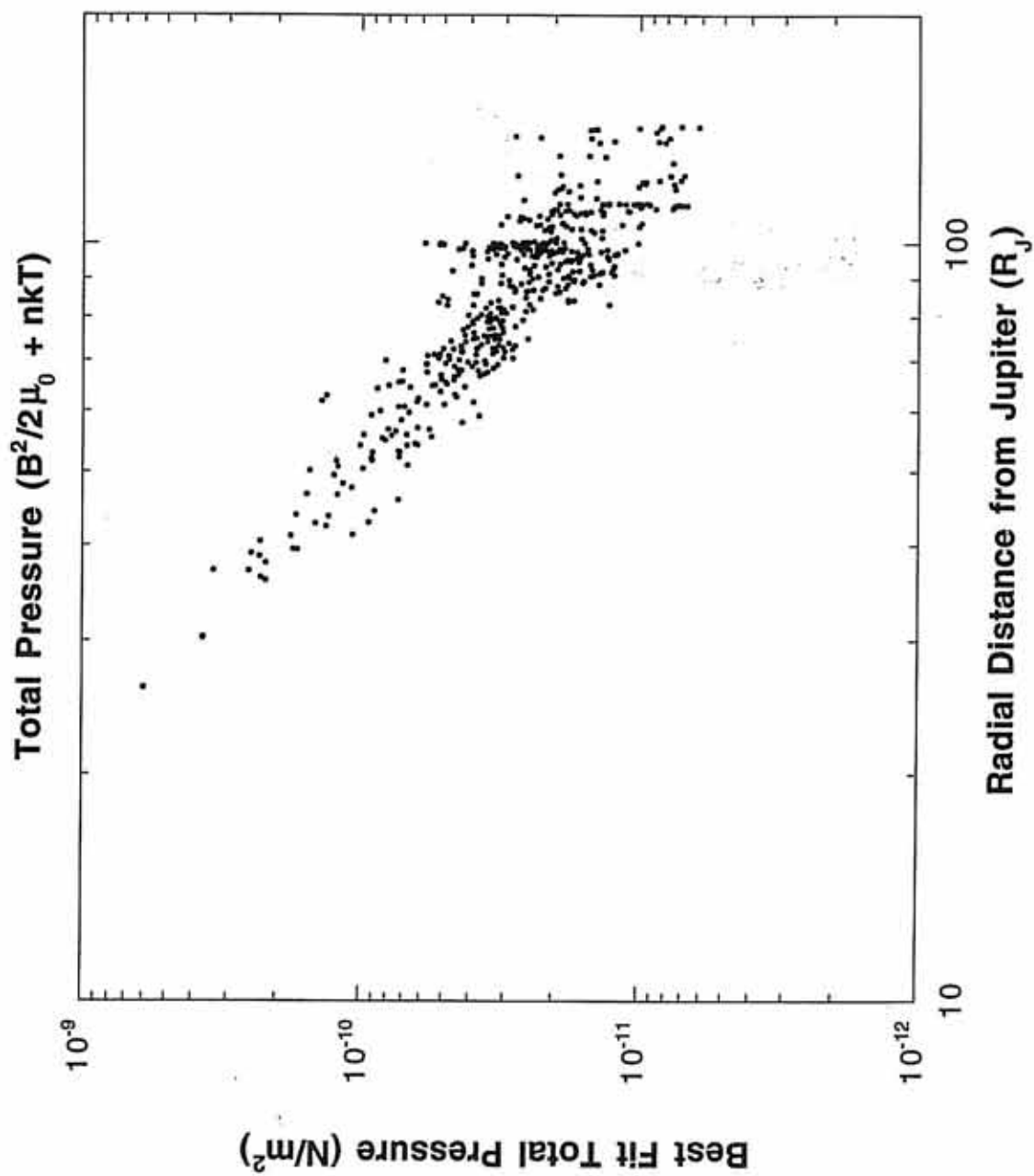


Figure 39. Total pressure. The best-fit (constant) total pressures in the plasma sheet, plotted as a function of radial distance from Jupiter.




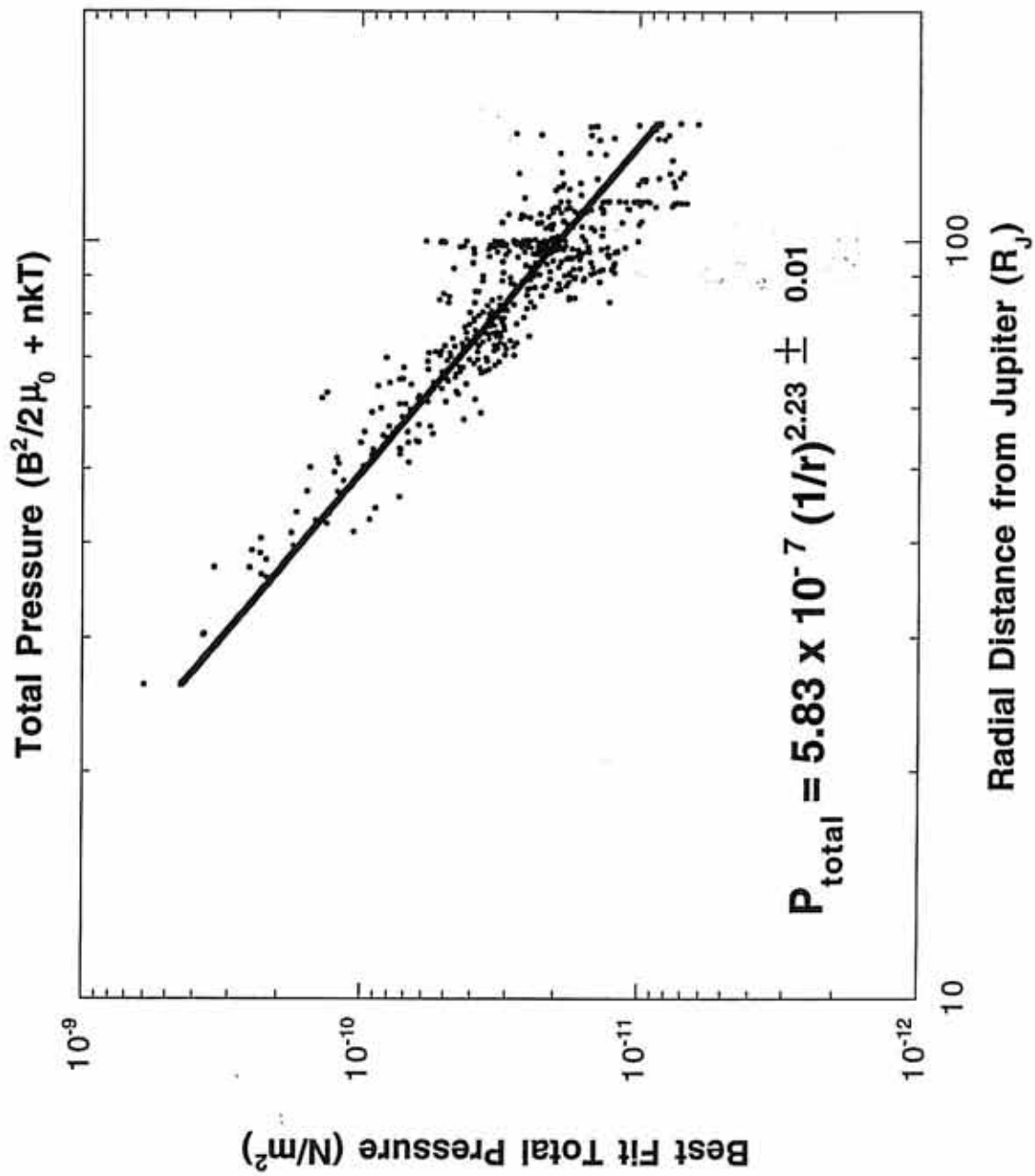


Figure 40. Radial total pressure profile. The same data in Figure 39, with a best fit power law to the data. There is significantly less scatter in this plot, and the power law indicates that average pressure in the plasma sheet decreases as $(1/r)^{2.23 \pm 0.01}$. Since the particle pressure is nearly zero outside the plasma sheet, this can be thought of as a measure of magnetic field pressure as a function of radial distance from Jupiter.




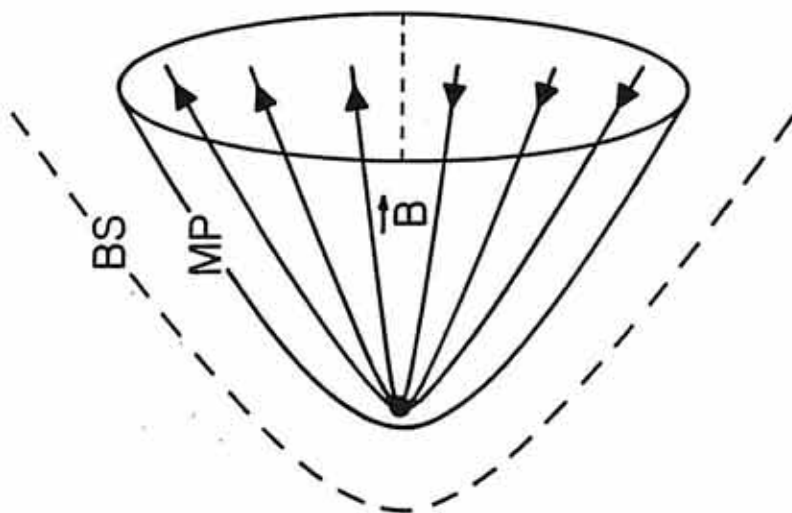


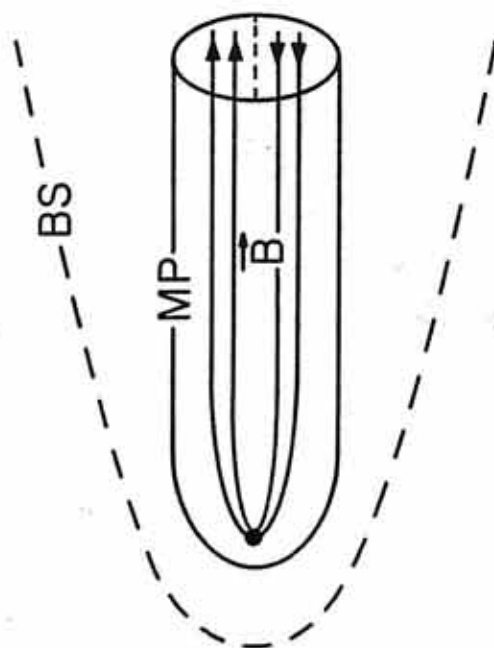
Figure 41. Tail magnetopause geometry. A diagram showing the two bounding cases for Jupiter's magnetopause configuration. If the magnetic field were radial in the magnetotail, (a conical magnetopause), magnetic pressure (B^2) would scale as $(1/r)^4$. If the field were everywhere parallel in the tail (a cylindrical magnetopause), magnetic pressure would be seen to scale as $(1/r)^0$. The data shown in Figure 40 indicate a situation somewhere in between.

A-GOI-138

TO SUN
←



$$B_{\text{tail}} \propto \frac{1}{r^2}$$



$$B_{\text{tail}} \propto \frac{1}{r^0}$$

CHAPTER VII: SUMMARY AND RESULTS

Plasma wave data from the entire Galileo primary mission has been processed and an electron density data set has been generated with 37.33-second time resolution. This data set constitutes the first measurements of the global electron density at Jupiter. The density values are accurate to within about 17% and are a proxy for the electron density at the location of the spacecraft. During limited portions of the Galileo mission, the plasma wave instrument does not detect continuum radiation, or other wave modes prohibit accurate determination of the plasma frequency. In regions close to Jupiter (approximately $r < 30 R_J$), electron density can be determined using the upper hybrid frequency. When this data is added to the main data set, a radial profile of electron density at Jupiter can be produced. This radial profile shows a steep power law close to Jupiter proportional to $(1/r)^{6.65 \pm 0.05}$, and a more gentle decrease with radial distance for $r > 20 R_J$, proportional to $(1/r)^{2.14 \pm 0.01}$. This change of power law slope at about $20 R_J$ may be related to the change in the configuration of Jupiter's magnetic field at this distance from a dipolar field to a more stretched configuration. In addition, the magnetospheric plasma's departure from co-rotation with Jupiter and the subsequent azimuthal sweepback of field lines begins to occur at this distance. Though the density varies by a factor of 2 from the best fits, there is clear correlation between the average density and radial distance, and these power laws are reported as general trends.

Global displays of the magnetosphere of Jupiter indicate that the plasma sheet, as identified by the higher electron density close to the magnetic equator, loses its definition and identity at radial distances $r > 50 R_J$. The electron density close to the magnetic

equator has values similar to the electron density at higher magnetic latitudes in the outer magnetosphere. This "vanishing" of the plasma sheet has also been noted by looking at the plasma wave data itself. The occasional disappearance and reappearance of continuum radiation at large radial distances from Jupiter indicated that the spacecraft crossed the magnetopause and entered the magnetosheath several times during the orbit prior to the first close approach to the large moon Ganymede. Voyager models of the magnetopause in the region where the spacecraft was located, and magnetometer data from the same time periods confirm the spacecraft's encounters with Jupiter's magnetosheath.

The adoption of the Khurana magnetodisc model to organize the PWS density data with respect to different regions of the magnetosphere has been generally successful. The ability of this model to predict the location of Jupiter's current sheet, especially in the inner magnetosphere, has been utilized to further characterize the plasma sheet encounters and has helped to place the density data within a context for analysis. The Khurana model does a good job of predicting plasma sheet crossings in the inner magnetosphere, but does a significantly poorer job at radial distances $r > 50 R_J$. The density data from this project preliminarily confirm the hinged-disc quality of the Khurana model, at least in the inner magnetosphere. However, a more detailed comparison of density data to specific other predictions of the model would be useful. A cartoon sketch of Jupiter's magnetosphere based upon the density data and the general predicted shape from the Khurana model is shown in Figure 42.

Using the Khurana model to find the maximum spacecraft positions away from the plasma sheet, five-hour half-rotations, each containing a plasma sheet crossing, were examined to study pressure balance across the plasma sheet. Using magneto-hydrodynamic equations, a simple relationship between the plasma pressure and

magnetic field pressure has been derived. This pressure balance equation has been incorporated into a least squares fitting program designed to calculate temperature and total pressure parameters through the plasma sheet. Analysis of these output values over large radial distances provides a pressure and temperature profile in Jupiter's plasma sheet at radial distances between $20 R_J$ and $140 R_J$.

The temperatures computed by the least squares fit program are typically around 10^8 K, which correspond to energies around 10 keV. These values fall within the ranges for plasma temperatures reported by Pioneer and Voyager at Jupiter. The average total pressure showed a radial power law fall-off proportional to $(1/r)^{2.14 \pm 0.01}$. The average temperature was nearly constant, but decreased slowly with radial distance, scaling as a power law proportional to $(1/r)^{0.81 \pm 0.01}$. There is a large statistical scatter about these best-fit values, but in each case (most clearly with the pressure), there is a 99.9% confidence that correlation between these quantities and radial distance from Jupiter is not random. The exponents on the power laws should be considered representative of global average trends rather than a specific functional dependence.

The pressure change over large radial distances is indicative of the magnetic field pressure in the lobes of Jupiter's magnetosphere, and affects the shape of the magnetopause at large distances in the magnetotail. Looking at limiting geometric cases for the tail magnetopause configuration, constraints can be placed on the expected fall-off of pressure in the magnetotail. The pressure profile determined herein implies a shape somewhere between a cylindrical magnetotail and a conical one. This shape is consistent with spacecraft observations. A summary of the radial profile parameters discussed throughout the text, and their statistical analysis parameters can be found in Table 3. The large degree of scatter about the best fit in each of the radial profile plots indicate that there is a large degree of variability in density, temperature, and pressure conditions in

Jupiter's magnetosphere. Despite the assumed dominance of internal forces at Jupiter, this variability is likely caused by solar wind variations or production of plasma at Io occurring on time scales much shorter than the length of coverage of this dataset. This may indicate the presence of substorm-like activity, though there is no clear evidence for that here. Further analysis of this density data set on short time scales (single orbits or less), rather than overviews of the entire mission, may improve our understanding of this variability.

Quantity	Symbol	Radial Power Law Dependence (best fit)	Reduced χ^2	R, Linear Correlation Coefficient
Peak Electron Density (Determined from Upper Hybrid Waves)	n_e	-6.55 ± 0.05	12.90	0.98
Peak Electron Density in Plasma Sheet (Determined from Continuum Cutoff)	n_e	-2.14 ± 0.01	19.89	0.80
Best-Fit Total Pressure in Plasma Sheet	P_{total}	-2.23 ± 0.01	13.00	0.89
Best Fit Temperature in Plasma Sheet	T	-0.81 ± 0.01	58.25	0.38

Table 3. Radial Profile Fit Parameters

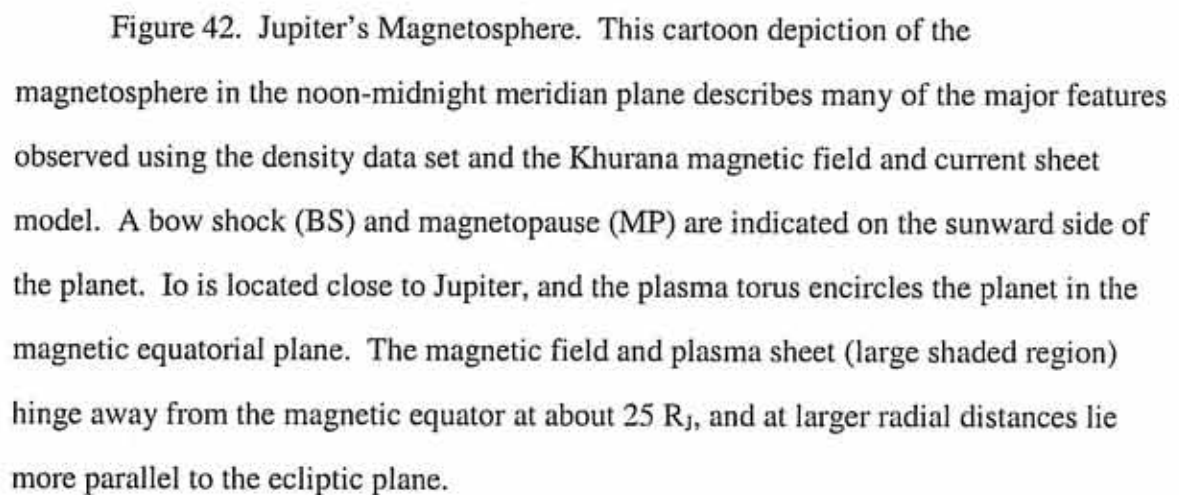
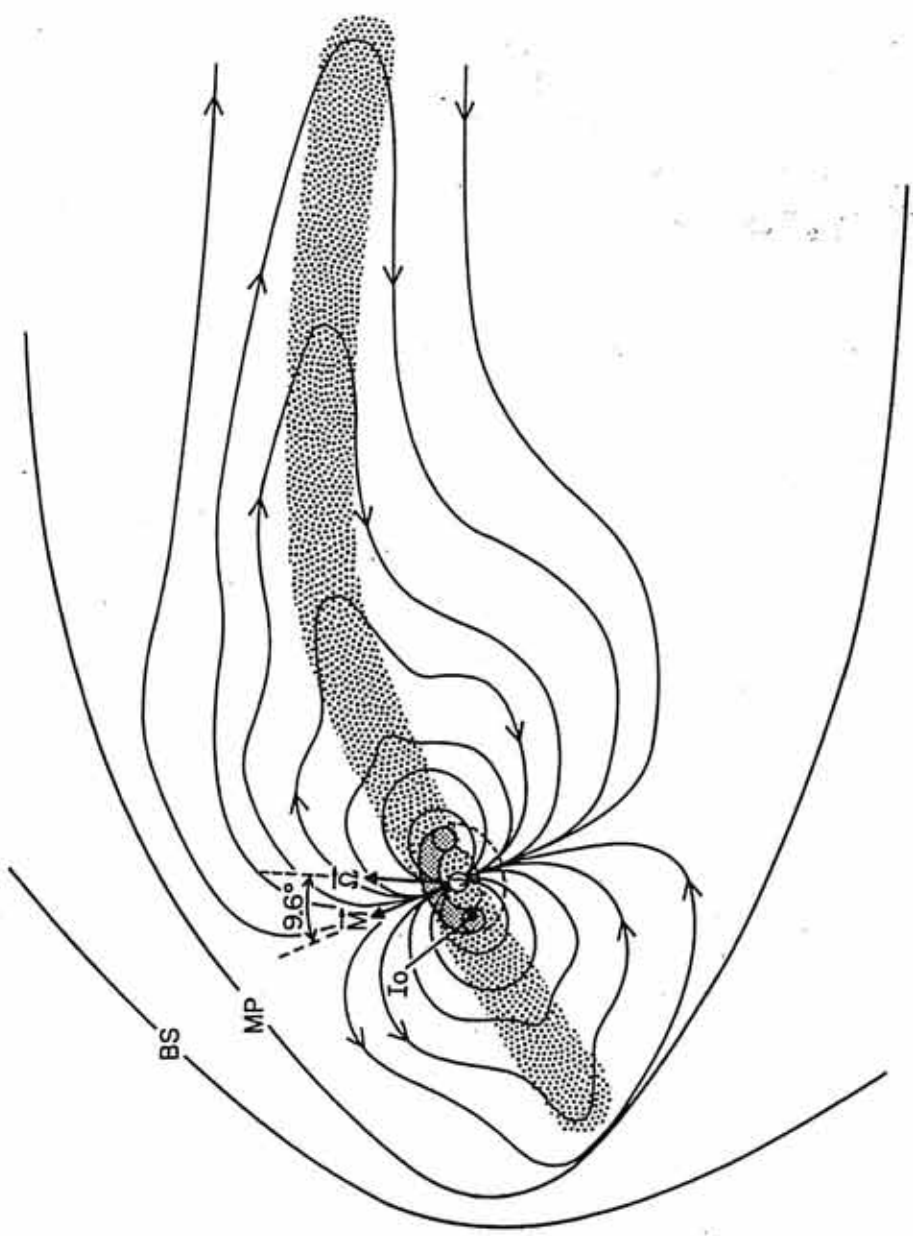


Figure 42. Jupiter's Magnetosphere. This cartoon depiction of the magnetosphere in the noon-midnight meridian plane describes many of the major features observed using the density data set and the Khurana magnetic field and current sheet model. A bow shock (BS) and magnetopause (MP) are indicated on the sunward side of the planet. Io is located close to Jupiter, and the plasma torus encircles the planet in the magnetic equatorial plane. The magnetic field and plasma sheet (large shaded region) hinge away from the magnetic equator at about $25 R_J$, and at larger radial distances lie more parallel to the ecliptic plane.

A-601-139



CHAPTER VIII: FUTURE RESEARCH

General Comments About the Data Set

The data from Galileo's primary mission is the focus of this dissertation project, however with additional funding that was made available, the plasma wave instrument (PWS) was operated for a large portion of the extended Galileo Europa Mission (GEM). A somewhat smaller data set than that of the primary mission has been available for analysis. A future project adding the additional GEM density data to the primary mission analysis is possible. The data will eventually be made available to other members of the scientific community, and further analysis of the data may be carried out. Specific regions of interest may be scrutinized, and global orbit-to-orbit features could be compared, to better understand time-dependent phenomena.

In some cases, multiple radio wave signals exist in the same frequency range as the plasma frequency. A well-defined method for deriving a density from these time periods should be developed. This would add a significant amount of density data to the data set. Many of the regions where the overlapping of wave modes complicates density determination occur during regions of interest (e.g. plasma sheet boundaries).

Analysis Projects

Time Dependent Phenomena and Substorms

Because of Galileo's unique capability to encounter some regions of the Jovian system multiple times, it is possible to compare a given region in magnetosphere at different times to get a time dependent picture of its behavior and structure. Such a time dependent picture may help us compare Jupiter's magnetosphere to our current working

understanding of magnetic substorms and magnetospheric convection at the Earth. There has been some evidence of Jovian auroral enhancements, energetic particle populations, and other periodic wave phenomena that are attributed to substorm activity at the Earth. Galileo is making multiple orbits of Jupiter, and can study these phenomena over long time periods. Some recent papers have been published that try to address the question of whether Jupiter experiences substorms in a similar manner to the Earth.

Louarn et al. [1998] describe periodic "energetic phenomena" in Jupiter's magnetosphere. They use the PWS instrument to describe the plasma sheet and the large-scale magnetospheric structure, but they focus on disturbances in the radio emissions. Russell et al. [1999] also consider the current sheet, but describe it using the magnetic field configuration. They are more concerned with small-scale magnetic field structures and their relationships to explosive reconnection events at large radial distances.

Plasma Transport

The electron density data set can be used in identification of plasma enhancements and rarefactions in Jupiter's magnetosphere. This information can be used to test theories of plasma transport. It can be compared to previous work in this area using Voyager data, and it can also be compared to numerical models. If the data indicate it is necessary, additions or corrections can be made to existing models, or a new model of plasma transport could be developed.

Test of Current Sheet Models

A technique that could be developed further is to model the density during the plasma sheet crossings using a mathematical function. Many of the plasma sheet encounters have been identified and plotted using the Khurana current sheet model. There are a wide variety of shapes, sizes, and configurations among the plasma sheet encounters in the data set. The individuality in appearance makes it difficult to compare

the crossings without establishing a common system for describing them. One suggested solution has been to model each crossing mathematically and have a computer algorithm find the best fit to the density data of each crossing. This database of sheet crossings can then be drawn upon to make many comparisons. One inbound pass or one orbit can be studied, and the plasma sheet parameters can be plotted to indicate any trends or variations in thickness or "vertical shift" of the plasma sheet. The properties of the plasma sheet represented by the best-fit parameters hold some importance in determining the large-scale behavior of the plasma sheet, and the magnetosphere as a whole.

There have been recent theoretical predictions about the structure of the current sheet based upon particular magnetic field configurations [Vasyliunas, 1999]. A bunching of magnetic field lines at a measurable distance above or below a model current sheet could affect the predicted location for such a current sheet. The density data set can be used to test them.

Io Torus Models

Another possible project is to use the PWS-derived density values to try and calculate total flux tube plasma content. A flux tube can be described as a volume of plasma in the shape of a tube that centers on a particular magnetic field line. The total plasma content of a flux tube should stay constant as it convects through space, and is given by the expression:

$$\eta = \int \frac{n_e}{B} ds \quad (16)$$

where η is the plasma content, n_e is the electron density, B is the magnetic field magnitude (a function of position along the field line), and the path integral is taken along the field line. Because the PWS density measurements are at only a single location along

the flux tube (near the equator), some model of density along the magnetic field line would be needed to carry out such an analysis.

REFERENCES

- Acuña, M. H., K. W. Behannon, and J. E. P. Connerney, Jupiter's Magnetic Field and Magnetosphere, in *Physics of the Jovian Magnetosphere*, edited by A. J. Dessler, pp. 1-50, Cambridge University Press, New York, 1983.
- Akasofu, S.-I., *Polar and Magnetospheric Substorms*, Springer-Verlag, New York, 1968.
- Ansher, J. A., W. S. Kurth, D. A. Gurnett, and C. K. Goertz, High Resolution measurements of density structures in the Jovian plasma sheet, *Geophys. Res. Lett.*, 19, 2281, 1992.
- Ansher, J. A., *Density Structures in the Jovian Magnetosphere*, M.S. Thesis, Department of Space Physics and Astronomy, Rice University, 1994.
- Bagenal, F., J. D. Sullivan, and G. L. Siscoe, Spatial distribution of Plasma in the Io torus, *Geophys. Res. Lett.*, 7, 41, 1980.
- Barbosa, D. D., D. A. Gurnett, W. S. Kurth, and F. L. Scarf, Structure and properties of Jupiter's magnetoplasma disc, *Geophys. Res. Lett.*, 6, 785, 1979.
- Bridge, H. S., J. W. Belcher, A. J. Lazarus, J. D. Sullivan, F. Bagenal, R. L. McNutt, Jr., K. W. Ogilvie, J. D. Scudder, E. C. Sittler, V. M. Vasyliunas, and C. K. Goertz, Plasma observations near Jupiter: Initial results from Voyager 2, *Science*, 205, 972, 1979.
- Burke, B. F., and K. L. Franklin, Observations of a variable radio source associated with the planet Jupiter, *J. Geophys. Res.*, 60, 213, 1955.
- Dessler, A. J., and T. W. Hill, High-order magnetic multipoles as a source of gross asymmetry in the distant Jovian magnetosphere. *Geophys. Res. Lett.*, 2, 567, 1975.
- Dessler, A. J., (Ed.), *Physics of the Jovian Magnetosphere*, 544 pp., Cambridge University Press, New York, 1983.
- Dungey, J. W., Interplanetary magnetic field and the auroral zones, *Phys. Rev. Lett.*, 6, 47, 1961
- Dungey, J. W., The length of the magnetospheric tail, *J. Geophys. Res.*, 70, 1753, 1965.
- Goertz, C. K., D. E. Jones, B. A. Randall, E. J. Smith, and M. F. Thomsen, Evidence for open field lines in Jupiter's magnetosphere, *J. Geophys. Res.*, 81, 3393, 1976.

- Goertz, C. K., A. W. Schardt, J. A. Van Allen, and J. L. Parish, Plasma in the Jovian current sheet, *Geophys. Res. Lett.*, 6, 495, 1979.
- Gurnett, D. A., and R. R. Shaw, Electromagnetic radiation trapped in the magnetosphere above the plasma frequency, *J. Geophys. Res.*, 78, 8136, 1973.
- Gurnett, D. A., and L. A. Frank, Thermal and suprathermal plasma Densities in the outer magnetosphere, *J. Geophys. Res.*, 79, 2355, 1974.
- Gurnett, D. A., The earth as a radio source: The nonthermal continuum, *J. Geophys. Res.*, 80, 2751, 1975.
- Gurnett, D. A., W. S. Kurth, and F. L. Scarf, Plasma wave observations near Jupiter: Initial results from Voyager 2, *Science*, 206, 987, 1979.
- Gurnett, D. A., W. S. Kurth, and F. L. Scarf, The structure of the Jovian magnetotail from plasma wave observations, *Geophys. Res. Lett.*, 7, 53, 1980.
- Gurnett, D. A., F. L. Scarf, W. S. Kurth, R. R. Shaw, and R. L. Poynter, Determination of Jupiter's electron density profile from plasma wave observations, *J. Geophys. Res.*, 86, 8199, 1981.
- Harel, M., R. A. Wolf, P. H. Reiff, R. W. Spiro, W. J. Burke, F. J. Rich, and M. Smiddy, Quantitative simulation of a magnetospheric substorm1, model logic and overview, *J. Geophys. Res.*, 86, 2217, 1981.
- Hill, T. W., Inertial limit on corotation, *J. Geophys. Res.*, 84, 6554, 1979.
- Hill, T. W., Corotation lag in Jupiter's magnetosphere: Comparison of observation and theory, *Science*, 207, 301, 1980.
- Hill, T. W., A. J. Dessler, and L. J. Maher, Corotating magnetospheric convection, *J. Geophys. Res.*, 86, 9020, 1981.
- Hill, T. W., Solar-wind magnetosphere coupling, in *Solar-Terrestrial Physics*, edited by R. L. Carovillano and J. M. Forbes, pp.261-302, D. Reidel Publishing Co., Dordrecht-Holland, 1983.
- Hill, T. W., A. J. Dessler, and C. K. Goertz, Magnetospheric Models, in *Physics of the Jovian Magnetosphere*, edited by A. J. Dessler, pp.353-394, Cambridge University Press, New York, 1983.
- Hill, T. W., and A. J. Dessler, Plasma Motions in Planetary Magnetospheres, *Science*, 252, 410, 1991.
- Hill, T. W., The shape and size of convection cells in the Jovian magnetosphere, in *Solar System Plasmas in Space and Time*, edited by J. L. Burch, and J. H. Waite, Jr., pp. 199-206, American Geophysical Union, Washington, DC, 1994.
- Joy, S., private communication, October 26, 2000.

- Kaufmann, W. J., and N. F. Comins, *Discovering the Universe*, 436 pp., Freeman and Co., New York, 1996.
- Khurana, K. K., M. G. Kivelson, T. P. Armstrong, and R. J. Walker, Voids in Jovian magnetosphere revisited: Evidence of spacecraft charging, *J. Geophys. Res.*, 92, 13399, 1987.
- Khurana, K. K., A generalized hinged-magnetodisc model of Jupiter's nightside current sheet, *J. Geophys. Res.*, 97, 6269, 1992.
- Kivelson, M. G., and C. T. Russell, eds., *Introduction to Space Physics*, 567 pp., Cambridge University Press, New York, 1995.
- Krimigis, S. M., J. F. Carbary, E. P. Keath, C. O. Bostrom, W. I. Axford, G. Gloeckler, L. J., Lanzerotti, and T. P. Armstrong, Characteristics of Hot Plasma in the Jovian Magnetosphere: Results from the Voyager Spacecraft, *J. Geophys. Res.*, 86, 8227, 1981.
- Krimigis, S. M., and E. C. Roelof, Low-Energy Particle Population, in *Physics of the Jovian Magnetosphere*, edited by A. J. Dessler, pp.106-156, Cambridge University Press, New York, 1983.
- Louarn, P., A. Roux, S. Perraut, W. Kurth, and D. Gurnett, A study of the large-scale dynamics of the Jovian magnetosphere using the Galileo plasma wave experiment, *Geophys. Res. Lett.*, 25, 2905, 1998.
- McNutt, R. L., Jr., J. W. Belcher, J. D. Sullivan, F. Bagenal, and H. S. Bridge, Departure from rigid corotation of plasma in Jupiter's dayside magnetosphere, *Nature*, 289, 803, 1979.
- McNutt, R. L., Jr., J. W. Belcher, and H. S. Bridge, Positive ion observations in the middle magnetosphere of Jupiter, *J. Geophys. Res.*, 86, 8319, 1981.
- Ness, N. F., M. H. Acuna, R. P. Lepping, L. F. Burlaga, K. W. Behannon, and F. M. Neubauer, Magnetic field studies at Jupiter by Voyager 1: preliminary results, *Science*, 204, 982, 1979.
- Northrop, T. G., C. K. Goertz, and M. F. Thomsen, The magnetosphere of Jupiter as observed with Pioneer 10 2. Nonrigid rotation of the magnetodisc, *J. Geophys. Res.*, 79, 3579, 1974.
- Pontius, D. H., T. W. Hill, and M. E. Rassbach, Steady state plasma transport in a corotation dominated magnetosphere, *Geophys. Res. Lett.*, 13, 1097, 1986.
- Pontius, D. H., and T. W. Hill, Rotation driven plasma transport: The coupling of macroscopic motion and microdiffusion, *J. Geophys. Res.*, 94, 15041, 1989.
- Richardson, J. D., and R. L. McNutt, Jr., Observational constraints on interchange models at Jupiter, *Geophys. Res. Lett.*, 14, 64, 1987.

- Russell, C. T., D. E. Huddleston, K. K. Khurana, and M. G. Kivelson, Structure of the Jovian magnetodisk current sheet: initial Galileo observations, *Planet. Space Sci.*, 47, 1101, 1999.
- Scarf, F. L., D. A. Gurnett, and W. S. Kurth, Jupiter plasma wave observations: An initial Voyager 1 overview, *Science*, 204, 991, 1979.
- Siscoe, G. L., and D. Summers, Centrifugally driven diffusion of Iogenic plasma, *J. Geophys. Res.*, 86, 8471, 1981.
- Tascione, T. F., *Introduction to the Space Environment*, 116 pp., Orbit Book Company, Malabar, Florida, 1988.
- Thorne, R.M., Microscopic Plasma Processes in the Jovian Magnetosphere, in *Physics of the Jovian Magnetosphere*, edited by A. J. Dessler, pp. 454-488, Cambridge University Press, New York, 1983.
- Van Allen, J. A., D. N. Baker, B. A. Randall, M. F. Thomsen, D. D. Sentman, and H. R. Flindt, Energetic electrons in the magnetosphere of Jupiter, *Science*, 184, 309, 1974.
- Van Allen, J. A., High-energy particles in the Jovian magnetosphere, in *Jupiter*, edited by T. Gehrels, pp. 928-960, The University of Arizona Press, Tucson, 1976.
- Van Allen, J. A., Energetic electrons in Jupiter's dawn magnetodisc, *Geophys. Res. Lett.*, 6, 309, 1979.
- Vasyliunas, V. M., Theoretical models of magnetic field-line merging, 1, *Rev. Geophys. Space Phys.*, 13, 303, 1975.
- Vasyliunas, V. M., Plasma distribution and flow, in *Physics of the Jovian Magnetosphere*, edited by A. J. Dessler, pp. 395-453, Cambridge University Press, New York, 1983.
- Vasyliunas, V. M., Effects of dipole tilt on the structure of the Jovian magnetosphere, Oral Presentation at Magnetospheres of the Outer Planets meeting, August, 1999.
- Wolf, R. A., The quasi-static (slow-flow) region of the magnetosphere, in *Solar-Terrestrial Physics*, edited by R. L. Carovillano and J. M. Forbes, pp. 303-368, D. Reidel, Boston, 1983.
- Wolf, R. A., R. W. Spiro, and F. J. Rich, Extension of the Rice Convection Model into the high-latitude ionosphere, *J. Atm. Terrest. Phys.*, 53, 817, 1991.
- Yang, Y. S., R. A. Wolf, R. W. Spiro, and A. J. Dessler, Numerical simulation of plasma transport driven by the Io torus, *Geophys. Res. Lett.*, 19, 957, 1992.
- Yang, Y. S., R. A. Wolf, R. W. Spiro, T. W. Hill and A. J. Dessler, Numerical simulation of torus-driven plasma transport in the Jovian magnetosphere, *J. Geophys. Res.*, 99, 8755, 1994.